Year XXXIV Nº 48 June 2026

UNDERGROUND MINING ENGINEERING

Podzemni radovi

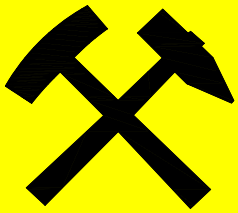

University of Belgrade – Faculty of Mining and Geology

UDK 62

eISSN 2560-3337

UNDERGROUND MINING ENGINEERING

PODZEMNI

RADOVI N°48

http://ume.rgf.bg.ac.rs
e-mail: editor.ume@rgf.bg.ac.rs

Belgrade, June 2026.

UNDERGROUND MINING ENGINEERING 48 (2026) UDK 62
UNIVERSITY OF BELGRADE - FACULTY OF MINING AND GEOLOGY eISSN 2560-3337

UNDERGROUND MINING ENGINEERING - PODZEMNI RADOVI

Publishing supported by: University of Belgrade – Faculty of Mining and Geology, Mining Section

Publisher: University of Belgrade - Faculty of Mining and Geology

For publisher: D.Sc. Aleksandar Cvjetić, Dean of Faculty of Mining and Geology

Availableonline: https://ume.rgf.bg.ac.rs/index.php/ume

The first issue of the journal "Podzemni radovi" (Underground Mining Engineering) was published back in 1982. Its founders were: Business Association Rudis - Trbovlje and the Faculty of Mining and Geology Belgrade. After publishing only four issues, however, the publication of the journal ceased in the same year.

Ten years later, in 1992, on the initiative of the Chair for the Construction of Underground Roadways, the Faculty of mining and Geology as the publisher, has launched journal "Podzemni radovi". The initial concept of the journal was, primarily, to enable that experts in the field of underground works and disciplines directly connected with those activities get information and present their experiences and suggestions for solution of various problems in this scientific field.

Development of science and technique requires even larger multi-disciplinarity of underground works, but also of the entire mining as industrial sector as well. This has also determined the change in editorial policy of the journal. Today, papers in all fields of mining are published in the "Underground Mining Engineering", fields that are not so strictly in connection with underground works, such as: surface mining, mine surveying, mineral processing, mining machinery, environmental protection and safety at work, oil and gas engineering and many others.

Extended themes covered by this journal have resulted in higher quality of published papers, which have considerably added to the mining theory and practice in Serbia, and which were very useful reading material for technical and scientific community.

A wish of editors is to extend themes being published in the "Underground Mining Engineering" even more and to include papers in the field of geology and other geo-sciences, but also in the field of other scientific and technical disciplines having direct or indirect application in mining.

The journal "Underground Mining Engineering" is published twice a year, in English language. Papers are subject to review.

This information represents the invitation for cooperation to all of those who have the need to publish their scientific, technical or research results in the field of mining, but also in the field of geology and other related scientific and technical disciplines having their application in mining.

Editors

TABLE OF CONTENTS

UNDERGROUND MINING ENGINEERING 48 (2026) 1-18 UDK 62
UNIVERSITY OF BELGRADE - FACULTY OF MINING AND GEOLOGY EISSN 2560-3337

Original scientific paper

TECHNICAL ANALYSIS OF THE POSSIBILITY OF EXPANDING THE QUARRY WITH DEEP BENCHES AT THE TREBAČKO BRDO

Ekrem Bektašević[1], Kemal Gutić[1],Toma Jovičić[2]

Received: March 12, 2026 **Accepted:** April 08, 2025

Abstract: This paper presents a comprehensive technical analysis of the potential expansion of the Trebačko Brdo quarry through the introduction of deep benches, with the aim of increasing extraction capacity while maintaining slope stability and ensuring compliance with environmental regulations. The geological, geomorphological, and engineering-geological characteristics of the site indicate favourable conditions for the continued exploitation of limestone. Laboratory testing confirms the high quality of the mineral resource, particularly in terms of its chemical composition (CaO > 50%) and physico-mechanical properties (compressive strength > 100 MPa).

The proposed expansion concept предусматри the successive development of benches down to an elevation of 470 m above sea level, increasing the total extraction height to 85 m. Slope stability has been verified through a calculated safety factor (F = 1.91), while the optimal working bench width (27.5 m) allows for the integration of spiral ramps, safety zones, and drainage systems. Special emphasis is placed on geotechnical challenges, including rock mass discontinuities, interaction with groundwater, and the need for adaptive planning.

The analysis also includes an assessment of environmental impacts, with particular focus on dust emissions, hydrogeological changes, and the necessity of technical reclamation. In conclusion, the proposed quarry expansion model demonstrates high technical feasibility, safety, and compliance with contemporary mining practices, thereby enabling the sustainable exploitation of technical stone at the Trebačko Brdo site.

Keywords: quary; deep benches; slope stability; limestone; geotechnical analysis

[1] University of Tuzla, Faculty of Mining, Geology and Civil Engineering, Urfeta Vejazgića 2, Tuzla, Federation of Bosnia and Herzegovina

[2] University of Belgrade, Faculty of Mining and Geology, Djusina 7, 11000 Belgrade, Serbia

E-mails: ekrem.bektasevic@untz.ba ORCID: https://orcid.org/0000-0001-6742-966X; kemal.gutic@untz.ba ORCID: https://orcid.org/0009-0008-9107-4641; toma.jovicic@rgf.bg.ac.rs ORCID: https://orcid.org/0009-0005-9748-2599

1 INTRODUCTION

The exploitation of technical construction stone, particularly limestone, plays a significant role in the construction industry, road infrastructure development, and the production of lime and cement. The importance of technical stone extraction has been confirmed in numerous national and international studies, especially in the context of environmental impact and industrial development (Bektašević, Sjerotanović & Baraković, 2011a; Bektašević, Sjerotanović & Baraković, 2011b; Valjevac et al., 2024) . Global trends indicate that demand for this resource is increasing in parallel with urbanization and infrastructure expansion (Carrasqueira et al., 2024; Zhang et al., 2025; Firoozi et al., 2024).

Bosnia and Herzegovina possesses numerous limestone deposits, one of the more significant being located within the Municipality of Tešanj, at the Trebačko Brdo site. This area is characterized by favorable geological, geomorphological, and mining-engineering conditions for exploitation, but also by certain constraints related to environmental considerations and spatial planning. Similar challenges associated with environmental restrictions and land-use planning have been documented in other quarries in Bosnia and Herzegovina, highlighting the need to balance resource extraction with spatial and environmental protection (Bektašević et al., 2023; Bektašević et al., 2024).

The Trebačko Brdo deposit is characterized by a well-developed hilly–mountainous relief, with elevations ranging from approximately 600 to 680 m above sea level, which enables the application of surface mining methods. Figure 1 presents the morphological appearance of the broader Trebačko Brdo area, providing insight into the relief characteristics relevant to exploitation planning.

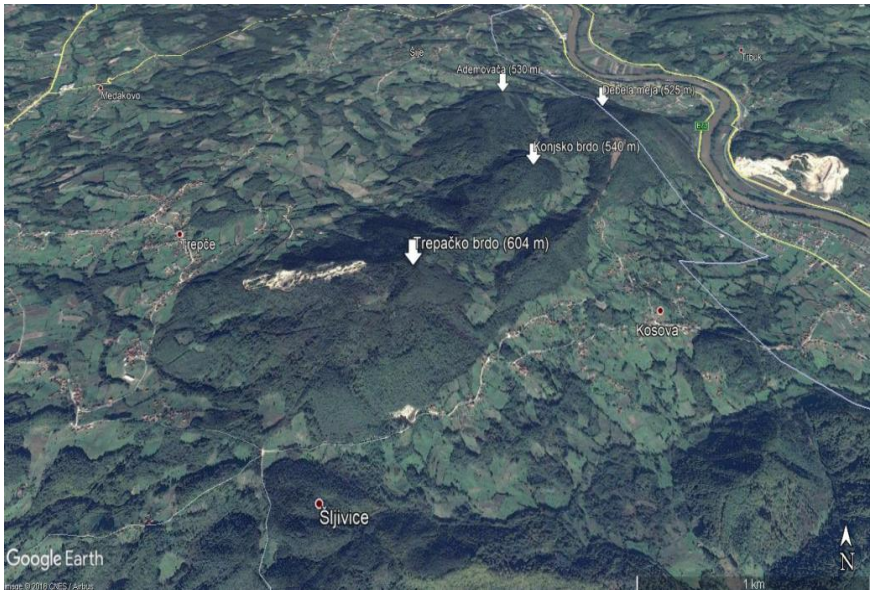

Figure 1 Morphological appearance of the wider Trebačko Brdo area [source: Google Earth]

Previous investigations included drilling operations, laboratory testing of the physico-mechanical properties of the rock mass, and reserve balance calculations. According to the available data, the deposit contains significant quantities of limestone suitable for various construction purposes. The chemical composition indicates a high $CaCO_3$ content, suggesting broad applicability in the construction materials industry (Kašić, Mihajlović & Đorđević, 2023).

In the context of technological development and the need to increase extraction capacity, the expansion of the quarry through the introduction of deep benches is being considered. This concept implies continuation of mining below the existing bench levels, while ensuring slope stability, adequate dewatering, and adaptation of the haulage system. The introduction of deep benches may substantially increase the volume of exploitable reserves; however, it also entails technical and safety challenges that require detailed analysis.

Slope stability represents one of the key factors in planning new bench development. The geomechanical characteristics of the rock mass—such as uniaxial compressive strength, modulus of elasticity, and resistance to water action—are crucial for determining optimal slope angles and bench heights (Hoek & Bray, 1981). Numerical methods, such as SWASE, have proven effective in calculating slope safety factors, particularly under complex geological conditions (Baraković, Bektašević & Sjerotanović, 2011).

Studies indicate that the mechanical properties of limestone change significantly with increasing confining pressure and under water-saturated conditions. Saturation may lead to strength reduction and increased deformability, which is particularly relevant when planning deep benches where interaction with groundwater is more likely (Šestak, 2006; Lama & Vutukuri, 1978).

In addition to geomechanical characteristics, the technological selection of excavation methods constitutes an important aspect. Quarries with deep benches require adequate planning of haul roads, drainage systems, and ventilation. Furthermore, the combined effects of surface and potential underground exploitation must be analyzed, as such systems may induce surface subsidence and alterations in the stress–strain state of the rock mass (Ma et al., 2023). Models developed in recent research enable the prediction of such displacements, thereby enhancing the safety and reliability of planned operations.

Alongside technical considerations, environmental issues are gaining increasing importance. Limestone extraction generates dust emissions, blasting-induced vibrations, landscape alteration, and potential disturbances to hydrogeological regimes. The impact of dust emissions on air quality has been extensively analyzed in several studies, which emphasize the need for the application of modern technologies and mitigation measures (Bektašević et al., 2012; Bektašević et al., 2015a; Bektašević et al., 2015b; Bektašević et al., 2018).

Contemporary approaches require the integration of environmental protection and sustainability measures into mining projects, including impact monitoring, controlled blasting techniques, and reclamation planning (Bell & Donnelly, 2006; Bektašević et al., 2013). Examples from other European quarries demonstrate that intensive exploitation can be successfully combined with high environmental protection standards through the use of modern technologies (Kaymierczak & Strazlkowski, 2019).

At the local level, the Trebačko Brdo quarry has specific social and economic significance. Stone exploitation represents a potential driver for the development of the local construction industry and the creation of new employment opportunities, while simultaneously raising concerns among part of the public regarding spatial and environmental protection. Decisions concerning capacity expansion and the introduction of deep benches must therefore consider technical, economic, environmental, and social factors in an integrated manner.

The objective of this paper is to provide a detailed technical analysis of the possibility of expanding the quarry at Trebačko Brdo through the introduction of deep benches. The focus will be on the assessment of the geomechanical characteristics of the rock mass, technical and technological solutions for excavation and haulage, as well as the evaluation of environmental and community impacts. Particular emphasis will be placed

on comparison with practical case studies and contemporary mining methods, with the aim of demonstrating the feasibility and sustainability of the proposed solutions.

2 GEOLOGICAL, GEOMORPHOLOGICAL, HYDROGEOLOGICAL AND ENGINEERING-GEOLOGICAL CHARACTERISTICS OF THE DEPOSIT AND LABORATORY TEST RESULTS

2.1 Geological and geomorphological characteristics

The Trebačko Brdo area belongs to the spatial unit known as the southern margin of the Pannonian Basin, characterized by complex geotectonic and geomorphological features. The relief consists of a series of hills aligned in the Dinaric strike direction (NW–SE), composed of magmatic–sedimentary rocks of Jurassic–Cretaceous and Neogene age. These geomorphological units are the result of the combined action of endogenous and exogenous processes, with fluvial–nival erosion playing a significant role (Rudarsko Projektovanje, 2023).

Within the broader area, three main morphological units can be distinguished: the lowland zone along river valleys (150–250 m a.s.l.), the hilly terrain (250–500 m a.s.l.), and the low-mountain zone (500–750 m a.s.l.). The maximum elevation of the investigated area reaches 604 m (Trebačko Brdo), while the terrain descends toward the Bosna River valley to elevations of 160–190 m a.s.l. Such hypsometric differences provide favorable conditions for surface mining, but simultaneously require careful slope design due to the pronounced relief dissection (Rudarsko Projektovanje, 2023).

Lithologically, the deposit belongs to the Upper Cretaceous (Turonian and Senonian), and is predominantly composed of limestones, calcarenites, and calcrudites. The limestones are gray to reddish in color, massive in texture, and crystalline in structure, exhibiting a vigorous reaction to diluted HCl acid (Geo IterMax, 2022). The stratigraphic position and lithological uniformity indicate significant potential for exploitation as technical construction stone, as confirmed by previous studies of similar deposits in Bosnia and Herzegovina (Ćosić, Kurtanović & Begović, 2007; Majstorović, Malbašić & Čelebić, 2015).

The bedding of the rock mass is characterized by variable thicknesses (5–25 cm), with a general strike direction of 310–330° and a dip angle of 25–32°. This layer orientation, together with the presence of joints and fractures, significantly influences the geomechanical behavior of the rock mass and slope stability, which is of particular importance when planning deep bench development (Hoek & Bray, 1981).

2.2 Hydrogeological and engineering-geological characteristics

The limestone massif of Trebačko Brdo is characterized by fracture–fissure and cavernous porosity, which conditions the formation of local aquifers with limited capacity. Recharge occurs predominantly through the infiltration of atmospheric

(precipitation) waters, accompanied by significant fluctuations in dynamic reserves. The bedded and fractured limestones enable rapid percolation of precipitation into the deeper parts of the massif, while karstification processes further enlarge fractures and increase flow conduits (Milanović, 2004).

From an engineering-geological perspective, the fundamental parameters of the working environment are determined by lithofacies composition, tectonic framework, and the spatial orientation of discontinuities. Observations from accessible cuts and bench exposures indicate that the layers exhibit variable physico-mechanical properties: lighter-colored limestones demonstrate more favorable characteristics, whereas darker varieties show lower strength values. It has also been observed that the rock mass exhibits improved properties with increasing depth, consistent with general trends in carbonate rocks (Deere & Miller, 1966).

Discontinuities, particularly sub-vertical fractures, represent a significant risk factor for slope stability. Their infill consists of secondary calcite and reddish-brown clay, which is easily washed out, leaving cavities of irregular dimensions. Such conditions require careful geotechnical analysis when designing new benches, with particular emphasis on close coordination between geologists and mining engineers in determining optimal slope angles (Song et al., 2025; Cui & Gratchev, 2024).

2.3 Laboratory test results

The results of chemical, mineralogical–petrographic, and physico-mechanical testing indicate that the limestones from the Trebačko Brdo site meet the requirements for use in the construction industry. Chemical analyses revealed a high CaO content (above 50%) and a loss on ignition of approximately 40–43%, which is typical of high-quality carbonate rocks (Rudex, 2023). The content of undesirable components, such as sulfates, sulfides, and chlorides, is very low (below 0.01%), further confirming the suitability of the material for application in concrete mixtures and asphalt (shown in Table 1).

Table 1 Results of chemical analysis

Parametar	TB-1 (4.2–4.8 m)	TB-1 (11.8–12.5 m)	TB-2 (6.2–7.0 m)	TB-2 (17.0–17.6 m)	TB-3 (4.1–4.7 m)	TB-3 (11.0–12.6 m)
Loss on ignition (LOI)	40.79	41.67	41.12	41.00	41.24	40.27
SiO_2 + insoluble residue	7.20	3.43	4.8	5.15	5.25	6.85
Fe_2O_3	0.10	0.18	0.25	0.21	0.27	0.28
Al_2O_3	0.00	0.00	0.00	0.00	0.00	0.00
CaO	51.04	53.98	53.14	53.00	52.44	51.58
MgO	0.22	0.22	0.21	0.24	0.21	0.27
Na_2O	0.09	0.09	0.09	0.13	0.12	0.12

K_2O	0.01	0.01	0.02	0.02	0.02	0.03
MnO	0.02	0.02	0.023	0.025	0.035	0.033
TiO_2	0.00	0.00	0.00	0.00	0.00	0.00
SO^3	0.01	0.011	0.009	0.015	0.012	0.014
Chlorides (Cl^-)	0.001	0.0011	0.01	0.0011	0.01	0.0011
Sulfides	0.005	0.006	0.004	0.008	0.007	0.009

Mineralogical–petrographic analysis confirmed that the rocks belong to carbonate sediments, specifically crystalline limestones, calcarenites, and calcrudites. The primary mineral constituent is calcite, while quartz and siliceous fragments occur in minor proportions. No components were identified that could cause concrete degradation or undesirable reactivity under adverse conditions.

Physico-mechanical testing showed that the limestones exhibit high uniaxial compressive strength (exceeding 100 MPa in dry conditions), whereas in saturated conditions the values are slightly lower but still remain above the minimum standard requirements (presented in Table 2).

Table 2 Results of physico-mechanical testing

Parameter	B–1 (32.0–33.0)	B–2 (32.0–32.4; 32.5–32.8)	Asphalt concrete (requirement)	Concrete (specification limit)
Compressive strength (MPa) – dry condition	108.9	50.7	≥ 80.0	≥ 120.0
Compressive strength (MPa) – water-saturated condition	103.7	46.1	≥ 64.0	-
Compressive strength (MPa) – after 25 freeze–thaw cycles	97.3	38.5	-	≥ 96.0
Abrasion resistance by grinding ($cm^3/50\ cm^2$)	20.2	36.1	≤35	
Abrasion resistance (Los Angeles coefficient)	21.8	35.5	≤35	
Water absorption (%)	0.68	1.52	≤0.75	
Mass loss in Na_2SO_4 (%) – freeze resistance (%)	3.06	5.61	≤5.0	
Porosity (%)	0.98	1.93	-	-
Bulk density (g/cm^3)	2.643	2.492	2.0-3.0	
Specific gravity (g/cm^3)	2.678	2.541	-	-

Freeze resistance and abrasion resistance indicate suitability for use in road construction, while water absorption is generally below 1%, confirming the good durability of the rock mass (Milišić, 2022).

Considering all evaluated parameters, the material from the Trebačko Brdo deposit can be used in a wide range of construction applications:

- as an aggregate material in cement concrete mixtures,
- for the construction of upper load-bearing layers in pavement structures,
- for precast concrete elements, bank protection structures, lean concrete, and stone cladding.

3 MINING CONDITIONS AND POTENTIAL FOR QUARRY EXPANSION

3.1 Current operational status

The quarry at the Trebačko Brdo site is currently being developed within a limited area with clearly defined quarry boundaries. To date, mining has been conducted in accordance with conventional surface extraction methods, whereby the material is obtained through drilling, blasting, and subsequent loading into haulage equipment.

Figure 2 presents the boundaries of the existing quarry at the Trebačko Brdo site, together with the associated infrastructure elements and the topographic characteristics of the terrain.

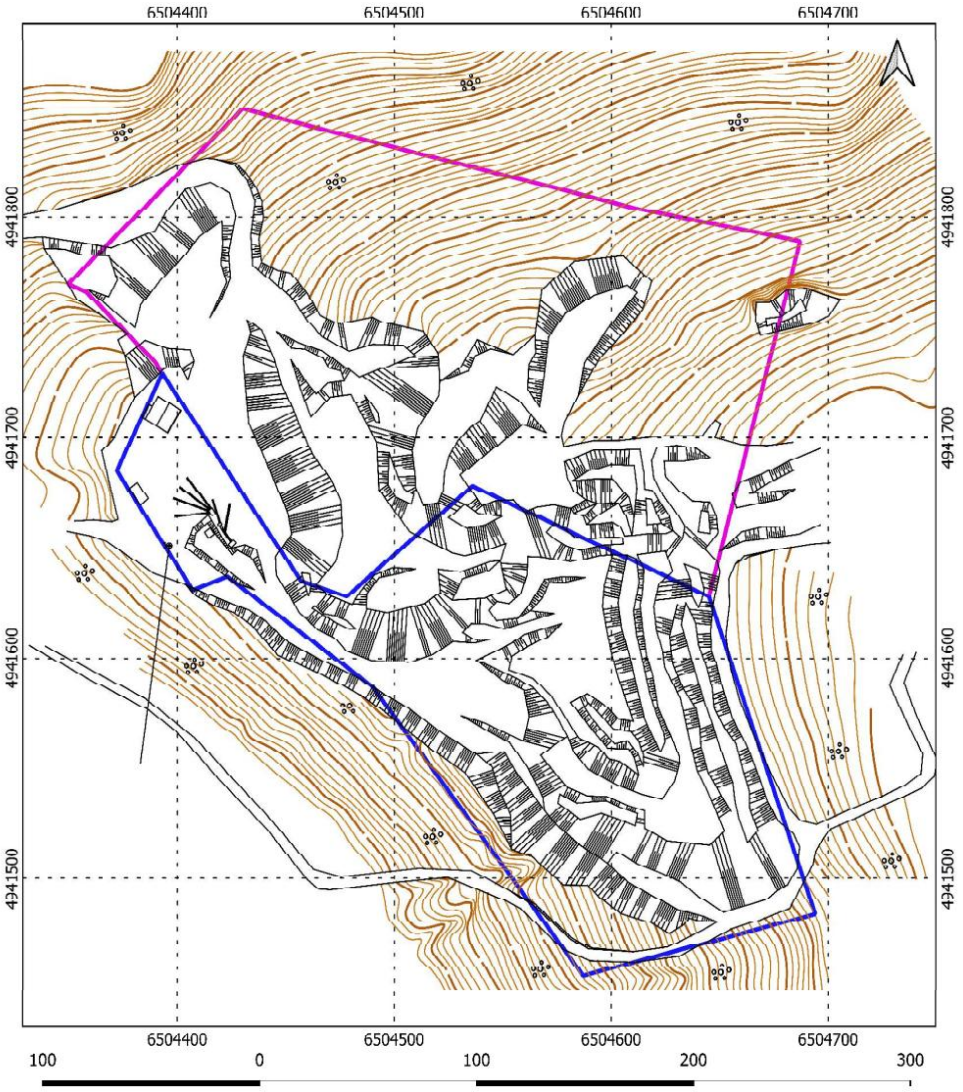

Figure 2 Topographic map of the Trebačko Brdo site with indicated quarry boundaries and infrastructure

The geometry of the benches is aligned with the natural stratification of the limestone rock mass, which has resulted in relatively good stability of the working slopes. However, the existing exploitable reserves in the upper parts of the massif are gradually being depleted, raising the issue of expanding the quarry to greater depths. Regional

trends indicate that many quarries, upon transitioning to deeper benches, face increased technical and safety requirements (Sjoberg. 1996).

3.2 Concept of quarry expansion to deeper bench levels

The expansion of the quarry through the introduction of deeper benches represents a technically optimal solution for securing additional exploitable reserves, without the need for lateral expansion of the quarry. The concept is based on the formation of successive deeper benches below the final mining level, while maintaining geometric stability and operational functionality.

The current designed condition is shown in Figure 3, where the final quarry configuration is visible, with an elevation range from 520 to 570 m above sea level.

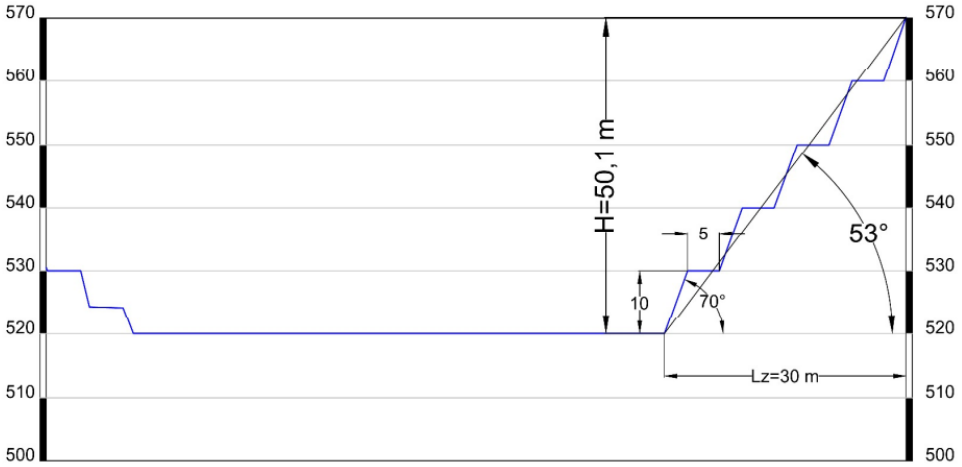

Figure 3 Existing designed cross-section of the Trebačko Brdo quarry

The planned expansion envisages the deepening of the quarry down to the elevation of 470 m above sea level, thereby increasing the total mining height from the current 50 m to 85 m. New benches will be formed successively below the existing mining level, with heights ranging from 10 to 15 meters, in accordance with the terrain geometry and the stability of the rock mass.

Access to the lower benches is provided by spiral ramps integrated into the existing quarry configuration, ensuring adequate working areas, safety zones, and haulage routes.

The working slopes in the expansion area are designed with an inclination of 70°, while the overall final quarry slope angle will be 56°, in accordance with stability requirements. The width of the final berm is 5 meters, providing additional safety during the final phase of exploitation.

The designed condition with the newly formed deeper benches is shown in Figure 4, illustrating the expanded quarry configuration with an increased elevation range from 470 m to 570 m above sea level.

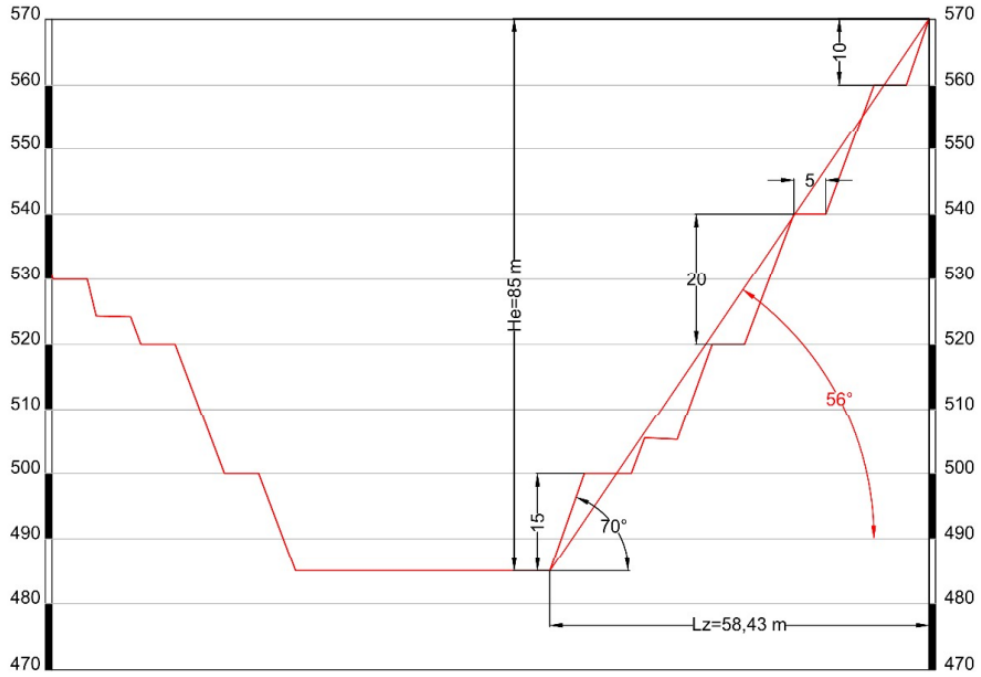

Figure 4 Presentation of the designed quarry profile with deeper benches at the Trebačko Brdo

The advantages of this approach include:

- increasing the volume of available reserves without the need to occupy additional land,
- maintaining continuity of mining operations,
- enabling more rational use of the existing infrastructure (roads, processing facilities, drainage systems).

The main challenges include the need to ensure the stability of deeper slopes, increased interaction with groundwater, and the adaptation of the haulage system to operating conditions at greater depths (Safari et al., 2025).

3.3 Slope Stability and Associated Geotechnical Challenges

Slope stability under conditions of deeper benches depends on the lithological and tectonic characteristics of the rock mass, the spatial orientation of bedding and

discontinuities, as well as hydrogeological conditions. Numerical analyses (e.g., the finite element method and the limit equilibrium method) have proven particularly effective for calculating the factor of safety of slopes in complex carbonate massifs.

When planning new benches, it is necessary to:

- precisely define the slope angle and bench height,
- conduct geotechnical investigations for each bench,
- provide a drainage system to reduce pore water pressures,
- implement stabilization measures where necessary (anchors, mesh, retaining structures) in zones of weakened rock mass.

Previous experience from quarries in Croatia and Slovenia shows that the combination of geotechnical monitoring and adaptive bench planning significantly reduces the risk of landslides and rockfalls in deep mining operations (Markus, 2018; Lazar et al., 2020).

In order to confirm the technical feasibility of the expansion, two basic calculations were carried out: the slope stability factor and the optimal working bench width. These calculations contribute to a quantitative assessment of safety and the geometric functionality of the planned benches.

For the assessment of slope stability in clayey–marly rock mass, a simplified version of Bishop's method is applied:

$$F = \frac{c' \cdot L + (W \cdot \cos\alpha - u \cdot L) \cdot \tan\emptyset'}{W \cdot \sin\alpha} \quad (1)$$

Where:

- Effective cohesion: c' = 28 kPa,
- Effective internal friction angle: φ' = 20°,
- Pore water pressure: u = 10 kPa,
- Weight of the sliding slice (segment): W = 200 kN,
- Length of the slip surface: L = 13.75 m,
- Slip (inclination) angle: α = 70°.

By substituting the given parameters $F = \frac{28 \cdot 13{,}75 + (200 \cdot \cos 70^0 - 10 \cdot 13{,}75) \cdot \tan 20^0}{200 \cdot \sin 70^0} = 1{,}91$

The slope stability analysis was carried out on clayey–marly rock mass to represent the most unfavorable scenario and to account for discontinuities filled with clay and marl. This approach ensures a conservative design, as the actual values for limestone indicate considerably higher slope stability.

For determining the minimum working platform width, the empirical formula proposed by Singh & Goel (2011) is used:

$$B = H \cdot \tan\theta \quad (2)$$

Where:

- B – working bench width,
- H = 10 m – bench height,
- θ = 70° – designed slope angle.

By substituting the given parameters $B = 10 \cdot \tan 70^0 = 27{,}5m$.

The obtained value represents the optimal working platform width, which includes space for the working area, safety berm, access ramp, and lateral stabilization zones. Considering that the technical documentation prescribes a minimum width of 8 meters, the designed value of 27.5 meters ensures additional safety and functionality during the deep mining phase.

The calculated factor of safety significantly exceeds the prescribed limit values (F = 1.05–1.10), thereby confirming the stability of the designed slopes under deep mining conditions.

3.4 Haulage System and Drainage

Mining operations at deeper bench levels require a reliable and functionally optimized haulage system. In practice, spiral truck ramps are most commonly used, enabling safe and continuous movement of equipment to the lower working benches. Alternatively, in some quarries, a combination of conveyor belts and truck haulage is applied, which is suitable for the continuous transport of larger quantities of fragmented material.

Drainage represents one of the key factors for the uninterrupted operation of the quarry, particularly under conditions of increased interaction with groundwater. The negative impacts of inadequate drainage include:

1. Reduced slope stability due to increased pore water pressure,
2. Difficult operation of machinery and equipment in saturated zones,
3. Accelerated damage and degradation of haulage infrastructure.

Due to these risks, it is necessary to design an integrated system of drainage channels, pumping stations, and settling ponds to control surface and groundwater, along with mandatory regular monitoring of groundwater levels. Such technical solutions have already been implemented in carbonate rock quarries across Central Europe, where deep bench mining is standard practice (Kamilov et al., 2024).

4 CONCLUSION

The technical analysis of the Trebačko Brdo quarry has shown that the site possesses valid geological, geometric, and infrastructural conditions for the continuation of mining at greater depths. Based on the available technical documentation, geological profile, and configuration of the existing benches, it has been determined that additional deeper benches can be formed while maintaining slope stability, transport efficiency, and compliance with both national and international standards.

The calculated slope stability factor, F = 1.91, significantly exceeds the prescribed limit values (1.05–1.10), confirming the high safety level of the designed slopes in the clayey–marly rock mass. At the same time, the designed working bench width of 27.5 meters considerably surpasses the minimum technical requirements, enabling the integration of a spiral ramp, safety berm, and drainage channels without compromising functionality.

Previous experience from quarries in Croatia and Slovenia confirms that the application of geotechnical monitoring combined with phased adjustment of quarry geometry represents an effective approach for controlling stability in complex geological conditions. Such an approach enables timely response to local changes in the rock mass, optimization of slope angles, and reduction of the risk of landslides and rockfalls. Comparable drainage methods, including drainage channels, pumping stations, and settling ponds, are already applied in deep carbonate rock mining operations in Central Europe, thereby confirming the technical justification of the proposed solutions.

REFERENCES

E. BEKTAŠEVIĆ, I. SJEROTANOVIĆ, A. BARAKOVIĆ (2011a) Research of influence of application of the best available techniques for processing sedimentary and igneous rocks on the air pollution in Bosnia and Herzegovina, 11-th International Multidisciplinary Scientific Geoconference SGEM 2011, Conference Centre Flamingo Grand Albena Complex, Bulgaria 20 – 25 June 2011, (Conference proceedings volume III 595 - 602), (ISSN 1314-2704 DOI: 10.5593/sgem2011), Scietific chairmen Acad. Nikola Sabotinov, Prof. Metodi Mazhdrakov

E. BEKTAŠEVIĆ, I. SJEROTANOVIĆ, A. BARAKOVIĆ (2011b) Influence of limestone and spilite processing at SM „Kota“ near Vares to environment, 11-th International Multidisciplinary Scientific Geoconference SGEM 2011, Conference Centre Flamingo Grand Albena Complex, Bulgaria 20 – 25 June 2011, (Conference proceedings volume III 419 - 426), (ISSN 1314-2704 DOI: 10.5593/sgem2011), Scientific chairmen Acad. Nikola Sabotinov, Prof. Metodi Mazhdrakov

M. VALJEVAC, E. BEKTAŠEVIĆ, K. GUTIĆ, N. SAKIĆ, DENIJEL SIKIRA (2024) Exploitation and processing of technical stone from quarries Plješevac near Kiseljak,

University of Tuzla, Journal of faculty of mining, geology and civil engineering, (Professional Paper), 12/2024, Article DOI: 10.51558/2303-5161.2024.12.12.23

CARRASQUEIRA, J., AFONSO, C., GIL, M. M., BERNARDINO, R., GAMBOA, R., BARROSO, S. D., & BERNARDINO, S. (2024). Digging Deeper: Assessing the Impact of Limestone Exploitation and Use Worldwide. Environments, 11(12), 283. https://doi.org/10.3390/environments11120283

ZHANG, W., WANG, J., LI, X. ET AL. (2025). Dynamic Mechanical Characteristics of Limestone Under Cyclic Impact of Various Confining Pressure. Indian Geotech J 55, 1506–1516 https://doi.org/10.1007/s40098-024-01027-z

FIROOZI, A., FIROOZI, A. A., OYEJOBI, D. O., AVUDAIAPPAN, S., & SAAVEDRA FLORES, E. (2024). Emerging trends in sustainable building materials: Technological innovations, enhanced performance, and future directions. Results in Engineering, 24, 103521. https://doi.org/10.1016/j.rineng.2024.103521

BEKTAŠEVIĆ, E., GUTIĆ, K., KADRIĆ, R., KADRIĆ, S., I SIKIRA, D. (2023). Influence of Dust Emission Emitted from the Surface Quarry of Technical Stone on Air Quality. Engineering And Technology Journal, 8(12), 3149-3155., https://doi.org/10.47191/ etj/v8i12.05

E. BEKTAŠEVIĆ, K. GUTIĆ, M. VALJEVAC, J. KONTA (2024) Unapređivanje mjera zaštite na radu u kamenolomima pri proizvodnji i preradi tehničkog kamena, Hrvatsko rudarsko geološko društvo Mostar - Rudarsko geološki glasnik, Mostar decembar 2024 godine, (strana 49-61), (ISSN 1840 0299), Glavni urednik: Josip Marinčić, dipl.inž.geol.

KAŠIĆ, V., MIHAJLOVIĆ, S., & ĐORĐEVIĆ, N. (2023). Geological characteristics of the limestone deposit "Dobrilovići" - Loznica and its preparation for use in agriculture. Podzemni Radovi, 2(43), 17-25. https://doi.org/10.5937/podrad2343017K

HOEK, E., & BRAY, J. W. (1981). Rock slope engineering (3rd ed.). London: Institution of Mining and Metallurgy.

A. BARAKOVIĆ, E. BEKTAŠEVIĆ, I. SJEROTANOVIĆ (2011) Određivanje faktora sigurnosti u stijenskom materijalu na primjeru Borskog ležišta numeričkom metodom „SWASE“, Institut za rudarstvo i metalurgiju Bor, Komitet za podzemnu eksploataciju mineralnih sirovina – Rudarski radovi 1/2011, Bor, Srbija mart 2011 godine, (strana 85 – 100), (UDC 622 YU ISSN 1451-0162), Glavni i odgovorni urednik Dr Milenko Ljubojev

ŠESTAK, I. (2006). J. OSWALD, Filozofija prakse u Hrvatskoj, Filozofsko-teološki institut Družbe Isusove u Zagrebu, Biblioteka Filozofski niz, knjiga 22, Zagreb, 2006, 133 str.. Obnovljeni Život, 61 (2), 249-251. Preuzeto s https://hrcak.srce.hr/3842

LAMA, R. D., & VUTUKURI, V. S. (1978). Handbook on mechanical properties of rocks. Clausthal: Trans Tech Publications.

MA, K., YANG, T., ZHAO, Y., GAO, Y., HE, R., LIU, Y., HOU, J., & LI, J. (2023). Mechanical Model for Calculating Surface Movement Related to Open-Pit and Underground Caving Combined Mining. Minerals, 13(4), 520. https://doi.org/10.3390/min13040520

BEKTAŠEVIĆ, E., BARAKOVIĆ, A., FRLJAK, N., & KONTA, J. (2012). Utjecaj kamenoloma na okoliš u Federaciji Bosne i Hercegovine. Rudarsko-geološki glasnik, Hrvatsko rudarsko-geološko društvo Mostar, (decembar), 237–246. ISSN 1840-0299.

BEKTAŠEVIĆ, E., GOLETIĆ, Š., HASIĆ, E., & KEŠETOVIĆ, Z. (2015a). Modelling of airborne dust dispersion emitted from opencast mining in order to assess its impact on the air quality. In Š. Goletić & N. Imamović (Eds.), Proceedings of the 5th International Scientific Conference Environmental and Material Flow Management (Session IV, pp. 260–267). University of Zenica, Faculty of Mechanical Engineering. ISBN 978-9958-617-46-1.

BEKTAŠEVIĆ, E., OSMANOVIĆ, F., ŽUTIĆ, Đ., HASIĆ, E., HUSEJNAGIĆ, E., & KONTA, J. (2015b). Obračun emisije prašine emitovane sa površinskog kopa tehničkog kamena u cilju ocjene njenog utjecaja na kvalitet zraka. Rudarsko-geološki glasnik, Hrvatsko rudarsko-geološko društvo Mostar, (decembar), 83–91. ISSN 1840-0299.

BEKTAŠEVIĆ, E., GOLETIĆ, Š., SARAJLIĆ, I., HASIĆ, E., & ŽUTIĆ, Đ. (2018). Modelling of airborne dust PM10 dispersion emitted from quarry in order to assess its impact on the air quality. In Š. Goletić & N. Imamović (Eds.), Proceedings of the 8th International Symposium on Environmental and Material Flow Management (pp. 148–155). University of Zenica, Faculty of Mechanical Engineering. ISBN 978-9958-617-46-1.

BELL, F. G., & DONNELLY, L. J. (2006). Mining and its impact on the environment. Boca Raton: CRC Press.

BEKTAŠEVIĆ, E., SARAJLIĆ, M., FRLJAK, N., KONTA, J., & LAPANDIĆ, E. (2013). Provođenje tehničke rekultivacije na dijelu deformisanog rudarskog terena na PK "Koritnik" RMU Breza. Rudarsko geološki glasnik, decembar, 149–154. ISSN 1840-0299.

KAŹMIERCZAK, U., & STRZAŁKOWSKI, P. (2019) Environmentally Friendly Rock Mining—Case Study of the Limestone Mine "Górażdże", Poland. Applied Sciences, 9(24), 5512. https://doi.org/10.3390/app9245512

Rudarsko projektovanje d.o.o. Tuzla. (2023). Glavni rudarski projekat eksploatacije krečnjaka kao AG i TG kamena na PK-Kamenolomu "Trebačko Brdo", općina Tešanj (rudarsko-tehnološki dio).

Geo InterMax d.o.o. Tuzla (2022). Elaborat o klasifikaciji, kategorizaciji i proračunu rezervi krečnjaka kao arhitektonsko-građevinskog i tehničkog-građevinskog kamena na lokalitetu "Trebačko Brdo" – Trepče, Općina Tešanj, sa stanjem na dan 30.06.2022.

ĆOSIĆ, N., KURTANOVIĆ, R., & BEGOVIĆ, S. (2007). Ležišta krečnjaka iz sarajevsko-zeničkog krednog fliša. U Zborniku radova sa naučno-stručnog skupa „KVALITET 2007“ (str. 154–160). Neum: Univerzitet u Zenici. https://www.quality.unze.ba/zbornici/QUALITY%202007/120-Q07-154.pdf

MAJSTOROVIĆ, S., MALBAŠIĆ, V., & ĆELEBIĆ, M. (2015) Perspectives for development of technical building stone - limestone in the Republic Srpska. Arhiv za tehničke nauke, (12), 27–36. https://doi.org/10.7251/afts.2015.0712.027M

MILANOVIC, P. (2004) Water Resources Engineering in Karst (1st ed.). CRC Press. https://doi.org/10.1201/9780203499443

DEERE, D. U., & Miller, R. P. (1966) Engineering classification and index properties for intact rock (Technical Report No. AFWL-TR-65-116). Air Force Weapons Laboratory, Kirtland Air Force Base, New Mexico. https://apps.dtic.mil/sti/tr/pdf/AD0646610.pdf

SONG, L., BAI, Z., JIANG, Q., ZHU, B., WANG, G., & GU, Y. (2025) Advancing the understanding of infilled joint shear behavior: A review of modeling, measurement, and influential factors. Rock Mechanics and Rock Engineering, 58, 9265–9295. https://doi.org/10.1007/s00603-025-04559-9

CUI, C., & GRATCHEV, I. (2024) The Effect of Clay Infill on Strength of Jointed Sandstone: Laboratory and Analysis. Geotechnics, 4(2), 499-511. https://doi.org/10.3390/geotechnics4020027

Rudex d.o.o. Vogošća. (2023) Dopunski rudarski projekat optimiziranja bušačko-minerskih parametara sa mjerama zaštite objekata od negativnih seizmičkih uticaja izazvanim miniranjem pri izvođenju eksploatacionih radova na proizvodnji krečnjaka kao AG i TG kamena na PK – kamenolomu "Trebačko Brdo", općina Tešanj (rudarski dio).

MILIŠIĆ, K. (2022) Utjecaj dodataka na svojstva betona izloženog habanju (Diplomski rad). Sveučilište u Splitu, Fakultet građevinarstva, arhitekture i geodezije. https://zir.nsk.hr/islandora/object/gradst%3A2430

SJÖBERG, J. (1996) Large scale slope stability in open pit mining — a review (TR 96-10T). Luleå University of Technology. https://www.diva-portal.org/smash/get/diva2:995561/FULLTEXT01.pdf

SAFARI, M., DOULATI ARDEJANI, F., MAGHSOUDY, S., & TAHERDANGKOO, R. (2025) Hydro-mechanical modeling of groundwater-induced instability and

dewatering strategies in open-pit slope design. Indian Geotechnical Journal. https://doi.org/10.1007/s40098-025-01385-2

MARKUS, J. (2018) Eksploatacija tehničko-građevnog kamena iz kamenoloma Podvlaštica kod Orebića (Diplomski rad). Varaždin: Sveučilište u Zagrebu, Geotehnički fakultet. Preuzeto s https://urn.nsk.hr/urn:nbn:hr:130:473100

LAZAR, A., VIŽINTIN, G., BEGUŠ, T., & VULIĆ, M. (2020) The Use of Precise Survey Techniques to Find the Connection between Discontinuities and Surface Morphologic Features in the Laže Quarry in Slovenia. Minerals, 10(4), 326. https://doi.org/10.3390/min10040326

SINGH, BHAWANI & R. K. GOEL. (2011) Engineering rock mass classification. Boston: Butterworth-Heinemann, 2011.

KOMILOV, S., RUSTAMOV, K. J., AKRAMOVA, L., EGAMSHUKUROV, P., & TASTANOVA, G. (2024) Development of mining operations in deep quarries using automobile and combined transport. E3S Web of Conferences, 515, 03014. https://doi.org/10.1051/e3sconf/202451503014

UNDERGROUND MINING ENGINEERING 48(2026) 19-38 UDK 62
UNIVERSITY OF BELGRADE - FACULTY OF MINING AND GEOLOGY ISSN 03542904

Original scientific paper

UPGRADE OF A CONVENTIONAL PUMPING UNIT WITH A COMPRESSOR FOR PRESSURE REDUCTION IN THE CASING, AIMED AT INCREASING OIL AND GAS PRODUCTION AND REDUCING CO2 EMISSIONS

Stevica Jankov[1], Eleonora Desnica[2], Borivoj Novaković, Luka Djordjević

Received: January 11, 2026 **Accepted:** February 17, 2026

Abstract: In the paper, the authors are conducing research into designing and upgrading the conventional system of oil production using a compressor for pressure reduction in the casing, aimed at increasing oil and gas production and reducing CO2 emissions. As oil exploitation progresses, the natural pressure of a reservoir decreases, which results in reduced production from the wells. Therefore, compressor design becomes essential for production optimization. The paper analyses the methodology of designing a compressor which is integrated into the existing sucker rod pump systems, bearing in mind specific pumping unit dimensions, the annular pressure and the quantity of produced gas. The proposed approach includes precise flow dynamics measurement and analysis, as well as optimization of the geometry of compressor installation in order to achieve maximum efficiency. Pilot projects at nine wells have shown a significant increase in fluid production and decrease in CO2 emissions by using a closed casing and directing gas into the production line. The research provides an insight into possible benefits of integrating a compressor with production systems, thus ensuring a more sustainable approach to oil and gas exploitation

Keywords: Beam Gas Compressor, Oil, Wells

1 INTRODUCTION

At the initial stage of production, the natural reservoir energy enables the majority of wells to produce in self-flowing conditions. However, as exploitation progresses, the natural energy gradually becomes used up, leading to a continuous fall in the reservoir pressure, which results in a rapid drop in production in self-flowing wells. An ever-growing number of oil wells at a single oil field is faced with discontinued production, which seriously threatens an efficient and stable oil field production. Consequently,

[1] NAFTAGAS – Oil Services LLC, Novi Sad, Serbia

[2] University of Novi Sad, Technical Faculty "Mihajlo Pupin", Zrenjanin, Serbia

E-mails: stevica.jankov@nis.rs ORCID: https://orcid.org/0009-0000-6503-8200;
eleonora.desnica@tfzr.rs ORCID: https://orcid.org/0000-0002-4724-5764;
borivoj.novakovic@uns.ac.rs ORCID: https://orcid.org/0000-0003-2816-3584;
luka.djordjevic@tfzr.rs ORCID: https://orcid.org/0000-0003-4578-9060

accurate forecasts of natural flow suspension and of key parameters (such as reservoir pressure, bottom-hole flowing pressure and production rate) are essential for designing a diagram of a mechanical exploitation mode, ensuring stable production and establishing production capacities (Gao et al., 2025). When a well is flowing, we analyse pressure drop trends at the wellhead to calculate pressure reduction speeds and determine the time when the pressure will reach its minimum - the time when the well will stop flowing.

By applying the nodal analysis method, we calculate Inflow Performance Relationship (IPR) and fluid production curves under different pressure conditions in the reservoir (Camargo et al., 2008). As Figure 1 shows, the shut-in pressure corresponds to the reservoir pressure at which the Inflow Performance Relationship (IPR) curves do not intersect the Tubing Performance Curve (TPC) under shut-in conditions.

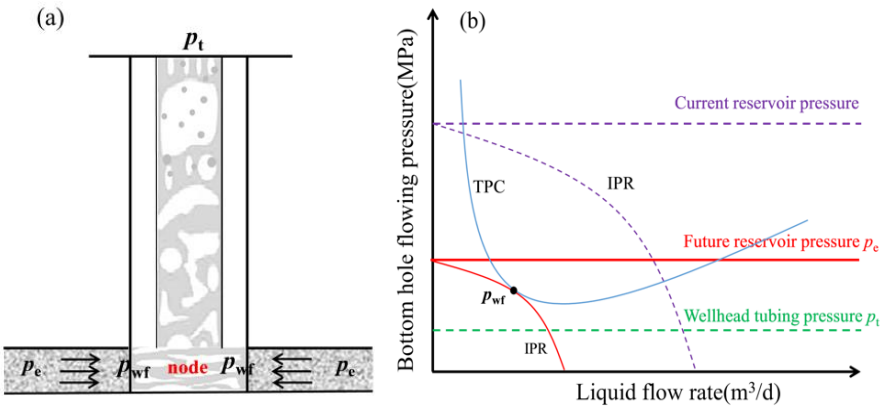

Figure 1 Schematic of fluid inflow into the wellbore (a) and a diagram showing the relationship between fluid production and bottom-hole pressure with inflow (IPR) curve and production (TPC) curve (Gao et al., 2025)

1.1 Sucker rod pumping system basics

After a well stops flowing, we proceed to the selection of a mechanical oil exploitation method to ensure maximum recovery from the oil reservoir. The paper presents the conventional system of oil recovery using sucker rod pumps. We can only speculate on the number of wells using this oil production method globally and these account for 21%, while their share in oil production is 7% (Kis, 2021). Given such large share in oil production, the basic goal of engineers is to safely manage well production with minimum operating expenses, downtime and equipment failures (Kis, 2021). Figure 2 shows the sucker rod pumping system

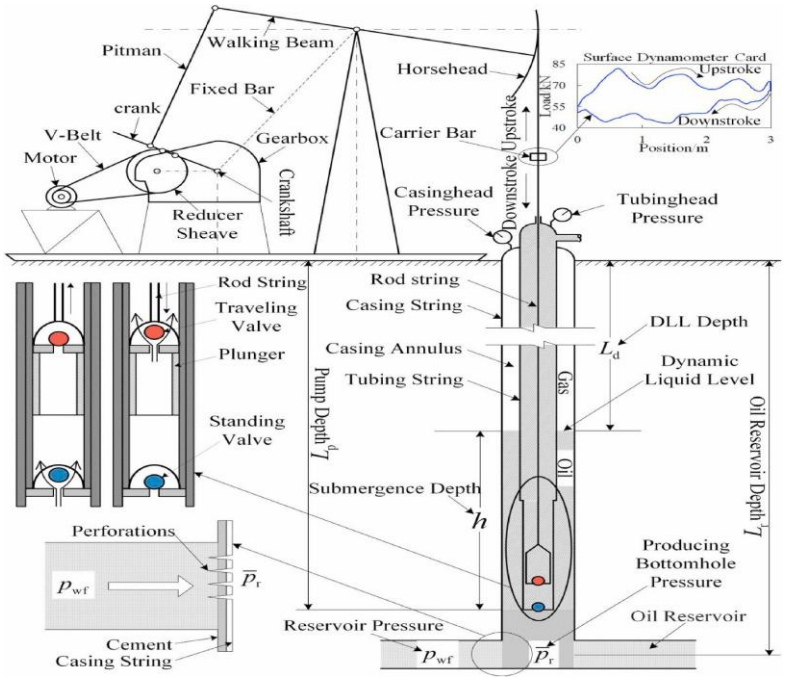

Figure 2 Schematic of the sucker rod pumping system (Chen et al., 2021)

The systems are simple to use owing to their design. However, there are several deficiencies, including loss of efficiency in wells containing gas, sucker rod friction in deviated wells and small installation depth (Bode, 2019).

The sucker rod pumping system and the intelligent three level management system (Aliev et al., 2018):

- Pumping unit level
- RMS level consisting of a controller for collecting data from the sensor and a frequency regulator for the actuator (electric motor) speed control. Furthermore, this level includes a modem equipped with an antenna for data exchange between RMS and the central control station via MODBUS-RTU protocol.
- Oil field centralised control station level consisting of an industrial computer and a wireless modem with an antenna.

During monitoring, it is possible to select an observation interval including all historical data accumulated through the application of the SCADA system.

Each of the parameters shown may be regarded and analysed individually. Given the large number of operation parameters, it is possible to detect a problem and forecast the time of system failure with high precision. The intelligent management system itself

gives reports on operation anomalies which the specialist detects and issues requests for the system servicing before it stops working (S. M. Jankov et al., 2025).

One of the preconditions for monitoring the operation of sucker rod pumps is the availability of dynamometer cards. The cards are generated using load and stroke sensors. The shape on the dynamometer card is that of a parallelogram. Technologists, based on the shape of the parallelogram, can identify more than 20 parallelogram types indicating different conditions in a well, and also problems in the operation (Aliev et al., 2018).

The data for examining the impact of the dynamic level were obtained by way of an automatic recorder which measures the depth of the dynamic fluid level in an oil well by applying the acoustic waves method. This principle uses the acoustic waves method based on the concept of acoustic distance measurement. The acoustic waves generator at the wellhead produces a signal and the wave spreads downwards along the annulus. When it reaches the tubing joint, a small part of the wave generates reflection received by a receiver at the wellhead. The largest part of the acoustic wave continues to spread downwards, with its energy gradually dissipating and the strength of the signal progressively reducing. Finally, a part of the wave reaches the liquid level, while the resulting wave (liquid level wave) is received by the receiver. (Jia et al., 2014; Davies et al., 2014; S. Jankov et al., 2025).

2 METHODOLOGY

Over time, oil production systems which use sucker rod pumps face problems due to gas backpressure which accumulates in the annular space (casing), preventing greater production of oil since it reduces the dynamic level which is often at the pump level (Escobar-Remolina et al., 2015). The gas problem is resolved by taking gas away from the well and burning it on the flare or releasing it into atmosphere, which poses great environmental problems and high operational risks (Sandler et al., 2012).

The gas released from a formation frequently creates problems in the operation of the sucker rod pump itself, which may result in oil production disruption due to the impact of gas, while the pressure the exerts on the reservoir may lead to the absence of fluid flow from the reservoir (Al-Khatib, 1984).

In 1971, Charlie McCoy found a solution to eliminate gas from annular space, after which the compressors he designed started being used globally (Al-Khatib, 1984).

2.1 Principle of compressor operation

The main advantage of compressors is in their use of the energy of the pumping unit without requiring any additional source of energy. When the polished rod moves upward, gas is taken and transported from the annulus over the check valve to the lower compressor chamber, while it is simultaneously compressed at the top of the compressor

and released into the discharge line through the discharge valve. Figure 3(a) shows blue gas absorbed from a well. When the piston moves, it is pressed (now red) and sent to the discharge line. The process of suction and compression is carried out alternatively in the upper and lower section. If it is suctioned from the lower pipe, the gas at the top of the piston is compressed, and if it is suctioned at the top of the compressor, then the bottom compresses and releases the gas (Figure 3(b)). The process repeats continuously.

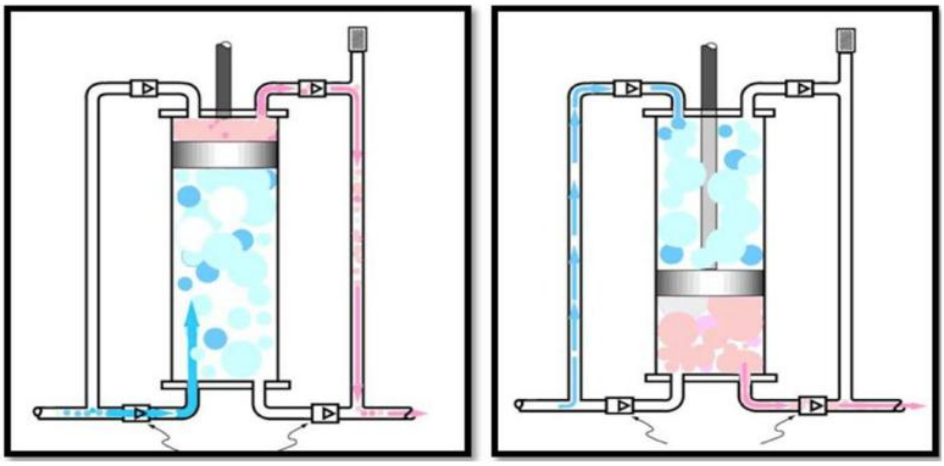

Figure 3 Lower suction (a) and upper suction (b) (Sandler et al., 2012)

It should be noted that the operating principle described here is based on double-acting operation. In case the quantity of gas that should be compressed is reduced, it is possible to use a simple combination of valve closing and opening to change the principle to a single-acting operation (Engl, 2009).

2.2 Compressor design

In his paper (Engl, 2009) describes in detail the Beam Gas Compressor (BGC) design. Several factors affect compressor design and the user should, therefore, provide the manufacturer with a comprehensive information sheet containing the type of the pumping unit with dimensions, quantity of produced gas sent to the production line, i.e. gas production measurements in conditions under which the compressor is to operate, gas content and the number of pumping unit strokes.

In order to design a compressor, it is necessary to have exact information about the quantity of gas that is compressed. System dimensions must be designed so as to enable compression 10 to 20% above the actual gas volume in order to ensure adequate working capacity in situations when gas production changes. Gas measurement, therefore, represents the key parameter in compressor design which must be carried out in conditions similar to the ones under which a well will operate, after compressor

installation. Additionally, there is a direct relationship between the calculation of compressor dimensions and the compression flow rate, which is proportional to the pump operating speed, as shown in the equation (1) (Escobar-Remolina et al., 2015).

$$Q = \frac{P * N * S * L}{K} \tag{1}$$

Where:

P – suction pressure (Pa),

Q – gas volume (Sm^3),

K = 0.07531 (for a single-acting compressor),

K= 0.03777 (for a double-acting compressor),

N – number of strokes min^{-1},

S – compressor piston area (m^2),

L – length of piston stroke (m).

Suction pressure for compressor selection is calculated according to the following formula (2):

$$P = \frac{Q * K}{N * S * L} \tag{2}$$

The basic compressor selection formula refers to the piston area calculated by the formula (3).

$$S = \frac{Q * K}{N * P * L} \tag{3}$$

NOTE: Coefficient K for a single-acting compressor is K = 0.07531, and for a double-acting compressor it is K=0.03777.

2.3 Compressor installation geometry

To ensure stable operation and the required length of the compressor piston movement, it is necessary to carry out the installation at the appropriate point of the pumping unit so as to meet the conditions for compressing the calculated gas volume and obtaining the target pressure in the casing.

The formula for the calculation of the point where the compressor is to be installed (4):

$$C = \frac{Y * A}{2 * B} \tag{4}$$

Where:

A – The distance of the walking beam bearing from the suspension point of Pitmen (mm)

B – The height from the Pitman suspension from the Crank to the point of compressor installation (mm)

C – The distance of the point of compressor installation on the Walking Beam to the Walking Beam bearing (the support point on the beam base) (mm)

Y – The length of compressor piston movement (mm)

Figure 4 shows the schematic of the pumping unit with marked A, B, C and Y values that will be used to calculate the point of compressor installation

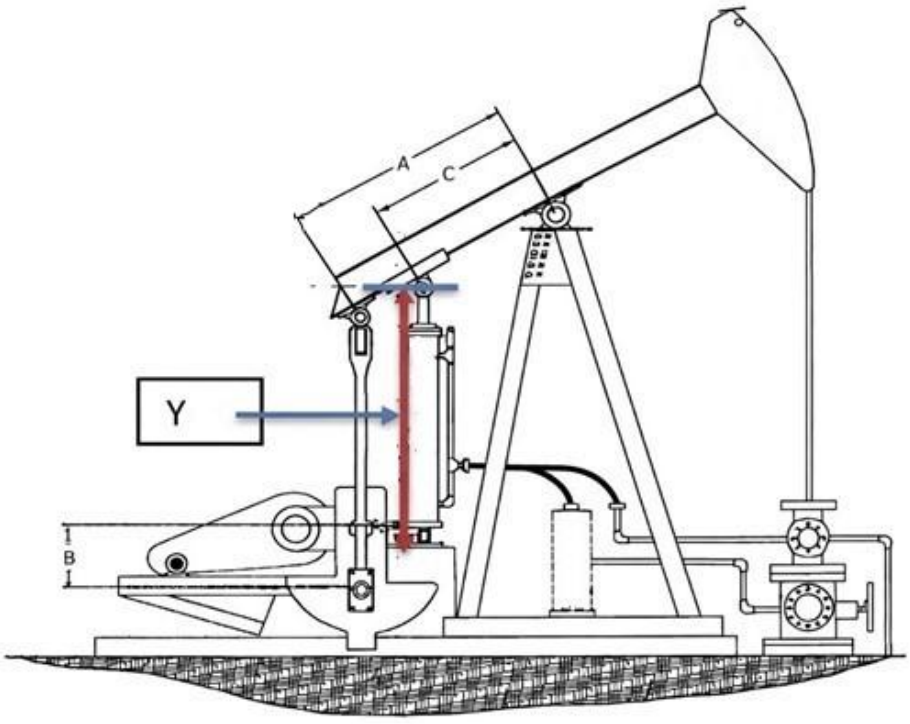

Figure 4 Schematic of the pumping unit with presented A, B, C and Y values that will be used in the calculation of the compressor unit point

3 EXPLORATION METHODOLOGY

3.1 Measurement flow chart

The study was conducted on nine producing oil wells equipped with sucker rod pumping units. Continuous monitoring of operational parameters was performed using a SCADA-based system integrated with stationary sensors. Dynamic fluid level and annular pressure were measured using a stationary acoustic level meter (sonolog), installed at the wellhead. Measurements were recorded four times per day, while gas production was measured at surface separators under reference conditions (101.325 kPa, 15 °C). Pumping unit operating parameters (stroke length, strokes per minute, load) were obtained from dynamometer cards generated by load and displacement sensors.

3.2 Filtering and validation of data

Raw sensor data were filtered to remove outliers caused by transient operating conditions, such as pump start-up or shutdown events and short-term pressure oscillations during compressor commissioning. Dynamic level measurements recorded at annular pressures below 80 kPa were flagged as potentially unreliable and excluded from quantitative analysis. Only stabilized operating periods of at least 24 h duration were considered for before/after comparison.

3.3 Calculation procedure

Gas volume rates were converted to standard conditions and used as input for compressor sizing. Compressor piston area and stroke length were calculated using Equations (1)–(3), based on measured suction pressure, gas volume, and pumping unit stroke frequency. The installation geometry of the compressor on the walking beam was determined using the kinematic relationship given in Equation (4), ensuring compatibility between pumping unit stroke and compressor piston travel. Fluid production before and after compressor installation was calculated from effective pump stroke length derived from dynamometer cards. CO_2 emissions were calculated based on measured gas volumes flared and standard emission factors, as described in Section CO_2 emission calculation

4 RESULTS AND DISCUSSION

In order to increase oil production and reduce CO2 emissions in unprofitable wells, a pilot project was carried out at nine wells. Gas extraction at five wells (E-001, E-002, E-003, E-004 and E-005) was resolved by a closed casing and by directing gas to the production line, thus preventing its emission into the atmosphere. However, in these wells, a pressure rise in the casing resulted in a fluid level drop in the well to the pump level, which led to reduced oil production.

At wells E-006, E-007, E-008 and E-009, oil was produced by taking gas away from the casing and burning it on the flare. In this case, oil production was satisfactory, though a

large quantity of gas was burnt on the flare, leading to CO2 emissions contrary to the legal regulations, and also to reduced well profitability due to the loss of gas produced from the reservoir. Table 1 shows the basic properties of wells operating with a closed casing where gas is not burnt on the flare but directed to the production line.

Table 1 Characteristics of Wells with Closed Casing Valve

Well	Sucker rod pump	Pump depth (m)	Well Level (m)	Pump Speed (o/min)	Stroke duration (mm)	Daily fluid production Qf (m^3)	Daily gas production Sm^3/day
E-001	25-175-RHAM-13-4-1-0	1499	1502	5.6	1710	12.6	555
E-002	25-175-RHAM-16-4-0-0	1095	1098	4.7	2021	6.8	222
E-003	25-175-RHAM-13-4-1-0	1480	1483	4.7	1874	10.3	477
E-004	25-175-RHAM-13-4-1-0	1320	1325	4.6	1660	9.7	222
E-005	25-175-RHAM-13-4-1-0	1603	1605	6	1479	11.3	413

Table 2 shows properties of the wells where gas is directed to the flare where it is subsequently burnt.

Table 2 Characteristics of Wells with Open Casing Valve

Well	Sucker rod pump	Pump depth (m)	Well Level (m)	Pump Speed (o/min)	Stroke duration (mm)	Daily fluid production Qf (m^3)	Daily gas production Sm^3/day
E-006	25-175-RHAM-13-4-1-0	1300	1223	4.8	2105	14.1	158
E-007	25-175-RHAM-12-4-2-0	1402	1328	5.6	2188	12.2	588
E-008	25-175-RHAM-13-4-1-0	1439	1356	4.3	2167	9.9	797
E-009	25-175-RHAM-12-4-2-0	1461	1392	6	1882	10.7	1300

The tables lead to the conclusion that wells with a closed casing have a much lower dynamic level. This is a consequence of pressure buildup (approximately 1000 kPa) in

the annular space between the casing string and the tubing. Experiments showed that the pressure of 100 kPa reduces the dynamic level by 10 m. Due to the low dynamic level (at the pump level), these wells were determined to have an incomplete filling of the sucker rod pump cylinder as a reduced effective piston stroke length and thus reduced fluid production, as well. The gas produced becomes utilised and together with oil and formation water goes to the production line to the gathering station.

The wells with an open casing were found to have the level around 80m above the pump, the cylinder was full, the effective length of the piston stroke was at the maximum, and production was greater. In this case the problem is in burning of the gas and CO2 emission resulting from burning natural gas from the well.

The data provided in the table were obtained from the sensors installed at the wells. They are transferred to the user by SCADA system and may be visually monitored on the AVEVA platform.

To record the dynamic level in this study, stationary sonolog was used, which measures the level four times a day, with the option to adjust the system for a higher number of measurements. The solonog also has the option of measuring and sending data about the annular pressure. The sonolog MGT APDU-1 is produced by Magmatek, Figure 5.

Figure 5 Sonolog MGT APDU-1 – stationary level meter in the annular space of a well (Приборы контроля параметров скважин https://www.mgtcontrol.ru/catalog/pribory-kontrolia-parametrov-skvazin

Technical characteristics of the device:

1. Measured level range	20 ÷ 6000 m
2. Level resolution	≤1 m
3. Measured pressure range	0 ÷ 10000 kPa
4. Pressure resolution	10 kPa
5. Operating pressure range	80 ÷ 5000kPa
6. Continuous operating time under normal conditions, without battery recharging	≥ 4000 level measurements
7. Installed battery recharging time	≤3 h
8. Sensor communication channel	Bluetooth LE
9. Communication channel range	≥30 m
10. Method of establishing communication	NFC
11. Operating temperature range	-40 ÷ +50 °C
12. Service life	≥5 years
13. Product weight	≤6 kg

Owing to the cutting-edge technologies applied, it is capable of operating in a stationary manner, in a fully automatic mode, for a very long time. When performing level measurement, 1-2 measurements per day may be done for over a year in one charging. Operating together with the information collection and transfer block BSPs, it may be connected to different automation and telemechanical systems over the RS-485 interface and also transfer data through GSM and LoRa WAN channels.

Tasks that are performed:

- Control of the static and dynamic fluid level in producing oil wells in the automatic and manual mode
- Creation of level change curves
- Long-term control of level change during well commissioning
- Operational level control in transfer mode
- Operational data transfer via different connection channels and into telemechanical systems

Produced gas volume is measured by the separator at atmospheric conditions, and the volumes are presented according to Reference conditions: 101,325kPa and 15°C.
Table 3 presents gas composition for the well E-002. Given the fact that all other wells are also situated in the same reservoir, gas composition is almost identical

Table 3 Composition of the gas produced from E-002 well

No	Characteristic	Unit	Method	Value
1	C_1	mol %	SRPS EN ISO 6974-5:2014	66,411
2	C_2	mol %	SRPS EN ISO 6974-5:2014	5,890
3	C_3	mol %	SRPS EN ISO 6974-5:2014	6.027
4	i-C_4	mol %	SRPS EN ISO 6974-5:2014	1,375
5	n-C_4	mol %	SRPS EN ISO 6974-5:2014	3.788
6	i-C_5	mol %	SRPS EN ISO 6974-5:2014	1.201
7	n-C_5	mol %	SRPS EN ISO 6974-5:2014	1.891
8	C_{6+}	mol %	SRPS EN ISO 6974-5:2014	3.709
9	N_2	mol %	SRPS EN ISO 6974-5:2014	2,417
10	CO_2	mol %	SRPS EN ISO 6974-5:2014	7,291
11	Av. molecular weight	g/mol	SRPS EN ISO 6976:2017	27.40
12	Density relative to air	/	SRPS EN ISO 6976:2017	0.9512
13	Density	kg/m³	SRPS EN ISO 6976:2017	1.1656
14	Vobes index (bottom)	MJ/m³	SRPS EN ISO 6976:2017	48.98
15	Lower heating value	MJ/m³	SRPS EN ISO 6976:2017	47.77
16	H_2S	mg/ms³	SRPS H.F8.507:1992	0.23

As specified in the previous section, the point of compressor installation is determined based on individual pumping unit dimensions so as to make the compressor operation optimal for the calculated gas volume and to simultaneously avoid additional load on the pumping unit operation and also prevent piston breakdown due to a pumping unit stroke larger than the compressor piston stroke. Tables 4 present the required pumping unit dimensions for the calculation of the installation point according to the previously given formula (5):

$$C = \frac{Y * A}{2 * B} \tag{5}$$

Table 4. Dimensions of pumping unit components

Well	Beam	A (in)	B (in)	C (in)	A (mm)	B (mm)	C (mm)
E-001	A 70	70.5	25.5	49.5	1791	648	1258
E-002	API 7.8	70	30	42.6	1778	762	1082
E-003	API 7.8	70.5	25.5	49.5	1791	648	1258
E-004	API 7.8	71	22.5	56.8	1803	572	1442
E-005	API 7.8	71	26	49.2	1803	660	1248
E-006	API 7.8	71	26.5	48.2	1803	673	1225
E-007	API 7.8	70.5	30	42.3	1790	762	1074
E-008	UL 90	82	32	46.1	2082	813	1171
E-009	A 90	82.5	31.5	47.1	2095	800	1197

Compressor selection

According to the parameters described and the compressor designing method, an appropriate compressor was determined for each well, and the point of compressor installation was identified for each pumping unit. The result of this selection is in Table 5.

Table 5 Installed compressor characteristics and dimensions

Well	Beam	Y (in)	Y (mm)	Piston diameter (in)	Piston diameter (mm)	Compressor Type
E-001	A 70	48	1219.2	6	239.2	Single Active
E-002	API 7.8	36	914.4	6	239.2	Single Active
E-003	API 7.8	36	914.4	6	239.2	Single Active
E-004	API 7.8	36	914.4	6	239.2	Single Active
E-005	API 7.8	36	914.4	6	239.2	Double Active
E-006	API 7.8	36	914.4	6	239.2	Single Active
E-007	API 7.8	36	914.4	6	239.2	Double Active
E-008	UL 90	48	1219.2	6	239.2	Double Active

E-009	A 90	48	1219.2	6	239.2	Double Active

At all nine wells, compressors were installed according to the schematic given in Figure 6:

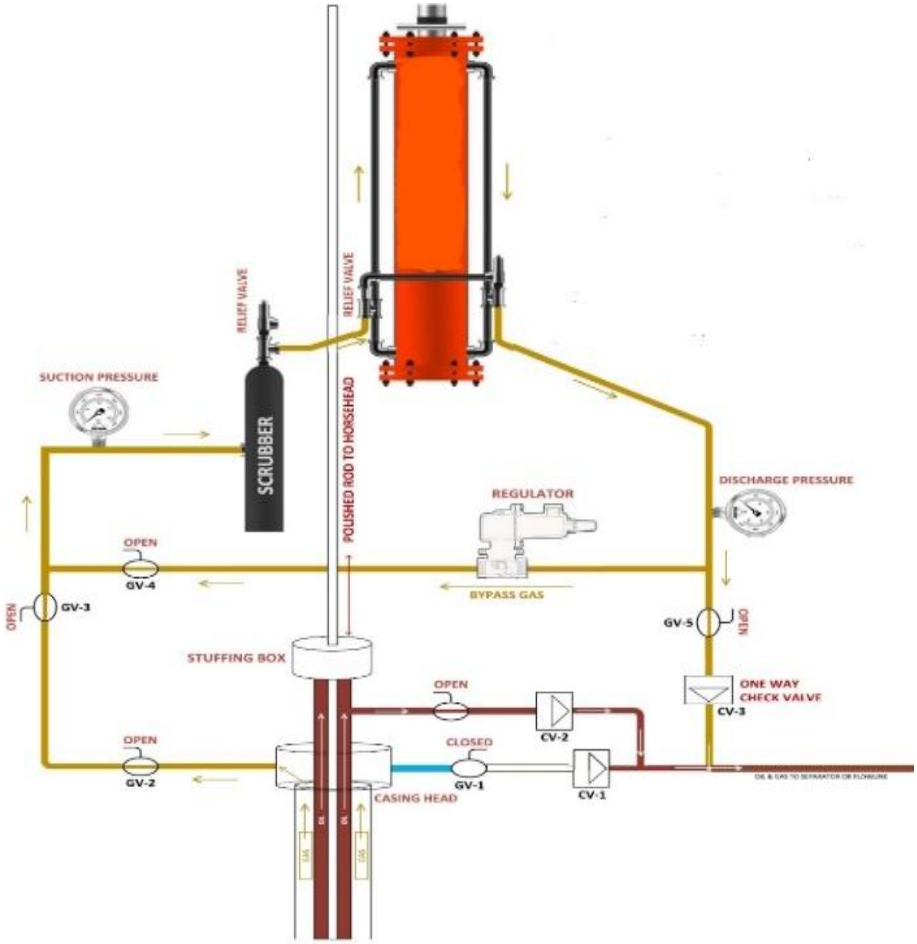

Figure 6 Schematic of the installed compressor with the supporting elements (https://www.creamco.ca/m3-casing-gas-compressor/technical-info/#tab-id-2)

Fluid production increase and CO_2 emission reduction

Gas extraction at five wells (E-001, E-002, E-003, E-004 and E-005) was resolved by a closed casing and by directing gas to the production line, thus preventing its emission into the atmosphere. However, in these wells, a pressure rise in the casing resulted in a fluid level drop in the well to the pump level, which led to reduced oil production. Compressor installation resulted in annular pressure reduction down to the target 170

kPa and fluid level increase in the well by about 80 m above the pump, which led to the increase in the effective length of the piston stroke, cylinder filling and fluid production. Table 6 shows the dynamic level and fluid production before and after compressor installation at wells E-001, E-002, E-003, E-004 and E-005.

Table 6. Dynamic level and fluid production before and after compressor installation at wells

Well	Pump depth (m)	Well Level (m) Before BGC	Well Level (m) After BGC	Pressure (kPa) Before BGC	Pressure (kPa) After BGC	Daily fluid product. Qf (m³) Before BGC	Daily fluid product. Qf (m3) After BGC	Product. increase Qf (m³)	Product increase Qf (%)
E-001	1499	1502	1417	1001	160	12.6	18.3	5.7	45%
E-002	1095	1098	1013	980	170	6.8	12.7	5.9	87%
E-003	1480	1483	1398	960	190	10.3	14.9	4.6	45%
E-004	1320	1325	1240	1050	150	9.7	13.5	3.8	39%
E-005	1603	1605	1520	1100	170	11.3	15.9	4.6	41%

Figure 7 shows fluid production increase after compressor installation at the well E-002. It can be seen that the compressor was installed on 24 December 2025. After the pumping unit was commissioned and the annular pressure reduced from p=980 kPa to p=170 kPa, fluid production rose from Qf=6,8 m³ to Qf=12,7 m³. The level in the well rose by 80 m which was enough for the pump to operate with the maximum cylinder filling.

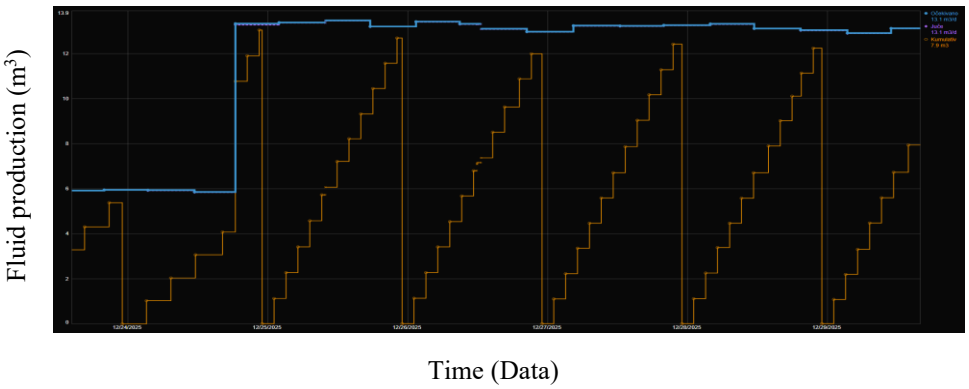

Figure 7 Fluid production increase after compressor installation

For production calculation purposes, the dynamometer cards recorded before and after compressor installation were used. Figure 8 shows the effective pump piston stoke length to be 630 mm. The dynamometer card was recorded on 24 December 2025 before compressor installation, while Figure 9 shows the effective pump piston stroke length to

be 1500 mm. This dynamometer card was recorded after compressor installation on 25 December 2025. It also shows complete pump cylinder filling. Furthermore, the maximum and minimum load in the diagrams indicate that compressor installation did not put any additional load on the oil production system using sucker rod pumps.

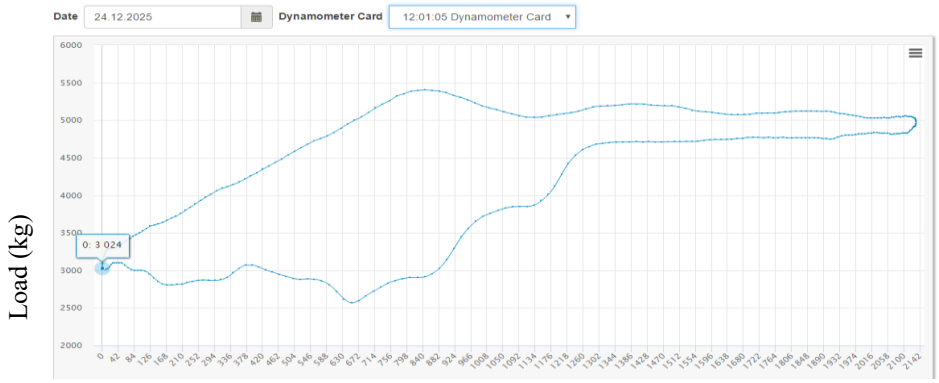

Figure 8 Dynamometer card recorder before compressor installation

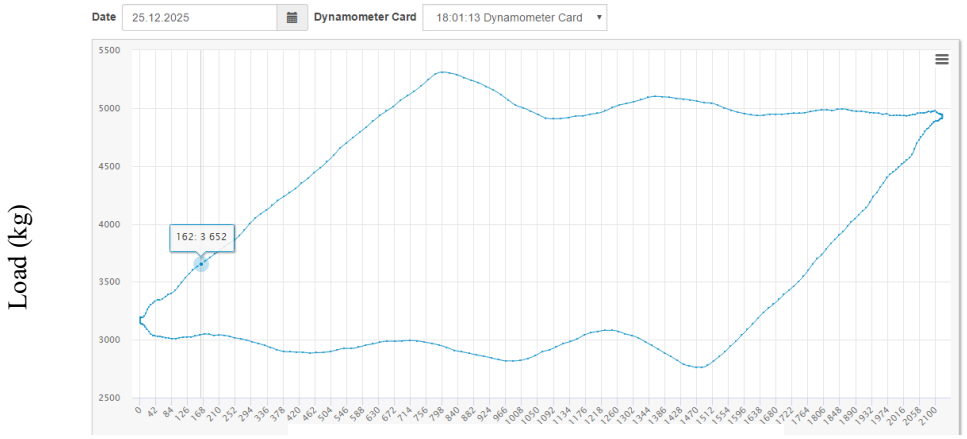

Figure 9 Dynamometer card recorder after compressor installation

4.1 CO_2 emission reduction

At wells E-006, E-007, E-008 and E-009, oil was produced by taking gas away from the casing and burning it on the flare. In this case, oil production was satisfactory, though a large quantity of gas was burned on the flare, leading to CO_2 emissions contrary to the legal regulations, and also to reduced well profitability due to the loss of gas produced from the reservoir. In these wells, due to the pressure of 100 kPa in the annular space,

there was no fluid inflow from the reservoir into the wellbore, and the problem was resolved by opening the casing valve and taking the gas away to the flare where it was burnt.

Compressor installation and annular pressure reduction enabled the gas to be transported to the production line and used further. The preserved gas volumes as profit are shown in Table 2 and they represent evident revenues of oil production from the well after compressor installation. Table 7 shows the quantity of released CO_2 when gas is burnt on the flare.

Table 7 Quantity of released CO_2 when gas is burnt on the flare

Well	Daily gas production Sm^3/day	Daily CO2 Production (kg)	Daily CO2 Production (t)
E-006	158	300.2	0.30
E-007	588	1117.2	1.11
E-008	797	1514.3	1.51
E-009	1300	2470.0	2.47

CO_2 emissions from gas flaring were calculated using the standard emission factor for natural gas combustion recommended by the IPCC Guidelines for National Greenhouse Gas Inventories and adopted by the Energy Agency of the Republic of Serbia (AERS).

This value corresponds to complete combustion of natural gas with an average composition consistent with the measured gas composition presented in Table 3.

Sample calculation (Well E-006):

$CO_2 = 158\ Sm^3 * 1.9 = 300.2$ kg/day

Where: 1,9 - Standard emission factor for natural gas combustion

The same calculation procedure was applied to all wells listed in Table 7.

AERS (2025) Energy Agency of the Republic of Serbia - Website, Available online https://www.aers.rs,

Accessed on [20 September 2025] IPCC (2025) The Intergovernmental Panel on Climate Change
https://www.ipccnggip.iges.or.jp/public/2006gl/pdf/2_Volume2/V2_2_Ch2_Stationary_Combustion.pdf , Accessed on 20 September 2025

4.2 Limitations and future works

There are several limitations to the design of upgrading conventional pumping units with BGC compressors.

- Level measurement in wells – A stationary sonolog which measures the level in a well operates optimally at an annular pressure of 80-5000 kPa. Although it was stressed that the annular pressure was 170 kPa, it actually varies during compressor operation and frequently reduces below 80 kPa which is inadequate for measuring the actual fluid level in a well. Since errors occur in measurements, an operator must be engaged to control the validity of the data transferred by the sonolog on a daily basis, which entails operator engagement for the purposes of control recording and increases costs, reducing the economic effect of the designed system.

- The produced gas composition is presented in Table 3 where the presence of higher fractions may be noticed which, under normal conditions, would be in a liquid state. In the compressor design, it was necessary to use a scrubber which collects liquid fraction to prevent its entry into the compressor and thus avoid problems in its operation. Given that the scrubber capacity for liquid phase collection is limited, the operator is required to visit the well on a daily basis to empty the scrubber. Scrubber design within the compressor system increases costs, as does operator engagement to empty the scrubber. All of the above reduces the system design efficiency.

Future research should include condition changing to ensure high-quality operation of the sonolog with regard to annular pressure variation, as well as valve opening automation without operator engagement

5 CONCLUSION

This paper studies upgrade of a conventional pumping unit with a compressor for pressure reduction in the casing, aimed at increasing oil and gas production and reducing CO_2 emissions. The analysis of the existing oil production systems showed that gas backpressure problems occur over time, significantly affecting production efficiency. In that context, compressor designing represents a key step towards optimisation of the existing systems.

Compressor designing requires careful analysis of several factors, including pumping unit type, dimensions, the volume of gas sent to the production line, as well as operating conditions under which the compressor is to work. This study used accurate formulas to calculate the compressor piston area and suction pressure, which enabled the optimal compressor size and type to be determined for each individual well. The data obtained

helped select the compressors which proved to be the most efficient for each individual well, taking into account specific characteristics and requirements.

Compressor installation enabled annular pressure reduction, which led to an increase in the fluid level in the wells. This change resulted in an increased effective piston stroke length and, consequently, increased fluid production. In cases when gas is directed towards a production line, instead of being burnt on the flare, significant CO_2 emission reduction is achieved, which corresponds with environmental standards and regulations.

Furthermore, it should be noted that compressor designing within the existing system upgrade required integration of modern technologies, such as automatic fluid level and pressure measurement sensors, which ensure continuous monitoring and work optimisation. The sensors, together with the SCADA system, enable operators to carry out real-time monitoring of system performances and to urgently respond to any possible problems.

Future research is recommended to be focused on improving the automation system, and also developing new technologies which would enable even more efficient pressure and fluid level control. Additionally, it is important to study options for reducing maintenance and operating costs in order to ensure sustainability and profitability of the upgraded systems.

In summary, an upgrade of the existing systems with a pressure reducing compressor represents an important step towards oil and gas production increase, simultaneously reducing adverse environmental effects. This approach may become standard in the industry, helping achieve a more sustainable development and a more efficient use of natural resources

REFERENCES

ALIEV, T., RZAYEV, A., GULUYEV, G., ALIZADA, T., & RZAYEVA, N. (2018). Robust technology and system for management of sucker rod pumping units in oil wells. Mechanical Systems and Signal Processing, 99, 47–56.

AL-KHATIB, A. M. (1984). Improving oil and gas production with the beam-mounted gas compressor. Journal of Petroleum Technology, 36(02), 276–280.

BODE, C. (2019). Measurement and Hardware Simulation on Torque, Speed & Load of a Prime Mover for optimization of a Sucker Rod Pumping System.

CAMARGO, E., AGUILAR, J., RÍOS, A., RIVAS, F., & AGUILAR-MARTIN, J. (2008). Production improving in gas lift wells using nodal analysis. Signal Processing, Robotics and Automation, 99–102.

CHEN, L., GAO, X., & LI, X. (2021). Using the motor power and XGBoost to diagnose working states of a sucker rod pump. Journal of Petroleum Science and Engineering, 199, 108329.

ENGL, N. (2009). Ascertainment of potential increase in production of RAG oil wells due to casing pressure drop.

ESCOBAR-REMOLINA, J., BARRIOS-ORTIZ, W., FRANCO-SANDOVAL, L., SACHICA-AVILA, J., MCCOY, C., & RIOS-RECUERO, R. (2015). Reduced Emissions and Increased Production Through gas Compressors: Pilot Case in Colombia. SPE-173601.

GAO, L., LIU, Y., LUO, C., LI, S., & PENG, Z. (2025). Wellbore Flow Behavior and Natural Flow Cessation Prediction in Ultra-Deep Wells: A Case Study of Shunbei Oilfield. Energy Science & Engineering, 13(11), 5385–5400.

JANKOV, S. M., STANISAVLJEV, S. M., NOVAKOVIĆ, B. Z., & ĐORĐEVIĆ, L. R. (2025). Visualization of operation parameters and remote management of oil production through the implementation of SCADA system. Tehnika, 80(5), 501–506.

JANKOV, S., NOVAKOVIĆ, B., IVANOV, G., & ĐORĐEVIĆ, L. (2025). Optimization of oil production using reciprocating pumps through corrective adjustment of operating parameters. Mining and Metallurgy Engineering Bor, 2, 21–34.

KIS, L. (2021). Torque Optimization of Sucker-Rod Pumping Units.

SANDLER, J., FOWLER, G., CHENG, K., & KOVSCEK, A. (2012). Solar-generated steam for oil recovery: Reservoir simulation, economic analysis, and life cycle assessment. SPE-153806.

Cream energy group https://www.creamco.ca/m3-casing-gas-compressor/technical-info/#tab-id-2

Приборы контроля параметров скважин https://www.mgtcontrol.ru/catalog/pribory-kontrolia-parametrov-skvazin

AERS (2025) Energy Agency of the Republic of Serbia - Website, Available online https://www.aers.rs, Accessed on [20.09.2025.] IPCC (2025) The Intergovernmental Panel on Climate Change - https://www.ipccnggip.iges.or.jp/public/2006gl/pdf/2_Volume2/V2_2_Ch2_Stationary_Combustion.pdf , Accessed on 20.09.2025.

UNDERGROUND MINING ENGINEERING 48(2026) 39-51 UDK 62
UNIVERSITY OF BELGRADE - FACULTY OF MINING AND GEOLOGY ISSN 03542904

Original Scientific paper

SPECIFICITIES OF GEOLOGICAL SAMPLING METHODS IN ALLUVIAL DEPOSITS

Vladan Kašić[1], Slavica Mihajlović[1], Nataša Đorđević[2], Srđan Matijašević[1], Ana Radosavljević-Mihajlović[1]

Received: April 24, 2026 **Accepted:**May 27, 2026

Abstract: Sampling alluvial deposits is important in geological exploration, providing data for understanding sediment composition, stratigraphy, and resource potential. The study including testing alluvial wells, conducting examinations during shallow shaft mining operations, and assessing deposits through floating dredgers. Across all methods, the key requirement is proper sampling and ensuring a sufficient quantity of material. Analyses of the collected samples, supported by calculations, reveal both the concentration of valuable minerals within the deposit and the spatial consistency of their distribution. In drilling testing methods, it is essential to precisely measure the volume of the drilled rock column and to determine the concentration of the useful component in the material recovered through washing. During mining operations, the sample comprises all material removed while deepening the shaft by 0.5 or 1.0 m. Sampling of floating dredger is conducted during exploitation measurements as the dredger advances along the transverse profile from one end of the deposit to the other. The horizontal spacing between sampling points is typically 5 m. Samples are taken first at the greatest digging depth and then at every meter of sediment. Due to their mobility and precision, floating excavators are particularly suited for operations in remote or inaccessible regions.

Keywords: testing, alluvial deposits, boreholes, mining operations, floating dredger orts

1 INTRODUCTION

Geological exploration worldwide has involved continuous improvements to existing methods, the development of new testing approaches, and the introduction of sustainable

[1] Institute for Technology of Nuclear and Other Mineral Raw Materials, Franchet d`Esperey 86, Belgrade, Serbia

[2] Institute of General and Physical Chemistry, 12 Studentski Trg, 11000 Belgrade, Serbia

E-mails: v.kasic@itnms.ac.rs, ORCID: https://orcid.org/0000-0002-4430-567X; s.mihajlovic@itnms.ac.rs, ORCID: https://orcid.org/0000-0003-0904-3878; natasa.djordjevic@iofh.bg.ac.rs, ORCID: https://orcid.org/0000-0002-2353-6751; s.matijasevic@itnms.ac.rs, ORCID: https://orcid.org/0000-0002-3897-8085; a.radosavljevic@itnms.ac.rs, ORCID: https://orcid.org/0000-0002-9194-161X

technologies that enhance efficiency. Achievements in the field of geological sciences have contributed to the creation of scientifically grounded methods for investigating mineral resources, including those derived from alluvial deposits. In circumstances where useful minerals are present, it is essential to develop new methodological approaches both for the assessment of mineral reserves and for determining the content of valuable components. This enables a clear understanding of the prerequisites directly linked to decisions on initiating exploitation. Indeed, no mining activity can commence without prior quantitative mapping of the mineral content within the deposit. At the same time, evaluations of the quality of primary and associated minerals are conducted. Such practices contribute to the rational use of natural resources and the protection of areas within potential exploitation zones. Altogether, these considerations highlight the importance of geological activities in generating data that define the spatial regularity of mineral occurrence within the Earth's crust and the requirements of mining procedures, thereby ensuring rational resource utilization and the economic viability of deposit development (Malanchuk et al., 2024; Zuo, 2020; Zeng et al., 2020; Rysbekov et al., 2020).

A mandatory and inherent activity before the exploitation of alluvial deposits is the sampling of unconsolidated material, most commonly sand, gravel, clay, or other alluvial sediments. Following this, the content of valuable minerals (e.g., gold, platinum) is determined to assess the economic feasibility of opening the deposit. Since these are alluvial deposits, the processes of sampling and investigation differ from those applied to solid rock formations. It is particularly important to emphasize the necessity of collecting large quantities of material, as useful components occur in fine grains that are typically present throughout the deposit (Dominy, 2014; Balaram and Subramanyam, 2022). This so-called 'volumetric testing' is a prerequisite for subsequent stages, namely the exploitation of the alluvial deposit. Washing the samples with water follows, intending to separate heavy minerals from lighter sand and silt. The content of the valuable element is presented in grams or milligrams per cubic meter of material (mg/m^3 or g/m^3). The results obtained serve as indicators of the profitability of exploiting a given metal from the alluvium (Mathioudakis et al., 2023a; Mathioudakis et al., 2023b; Bettenay and Ross, 2026; Vakanjac, 1992).

2 BOREHOLE SAMPLING IN ALLUVIAL DEPOSITS

Proper sampling of alluvial sediments and the results of preliminary analyses of collected samples significantly impact decisions on the exploitation of valuable components and their profitability. Depending on when and how the alluvial deposits were formed, they differ in grain size, composition, layer thickness, orientation, and other characteristics. Accordingly, different sampling and testing techniques have been applied over time, which have become increasingly advanced (Ghorbani et al., 2023; Awal et al., 2019; Khomsin et al., 2021).

For the exploration of alluvial deposits containing precious and rare metals at shallow depths (up to 20 m), sets for manual impact rotary drilling are most commonly used. However, for deposits at depths of 20 to 50 m and beyond, mechanical rope driven impact drilling equipment is applied. In the method of testing (sampling) alluvial deposits by drilling, the most important aspect is the precise measurement of the volume of the drilled rock column. Equally important is the determination of the content of the valuable component in the material obtained by washing the drilled rock, expressed in units of mass (kg, g, mg) per cubic meter of rock (sand) (Karpov and Petreev, 2021; Oparin et al., 2022).

The accuracy of determining the initial volume of the extracted rock (sand) during drilling is influenced by several factors:

1. Rock disintegration: As the borehole penetrates the formation, the rocks pass into a loose state, which affects the increase in their volume. The degree of disintegration varies depending on the composition and physical condition of the rocks.

2. Loss in suspension: A portion of the rock extracted with a scoop (including flap scoops) is lost in the water suspension, with the percentage of loss depending on the amount of clay particles.

3. Displacement by chisel drilling: During chisel drilling, part of the rock is displaced outside the cased space, reducing the initial volume of rock that enters the casing column.

4. Hydrogeological conditions: In formations with higher water content (lower permeability), high groundwater levels, and insufficiently vigorous forcing of the casing column, significant inflow of rock into the casing may occur, along with the washing out of clay particles beneath the shoe of the casing column.

To ensure the most accurate sampling results during drilling, the shoe of the casing column must remain ahead of the drilling tool at all times. This is achieved through continuous or frequent forcing of the casing column.

During the normal course of drilling and testing, tools such as scoops or flap scoops are used to extract a column of sand from the casing. When rocks are loosened with a chisel and during the use of scoops, gold and other heavy minerals tend to sink into the lower parts of the borehole. To reduce the amount of gold that 'settles' during drilling of a gold bearing layer, 1–2 liters of clay solution are added at each casing stage. The addition of clay must be taken into account and included as a correction factor when determining the volume.

Samples are collected at regular drilling intervals, most often every 0.5 m. When drilling overburden rocks that are known to represent barren material, only control point samples are taken after each meter. The bedrock of the deposit (from bed + rock), usually composed of alluvial parent rocks, is also sampled, as it often contains significant

amounts of metals. When the bedrock is soft, the core must be carefully examined to determine whether it represents a weathered crust or alluvium. Occasionally, clayey rich 'false' bedrock may cover sand layers rich in metal.

During manual drilling of boreholes with diameters of 117 and 165 mm, accurate recording of the initial volume for samples is achieved by measuring the depth of the borehole before and after using the scoop. The difference in depth provides the actual height of the extracted rock column. In certain cases, the actual volume of rock extracted from the borehole is determined using a specific construction: a vertical pipe of defined height and diameter (the diameter must be such that the area of the inner circular cross-section equals 100 cm²). The pipe is fixed to a wooden tripod with an inclined steel chute. The sand sample from the scoop is poured into the chute, flows into the pipe, is compacted, and then measured. The height of the rock column in the pipe is multiplied by 100 to obtain the volume in cm³. For measuring the actual volume of rocks extracted during mechanical impact drilling with casing columns of 165 and 210 mm, a horizontal trough with a measuring box is used. The box has a precisely defined cross-section and height, and is graduated along its height. Material from the scoop is poured into the measuring box, and the height of the deposited material is read. Based on the known cross-section of the box and the measured height, the volume of the deposited material is determined.

When investigating gold bearing alluvial deposits by drilling, graphite grease is used for lubricating the threads of drilling (cased) pipes and rods. Standard greases are avoided because they penetrate the sand and cause 'gold flotation' during the washing process. In such cases, instead of remaining at the bottom, gold floats to the surface, resulting in the loss of a certain amount of this precious metal (Sillitoe and Hedenquist, 2010; Hedenquist, 2000; Robert et al., 2007; Kašić, 1995). The material obtained from washing the sample is dried, measured, and labeled according to the sampling location. The content of the valuable mineral in the alluvium (S), expressed in kilograms, grams, or milligrams per cubic meter of rock or sand, is calculated according to Formula 1:

$$S = \frac{M}{Z} \tag{1}$$

where: M-mass of the obtained mineral sample, (g); Z-volume of the sample, (m³).

It should be emphasized that there are two methods for calculating the content of valuable minerals in alluvial deposits: 1. Based on the theoretical volume of the sample and 2. Based on the actual volume of the sample.

In the calculation method based on theoretical volume, it is assumed that the entire rock mass pressed by the shoe of the casing column enters the column and is extracted by the drilling tool. Therefore, the rock volume is taken as the volume of a cylinder, expressed according to the following formula:

$$Z = \frac{\pi \cdot p^2}{4} \cdot d \tag{2}$$

Where: *d*-length of the coated column, (m); *P*-external diameter of the shoe of the coated columns, (mm).

In this case, the formula for determining the content of useful minerals takes the following form:

$$S = \frac{M}{Z} \cdot 1000000 = \frac{M}{d} \cdot \frac{4 \cdot 1000000}{\pi \cdot P^2} = \frac{M}{d} = k \tag{3}$$

Where:

1000000-multiplier for the transition from the cross-section expressed in mm² to m²;

k-constant coefficient.

However, the volume of rock that in practice reaches the lining columns of a smaller diameter can be significantly different from the theoretical volume. Therefore, the theoretical method can only be applied to boreholes that are drilled with large diameter drills (eg Nevjan drill with a diameter of 530 mm).

When drilling with smaller diameters of 117 and 165 mm, the volume of the samples is determined according to the inner diameter of the pipe and the difference in the height of the column before and after filling the drill. The loosening of rock pillars in the cladding columns is not considered. The metal or valuable mineral content is calculated according to the formula:

$$S = \frac{M \cdot 4 \cdot 1000000}{\pi \cdot P^2 \cdot V} \tag{4}$$

Where: *V*-height of the column that is pulled out (difference in height before and after working with the pusher), (m).

At P-93 mm, the constant coefficient is:

$$k = \frac{4 \cdot 1000000}{\pi \cdot 93^2} \tag{5}$$

For percussive drilling with a rope of 165 and 210 mm diameter (whereas the inner diameters of the working casing columns are 145 and 195 mm) the value of the coefficient k is 65 and 33, respectively. All calculations are performed using special tables. Calculations must be absolutely accurate. Otherwise, the values of the content of the useful component in the sediment, which were obtained by calculation, can be significantly higher than the actual content. Potential errors can occur if the recovered

gold from the well is spread over a deposit volume corresponding to the inside diameter of the casing columns (mill shoes) instead of, as is correct, to the outside diameter. Likewise, an increase in the content and reserves of gold in the deposit can occur due to improper drilling technology, when the drilling equipment is ahead of the casing column cutter. In this case, material may seep into the well from the side (so-called "excess" material). Also, to the enrichment of the lower parts of the layer with gold due to the loose walls of the well that are not covered with a casing column and through which the gold falls on the bedrock itself. In that case, the bedrock shows a high gold content, which is not confirmed later during mining.

When coarse gold is encountered in a sample, the question arises regarding the threshold mass of nuggets to be included in reserve calculations. For each large alluvial deposit, or for a group of deposits of the same type, the threshold mass of nuggets is determined based on experimental data. Therefore, all metal obtained from the borehole is measured and subjected to sieve analysis. Based on the results, the class is identified from which the total mass of metal increases only slightly; the number of gold grains in that class is determined, as well as the average mass of a single grain in milligrams. This value is taken as the threshold mass for gold of normal grain size. The difference between the mass of nuggets and the mass of gold grains substituted for them in the calculation is accounted for in the estimation of total gold reserves in the alluvial deposit by introducing a correction coefficient, the value of which is always greater than one (Dominy and Annels, 2001a; Dominy and Hunt, 2001b; Dominy et al., 2006; Dominy, Xie and Platten, 2008).

3 TESTING DURING MINING WORKS

Sampling of materials and formation of samples during mining operations in shallow shafts is very specific. A sample is taken from the entire excavated alluvial material whose mass corresponds to a layer of material with a vertical thickness of 0.5 or 1.0 m. That is, practically, all the material taken when deepening the shaft by 0.5 or 1.0 m. Sample washing is carried out immediately, or at the latest 3-5 days after the sample is formed. If the sample remains for a longer time, it may lose its representativeness, especially if it is washed away by atmospheric precipitation or due to the rise of the water level in the riverbed.

The washing of the sand sample is carried out in a washing basin which is placed in the water approximately at the center of the investigation plot. The washing basin is a rectangular groove or structure, 2.5–3.0 m long and 0.7 m wide, made of thick boards and set at a slight slope (7–15°). The upper part consists of a square wooden box fitted with a horizontal grid with openings of 6–7 mm. To retain sand and water, a wooden frame made of four planks inclined toward the grid is placed above it. The inclined bottom of the washer serves as the working surface (“canvas”) on which the sand is washed. Sand for rinsing is manually placed on the grid and mixed while receiving a jet

of water from either a pump or gravity flow. The washed gravel fragments are removed from the grid and deposited in a designated area, while sand and clay pass through the grid openings and are carried away by the water along the wash surface. To capture schlich (German: "schlich" - a concentrate of heavy metals obtained by washing rock material) and gold particles, the work surface of the washer is covered with a material that retains schlich. It can be cloth (fabric made from wool or coarse cloth made from goat or camel hair). The material is attached with transversely placed wooden slats 1-2 cm thick. Under the washboard, in the part where the tailings are separated, a box is placed to control the separation of the sludge. Productivity of the washing machine when washing sand, in average conditions, is 1.5 to 4.0 m3 during a shift that lasts 8 hours.

After rinsing the sample, the so-called "crying out" is performed. With a small amount of water, the movable frame, the cloth, the surface of the washing machine and the entire slide, which is lowered into the bucket or the sample placed under the lower end of the washing machine are carefully washed (rinsed). A pan is a traditional wooden or metal pan used to separate gold from river sediment. In a bucket or a sample (with the addition of mercury in the presence of fine gold), the metal is separated from the slag. After drying, the cuttings are sampled (weight 50-100 g), packed and submitted for mineralogical analysis. The amalgam is heated to release the mercury. The obtained gold is measured and stored in a special cardboard box (capsule). Gold content in sand in g/m3 is determined by dividing the mass of washed metal in g by the volume of the sample in m3 (Boukari et al., 2025; Mathioudakis et al., 2023a).

The content of minerals in the sands is determined as follows: after drying, the slag from the washboard is measured, and its content in the sediment is determined, expressed as kg/m3 of washed sands. The magnetic fraction (magnetite) is separated from the slag with the help of a magnet, while pieces larger than 2 mm are separated by hand. All the separated classes are measured individually. The class smaller than 2 mm, is scattered on the glass, on the underside of which a white paper with a centimeter grid has been glued. A typical test strip, 10-12 cm long, is separated from the schist, preferably "one grain" in width, and the interesting mineral is separated with a needle. It is preferable to use a binocular magnifier. The ratio of the length of the parallel strip of the same mineral to the total length of the initial strip gives the approximate content of the useful mineral in percentage by volume. By introducing the specific mass into the calculation, volume percentages are converted into mass. The total mass of pure useful mineral in all grades, divided by the volume of the sample, gives its content in sands. During the exploitation of alluvium by underground mining works, excavation testing is of decisive importance, since the entire work in the pit depends on the results of the testing. Based on the test results, excavation work is interrupted or extended, and the thickness of the layer with the balance ore and the height of the excavation are determined. Bad or improperly organized testing entails improper exploitation of sediments, with all the consequences that result (Skrzypkowski et al., 2022; Lu et al., 2024).

Sampling in the metal-bearing layer should be done with a wide vertical channel, in the direction from the floor to the roof of the section. The channel sample is divided according to the height of the channel into three or four parts to take sectional samples. The first sample is taken covering 0.2 m of the substrate, while larger fragments of primary rocks are discarded. The sample material is poured into the trough to measure its exact volume. The troughs are made of boards or sheet metal, the volume is 25500 cm3, which corresponds to the volume of 0.02 m3 of massif sediment (compact rock). Before filling the trough, a badge with a number is placed on the bottom, which is recorded in the geologist's field log. The vertical channel above the first sample is divided into three unequal parts for taking sectional samples. The bottom sample is taken starting from the deposit base up to a height of 0.4-0.5 m. The middle sample covers the middle of the column with a section length of 1.2-1.4 m. The last upper sample with a length of 0.3-0.4 m reflects the metal content in the upper part of the column next to the roof itself. Dividing the sampling column by height into unequal parts excludes the possibility of enriching the upper and lower samples at the expense of the richer middle sample. In the case of the presence of pebbles, their primary content on the surface of the ort is determined macroscopically and based on the geological sketch of the column. Troughs filled with samples are sent for washing, usually on a smaller washboard. The metal content of the sample (g/m3) is calculated by multiplying the mass of the mineral by 50, because the bed volume represents 1/50th of a cubic meter. The average metal content on the ort is calculated as a weighted average value proportional to the length of the channel of individual samples. The metal content in the substrate (base, bedrock) is not taken into account during the calculation, because during normal exploitation, there must be no metal in the substrate test. Coarse grains of gold are a common occurrence in the underground mining of many deposits, which is why they are taken into account when calculating the average metal content of the ore, as well as the average content for the entire deposit.

4 SAMPLING OF FLOATING DREDGE

Proper testing of floating dredges has great practical importance. Based on testing, the average content of useful metal (minerals) in a cubic meter of excavated rock is determined, the contours of the excavation polygon (the balanced part of the deposit) are determined, and the purity of the bedrock or deposit base is controlled. The contour of the dredging polygon is drawn on the measurement plan based on the graphical interpolation of the marginal (minimum economic) metal content determined by testing shallow wells or wells. However, there are cases when the actual contour of the balanced part of the deposit was wider than the design contour determined based on the exploration. Namely, when determining the limit of dredging, one should be guided not only by the project polygon, but also by the results of testing in the process of working of the excavator. Sampling the dredging soil vertically can show the following: the existence of clay layers in deposits with increased metal content above them (the so-

called "false bedrock"), and confirm the complete capture of the bedrock during dredging. The testing of soil in the column of sediment on floating dredgers in operation has the following characteristics:

a) excavating section and sediment beds are underwater and are not available for direct observation;

b) samples should be taken from the dredger buckets that are moving during the operation of the floating dredger;

c) Quick regulation of the sampling site is necessary due to the constant movement of the excavator along the excavation section.

The simplest method of testing the soil during dredging is a test sample. The washer takes the sample from the buckets moving in the trough and, knowing its volume, washes it on the deck of the floating dredge. Such testing is not complex, but it does not reflect the quantitative distribution of the metal content on the ore and does not provide the exact coordinates of the sampling site for its application on the test plan. In order to ensure more accurate mapping of the sample locations on the sample plan, in the field, and on the plan, a square grid with sides of 5m2 and at the appropriate scale on the plan is set up. According to this grid, the exact position of the field in the plan at the time of sampling is determined. The vertical position of the sample taken on the transverse profile of the sediment is determined based on the angle of inclination, that is, the depth of the bucket carrier. The sample is washed on a special washboard placed on a floating dredge.

The testing is done on the day of measurement of exploitation works for a ten days or for a month, when the excavator moves along the cross-section, from one end of the deposit to the other. The distance between the tests in the plan, according to the horizontal line, is normally 5 m. Sampling should start from the greatest depth of digging. Then, when the frame is gradually raised, one sample is taken from each meter of deposit thickness. Special attention should be paid to testing the boundaries of the excavation site. Along the lines of the measurement survey and along the borders of the polygons, mean arithmetic contents are applied, calculated from a series of individual samples in each vertical section. During dredging, the method of mass sediment testing is also applied, where the volume obtained between two washes is measured. The entire mass of metal obtained by washing that amount of sand is divided by that value. The intermediate contents obtained in this way are applied to the plan of the excavation site. The application of the presented testing methods on floating dredgers enables the reduction of losses of useful metal (minerals) as well as the constant control of floating dredger operations. Also, these systems incorporate advanced technology for extracting gold particles with minimal environmental concerns. The mobility and precise operation of floating dredgers enable their application in remote and hard-to-reach places (Roshchupkin, 1975; Delgado, 2023).

5 CONCLUSION

In order to obtain representative samples, proper sampling and testing of alluvial deposits requires special techniques and compliance with rules during the execution of all geological activities. When choosing a sampling technique, it is necessary to take into account the heterogeneity of the sampling material and large variations in the size of the useful mineral particles. One of the applied methods is the testing of vertical boreholes, which provides a large volume sample from all layers of deposits. For drilling at shallower depths (up to 20 m), manual percussive-rotary drilling rigs are used, while for greater depths (20 to 50 m and more), mechanical rigs with percussive drilling with rope are used. In this method, the most important thing is the accurate measurement of the volume of the column of rock being drilled and the determination of the content of the useful component in the material obtained by washing the drilled rock, expressed in mass units (kg, g, mg) per 1 m3 of rock (sand). When performing mining works in shallow shafts, sampling of materials and formation of samples is very specific. From the entire excavated alluvial material, a sample is taken whose mass corresponds to a layer of material with a vertical thickness of 0.5 or 1.0 m. This is all the material taken when deepening the shaft by 0.5 or 1.0 m. Sample washing is carried out immediately, or at the latest 3-5 days after the sample is formed. Floating dredges are widely used due to their many advantages, which provide practical and sustainable solutions for sediment management, resource exploitation, and environmental protection. The mobility and precise operation of floating excavators enable their use in remote and hard-to-reach places. The testing is done on the day of measurement recording of exploitation works for a decade or for a month, when moving the excavator along the cross profile, from one end of the deposit to the other. The distance between the tests in the plan, according to the horizontal line, is normally 5 m. Sampling should start from the greatest depth of digging. Then, when the frame is gradually raised, one sample is taken from each meter of deposit thickness. Special attention should be paid to testing the limits of the excavation site

Acknowledgment: The authors would like to thank the Ministry of Science, Technological Development and Innovation of the Republic of Serbia for financial support for research (contract 451-03-33/2026-03/200023).

REFERENCES

AWAL, R., SAPKOTA, P., CHITRAKAR, S., THAPA, B.S., NEOPANE H.P. and THAPA,B. (2019) A General Review on Methods of Sediment Sampling and Mineral Content Analysis. Journal of Physics: Conference Series, 1266 012005. doi: 10.1088/1742-6596/1266/1/012005

BALARAM, V. and SUBRAMANYAM, K.S.V. (2022) Sample preparation for geochemical analysis: Strategies and significance. Advances in Sample Preparation, 1, 100010. https://doi.org/10.1016/j.sampre.2022.100010

BETTENAY, L.and ROSS, J. (2026) Alluvial gold' in Bronze Age Egypt and Nubia: from placers or clasts, and why it matters. Journal of Archaeological Science: Reports, 69, 105485. https://doi.org/10.1016/j.jasrep.2025.105485

BOUKARI, H., LEROY, L., NGUEYEP, M., SINI, A., NGUEYAP, S.A.A., TEMGOUA, J., DALABRA, M. and BOBDA, C.F. (2025) Optimizing panning operating parameters for alluvial gold processing: The case of the Wakaso panning plant. Engineering Reports, 7(11), e70496. https://doi.org/10.1002/eng2.70496

DOMINY, S.C. and ANNELS, A.E. (2001a) Evaluation of gold deposits - Part 1: Review of mineral resource estimation methodology applied to fault- and fracture-related systems. Applied Earth Science IMM Transactions section B, 110(3), pp. 145-166. doi: 10.1179/aes.2001.110.3.145

DOMINY, S.C. and HUNT, S.P. (2001b), Evaluation of gold deposits - Part 2: Results of a survey of estimation methodologies applied in the Eastern Goldfields of Western Australia. Applied Earth Science IMM Transactions section B, 110(3), pp. 167-175.n doi: 10.1179/aes.2001.110.3.167

DOMINY, S.C., SIDES, E. J., DAHL, O. and PLATTEN, I M (2006) Estimation and Exploitation in an Underground Narrow Vein Gold Operation-Nalunaq Mine. 6th International Mining Geology Conference Darwin, NT, Greenland, 21 - 23 August 2006, pp. 29-44. https://www.researchgate.net/publication/288186409_Estimation_and_exploitation_in_an_underground_narrow_vein_gold_operation__Nalunaq_mine_Greenland [Accessed 6/4/26].

DOMINY, S.C., XIE, Y. and PLATTEN, I M (2008) Characterisation of In Situ Gold Particle Size and Distribution for Sampling Protocol Optimisation. Ninth International Congress for Applied Mineralogy Brisbane, QLD, 8 - 10 September 2008, pp 175-186. https://www.researchgate.net/publication/289363579_Characterisation_of_in_situ_gold_particle_size_and_distribution_for_sampling_protocol_optimisation [Accessed 6/4/26].

DOMINY, S.C. (2014) Effects of sample mass on gravity recoverable gold test results in low-grade ores. Applied Earth Science IMM Transactions section B, 123(4), pp. 234-242. doi . 10.1179/1743275814Y.0000000061

DELGADO, J.P. (2023) The Archaeology of the Gold Dredge: The Final Phase of Placer Mining. Journal Maritime Archaeology, 18, pp. 269-295. https://doi.org/10.1007/s11457-023-09363-6

GHORBANI, Y., NWAILA, G.T., ZHANG, S.E., BOURDEAU, J.E., CANOVAS, M., ARZUA, J. and NIKADAT, N. (2023) Moving towards deep underground mineral resources: Drivers, challenges and potential solutions. Resources Policy, 80, 103222. doi: 10.1016/j.resourpol.2022.103222

HEDENQUIST, J. (2000) Exploration for epithermal gold deposits. Chapter 7-SEG Reviews, 13, pp. 245-277. https://www.researchgate.net/publication/228840402_Exploration_for_Epithermal_Gold_Deposits#full-text [Accessed 6/4/26].

KARPOV,V. and PETREEV, A.M. (2021) Determination of Efficient Rotary Percussive Drilling Techniques for Strong Rocks. Journal of Mining Science, 57, pp. 447-458. doi: 10.1134/S1062739121030108

KAŠIĆ, V. (1995) Komparativna analiza dosadašnjih istraživanja zlatonosnih nanosa Peka i predlog njihove optimizacije. Magistarski rad, Rudarsko-geološki fakultet, Univerzitet u Beogradu.

KHOMSIN K., MUKHTASOR, PRATOMO, D.G. and SUNTOYO, S. (2021) The Development of Seabed Sediment Mapping Methods: The Opportunity Application in the Coastal Waters. IOP Conference Series Earth and Environmental Science, 731(1),012039. doi: 10.1088/1755-1315/731/1/012039

LU, Y., ZHANG, B., WANG,X., LIU, H. and ZHOU, J. (2024) Characterization of metal-bearing nanoparticles observed in loess-covered terrain: Implications for prospecting. Journal of Geochemical Exploration, 262, 107488. https://doi.org/10.1016/j.gexplo.2024.107488

OPARIN, V.N., KARPOV, V.N., TIMONIN, V.V. and KONURIN, A.I. (2022) Evaluation of the energy efficiency of rotary percussive drilling using dimensionless energy index. Journal of Rock Mechanics and Geotechnical Engineering, 14(5), pp. 1486-1500. doi: 10.1016/j.jrmge.2021.12.021

ROBERT, F., BROMMECKER, R., BOURNE, B.T., DOBAK, P.J., MCEWAN, C., ROWE, R.R.and ZHOU, X. (2007) Models and exploration methods for major gold deposit types. Proceedings of "Exploration 07: Fifth Decennial International Conference on Mineral Exploration", 2007. pp. 691-711. https://www.researchgate.net/publication/284574136_Models_and_exploration_methods_for_major_gold_deposit_types [Accessed 6/4/26].

ROSHCHUPKIN, D.V. (1975) Increase in the effectiveness of excavation by floating dredges. Hydrotechnical Construction, 9, pp. 525-528. https://doi.org/10.1007/BF02379745

RYSBEKOV, K., TOKTAROV, A., KALYBEKOV, T., MOLDABAYEV, S., YESSEZHULOV, T.and BAKHMAGAMBETOVA, G. (2020). Mine planning subject

to prepared ore reserves rationing. E3S Web of Conference, 168, 00016. https://doi.org/10.1051/e3sconf/202016800016

SILLITOE, R.H. and HEDENQUIST, J. (2010) Gold exploration: Deposits and methodology. Mining journal, 37, pp. 3-5. https://www.researchgate.net/publication/283861540 [Accessed 3/4/26].

SKRZYPKOWSKI, K., ZAGÓRSKI, K., ZAGÓRSKA, A., and SENGANI, F. (2022) Access to Deposits as a Stage of Mining Works. Energies, 15(22), 8740. https://doi.org/10.3390/en15228740

MALANCHUK, Y., MOSHYNSKYI, V., KHRYSTYUK, A., MALANCHUK, Z., KORNIYENKO, V. and ZHOMYRUK, R. (2024) Modelling mineral reserve assessment using discrete kriging methods. Mining of mineral deposits, 18(1), pp. 89-98. https://doi.org/10.33271/mining18.01.089

MATHIOUDAKIS, S., XIROUDAKIS, G., PETRAKIS, E. and MANOUTSOGLOU, E. (2023a) Evolution of Alluvial Gold Mining Technologies. Materials Proceedings, 15(1), pp. 70. https://doi.org/10.3390/materproc2023015070

MATHIOUDAKIS, S., XIROUDAKIS, G., PETRAKIS, E., and MANOUTSOGLOU, E. (2023b) Alluvial Gold Mining Technologies from Ancient Times to the Present. Mining, 3(4), pp. 618-644. https://doi.org/10.3390/mining3040034

VAKANJAC, B. (1992) Geologija ležišta nemetaličnih mineralnih sirovina, Beograd: Katedra ekonomske geologije, Rudarsko-geološki fakulteta Univerziteta u Beogradu i Republički fond za geološka istraživanja. https://www.scribd.com/document/410095635/Nemetali-Vakanjac-doc [Accessed 3/4/26].

ZENG, X., ALI, S.H., TIAN, J. and LI, J. (2020) Mapping anthropogenic mineral generation in China and its implications for a circular economy. Nature communications, 11(1), pp. 1544. https://doi.org/10.1038/s41467-020-15246-4

ZUO, R. (2020) Geodata science-based mineral prospectivity mapping: A review. Natural Resources Research, 29, pp. 3415-3424. https://doi.org/10.1007/s11053-020-09700-9

UNDERGROUND MINING ENGINEERING 48(2026) 53-81 UDK 62
UNIVERSITY OF BELGRADE - FACULTY OF MINING AND GEOLOGY ISSN 03542904

Professional paper

IMPROVEMENT OF BUSINESS OPERATIONS THROUGH PHASES OF TECHNOLOGY DEVELOPMENT FOR MONITORING WELL PARAMETERS

Stevica Jankov[1], Vesna Makitan[2], Borivoj Novaković[2], Luka Djordjević[2]

Received: April 13, 2026 **Accepted:** May 25, 2026

Abstract: The subject of the paper is a comparative analysis of technologies for monitoring well parameters through three phases of development. The research is based on a case study conducted on an oil field with 152 wells in Serbia. The aim of the study is to determine the impact of digitalization and wireless data transmission on operational efficiency and reduction of production costs. The methodology includes analysis of operational data collected during years of field work, including parameters such as number of operators, response time, and logistics requirements. Results show that the transition from manual data recording to real-time systems reduces the number of required operators by 83 percent. The total response time to changes in well operation was reduced from more than seven days in the paper phase, through two to three days in the digitalization phase, to 30 seconds in the real time phase. Analysis of logistics parameters indicates a reduction in daily vehicle mileage from 230 to 14 kilometers, accompanied by a 94 percent decrease in CO2 emissions. The paper also identifies limitations regarding data resolution and the influence of human factors on the speed of implementation of new solutions. The findings confirm the economic and environmental justification of introducing modern measurement systems in the oil industry. Identified intermediate phases point to the need for gradual adaptation of work processes to new technologies. The obtained data serve as a basis for future research in predictive maintenance and application of artificial intelligence algorithms in oil exploitation.

Keywords: Oil Industry, Well Monitoring, Digital Transformation, Real-Time Data Transmission, Case Study, Operational Efficiency, Oil Production Optimization

[1] NAFTAGAS – Oil Services LLC, Novi Sad, Serbia

[2] University of Novi Sad, Technical Faculty "Mihajlo Pupin", Zrenjanin, Serbia

E-mails: stevica.jankov@nis.rs ORCID: https://orcid.org/0009-0000-6503-8200; vesna.makitan@tfzr.rs ORCID: https://orcid.org/0000-0002-0356-5993; borivoj.novakovic@uns.ac.rs ORCID: https://orcid.org/0000-0003-2816-3584; luka.djordjevic@tfzr.rs ORCID: https://orcid.org/0000-0003-4578-9060

1 INTRODUCTION

The issue of monitoring well parameters has been studied through different periods of technology development in oil production. A comparative analysis of the history of monitoring technologies was conducted based on available literature and practice. The analysis focused on operational data from the oil industry in Serbia. The topic was chosen due to its relevance and the limited number of studies based on long-term field data. The research is structured around phases identified through direct observation and work with equipment in the field. Each phase reflects real working conditions in a company operating 152 wells. The methodology was determined by technical specifications of instruments and machines used in different phases of exploitation, as well as the method of data transfer and processing. This approach allowed theoretical models to be tested through direct interaction with technology.

Data obtained reflect actual field conditions. Historical boundaries were set based on industry experience. These experiential data made it possible to identify turning points in operational processes that are not always visible in general scientific presentations. Each period reflects cycles in which changes in work methods and adoption of new solutions occurred.

Technology development is observed in historical context to explain how technical innovations influenced business processes. Each new phase brought changes in efficiency and speed of work. Analysis of these changes provides insight into how modernization of equipment reduced costs and increased output. The historical overview includes the transition from manual measurement methods to automated systems, which changed the structure of field work. The connection between technological progress and production optimization is the central part of the paper. Business improvement is considered a consequence of introducing solutions that changed resource management. Through analysis of practical examples, the paper shows how attitudes toward technology evolved and how its use led to more stable models of work in the oil industry. Technology is considered a tool that determines productivity level and precision of resource monitoring.

Parameters such as time, number of operators, vehicle mileage, and number of measurements were used in the study. These parameters changed during each phase, and the changes were used to analyze the justification of introducing new technologies in production. The following chapters present results of similar studies from scientific sources, a review of applied monitoring technologies, and comparison of their effects based on collected field data.

2 RELATED WORK

Oil exploitation using sucker rod pumps is a common artificial lift method that requires precise monitoring to maintain optimal production. Diagnostics of these systems went

through a development process that in early phases relied on mechanical laws of physics without microprocessor processing. The so-called paper phase involved use of explosive sonologs and mechanical dynamographs that converted tensile force into physical displacement of a pen on paper (Gibbs, 1982; Gibbs, 1963).

Traditional systems showed shortcomings due to subjectivity in data interpretation and safety risks related to use of explosives at the wellhead. A major problem was delay of information, where several days could pass between occurrence of a failure and notification of engineers, causing production losses (Clegg et al., 1993; J. N. McCoy et al., 1988).

Digitalization, initiated by introduction of electronic load cells, enabled high-frequency data collection and identification of material fatigue not visible with previous methods. Modern online transmission and SCADA analytics allow visualization of processes in real time, reducing response time to less than one minute (Gibbs, 1987; Danylenko & Sotnik, 2025).

The study analyzes three phases on a sample of 152 wells, focusing on optimization of human resources, reduction of operational costs, and application of predictive maintenance for long-term sustainability of the oil industry. Maintenance is divided into reactive, planned, and predictive. Reactive repairs are performed after failure, planned inspections follow fixed schedules, and predictive models use sensor signal analysis to forecast equipment failure. This approach reduces unplanned downtime and ensures stability of production processes (Liang et al., 2024; Meddaoui et al., 2023; Jankov et al., 2026).

SCADA systems of the fourth generation enable real-time information processing. Integration of Internet of Things into oil systems provides precise monitoring of mechanical and electrical parameters (Vani et al., 2024; Danylenko & Sotnik, 2025). These systems use software algorithms for automatic alarm management and equipment diagnostics. Digital solutions allow remote monitoring of sucker rod pumps and other well equipment (Osaretin, 2025; Godase, 2025).

Remote monitoring reduces need for frequent field visits by operators. Fewer interventions lower vehicle mileage and fuel consumption. Reduced wear of vehicles decreases overall company costs (Novaković et al., 2025). This organization allows control of more production units with fewer field staff (Snytko et al., 2025; Liang et al., 2024).

Sensor data analysis enables early identification of failures. Continuous monitoring of load trends and motor electrical values helps detect system degradation. Predictive maintenance is based on statistical methods and probability models of failure (Novaković et al., 2025). These models support planning of interventions only when data show actual technical need. Effective prediction of downtime reduces spare part and

overhaul costs (Liang et al., 2024; Meddaoui et al., 2023; Tian et al., 2021; Osaretin, 2025).

Machine learning algorithms are applied to large sets of historical data in the oil sector. Optimization of system operation is achieved through metaheuristic methods that improve energy efficiency (Marković et al., 2025). Timely action based on predictive indicators leads to higher profitability (Liang et al., 2024); (Ucar et al., 2024). Integration of artificial intelligence into control systems reduces risk of human error in decision making. Timely maintenance preserves equipment integrity and extends system life (Çınar et al., 2020); (Aderamo et al., 2024).

3 METHODOLOGY

The methodology is based on historical-comparative method and case study covering 152 wells. Field work and case study led to division of research into phases: paper phase, digitalization phase, and real-time data transmission phase. These phases were applied in practice of monitoring well parameters. Recognition and definition of phases were based on practice, and each new phase brought changes in oil production. Three phases were classified into periods: from mid-20th century to 1990s, from 1990s to 2020, and after 2020.

The criteria used to define each phase were based on the dominant diagnostic technology applied in the field (mechanical instruments in the paper phase, portable electronic devices in the digitalization phase, and permanently installed sensors with wireless transmission in the real-time phase). The data cover the period from the mid-20th century to the 2020s, with continuous records from 152 wells in Serbia. All wells were analyzed using the same methodological approach, with parameters including number of operators, response time, vehicle mileage, and measurement frequency. Reported values represent directly measured field data, aggregated into averages for each phase to ensure comparability.

The first period was characterized by use of mechanical dynamographs and explosive sonologs during direct field visits. Data were recorded on paper, and processing required manual counting of couplings and use of planimeter for calculation of power. Traditional systems carried safety risks due to use of explosives in flammable environments and work near moving parts of pump units (J. N. McCoy et al., 1988; Gibbs, 1963). Information delays of several days caused production losses. The second phase introduced electronic load cells that enabled high-frequency data collection (Gibbs, 1987; Clegg et al., 1993). Digitalization reduced human factor influence but still required operator presence to collect files. Portable units shortened reaction time compared to paper methods. The third phase involved permanently installed sensors and wireless real-time data transmission (Danylenko & Sotnik, 2025; Takacs & Kis, 2021).

Modern maintenance integrates artificial intelligence to predict system condition. Machine learning algorithms analyze sensor signals and identify wear patterns (Ucar et al., 2024; Vani et al., 2024). Deep learning methods allow automatic diagnostics of well operating states based on field data. Integration of product quality parameters into maintenance models influences reliability of the process. These systems reduce unplanned downtime and optimize operating costs. Use of artificial intelligence is considered a fourth phase of technology development for data transmission and predictive maintenance (Riccio et al., 2024; (Wang et al., 2021).

Each phase was followed by selection of device characteristics and parameters, allowing monitoring of technology development and production changes. Field measurements showed that data transmission and physical characteristics of instruments directly influence work processes. Comparison of characteristics showed that instruments became more adapted to operators over time. Reduction in instrument weight made use easier, reduced installation time, and lowered number of operators needed. For each instrument, characteristics were presented in tables to show innovation flow and impact on field processes.

Results indicate existence of intermediate phases between main periods, caused by lack of trust in new technologies. These transitional periods were marked by attempts of operators and engineers to control new systems while still relying on old equipment. Adaptation to new solutions was accompanied by resistance due to fear of job loss and reduced importance of their role. The intermediate phase between the first and second phases occurred gradually, with partial modifications of devices. The third phase was introduced quickly through investment in modern equipment. However, resistance was still present, with operators trying to prove malfunction of new equipment. This resistance was based on fear of innovation, doubts about the ability to operate new systems, and concerns about job security. These transitional phases were noted during direct field work and may serve as a basis for future studies. The authors did not conduct a separate analysis of them in this paper.

4 THE PAPER PHASE

The paper phase, covering the mid-20th century to the 1990s, was characterized by diagnostic methods based on mechanical physics and chemical reactions without microprocessor technology. Monitoring was periodic, with mechanical dynamographs placed directly on the polished rod. A system of springs and levers transformed tensile force into mechanical displacement of a pen that drew a force-stroke diagram on paper (Gibbs, 1963).

At the same time, explosive sonologs were used to determine fluid level. The process involved activating a charge in the annulus of the well, generating a sound wave. The echo reflected from couplings and fluid surface was recorded by a mechanical printer.

Depth was determined manually by counting amplitudes with a ruler (J. N. McCoy et al., 1988).

These methods were considered standard at the time due to robustness and independence from electrical power, which allowed stable operation in extreme conditions (Gibbs, 1992). Paper records provided permanent evidence without risk of software errors (Nicol & Purcupile, 1984). Manual data processing supported development of engineering intuition, enabling experts to identify valve irregularities by visual analysis of curve shape. The explosive impulse provided strong penetration of sound waves in deep wells (J. McCoy et al., 1997).

From today's perspective, these methods had significant shortcomings (Clegg et al., 1993). Subjectivity in interpretation and use of planimeters for manual measurement led to errors. Safety risks were present due to explosives in flammable environments and work near moving parts. Information delays caused production losses. Archiving paper documentation prevented long-term statistical analysis, while low resolution concealed early material fatigue.

Diagnostics in this phase included planimeter use, which connected mechanical records with mathematical calculation of power. After drawing the curve, engineers used a planimeter to determine surface area of irregular shapes. The measured area represented work performed during one cycle. Power was calculated using a formula with device constants(Garrett et al., 1996; Takacs, 2015).

The obtained area represented the work performed during one cycle. To calculate the power, a formula was used that included device constants (Takacs & Kis, 2021)

$$P = \frac{A * S * C * N}{K} \quad (1)$$

Where:
P - Power (kW)
A - Area measured by planimeter (cm2)
S – Spring scale (kg/mm)
C - Constant of pen stroke
N - Number of strokes per minute (min^{-1})
K - Conversion factor (6116 for kW).

Figure 1 shows the dynamograph used during the paper phase, while Table 1 presents the technical characteristics of the DYN 77 dynamograph.

Figure 1 Mechanical dynamograph with a paper display of the dynamograph card (Dynamograph DYN 77 | Sonoecho™, n.d.)

Table 1 Technical Specifications of the Dynamograph DYN 77

Characteristic	Description
Max. load:	140 kN / 14.5 t / 31,000 lbs
Max. stroke:	1 to 8 m (39 to 315")
Min. distance between bridels:	190 mm (7 1/2")
Weight	9.1 kg (20.0 lbs)

Figure 2 shows the sonolog used during the paper phase.

Figure 2 Powder-actuated Sonolog Model M (Echometer Model M Strip Chart Recorder - UPC Global, n.d.)

Table 2 presents the technical characteristics of the Sonolog Model M.

Table 2 Technical characteristics of the Sonolog Model M

Characteristic	Description
Enclosure / Housing	Compact plastic case
Cables	1.5 m cable for microphone and amplifier, 12 VDC car cigarette lighter cable
Power Supply	110/220 VAC automatic battery charger
Accessories	11-point divider, 10 paper rolls
Measurement Equipment	200 PSI gauge with quick connector
Spare Parts	O-ring set and small parts
Gas Cylinder	2.2kg cylinder for CO2 or nitrogen
Gas Accessories	Hose and cylinder charging connector

The plastic enclosure contains cable for connecting the microphone and amplifier. The device features an automatic battery charger supporting 110 or 220 volts, as well as a 12-volt power cable for a car cigarette lighter socket.

The package includes a divider, paper rolls, and a pressure gaugewith a quick connector. A set of O-rings and related parts are provided with the equipment. The standard offering includes a 2.2 kg cylinder for CO2 or nitrogen, unless otherwise specified. A hose and a cylinder charging connector are part of the standard equipment.

5 DIGITALIZATION PHASE

The digitalization phase, from the mid-1990s to early 2010s, marked transition from paper systems to semiconductor memory. Mechanical dynamographs were replaced by electronic load cells. Instead of mechanical pen movement, force on the polished rod changed electrical resistance in strain gauges, allowing high-frequency sampling and detection of vibrations not previously visible (Gibbs, 1987).

Explosives in sonologs were replaced by compressed gas, while microphones sent signals to processors that identified pipe couplings (J. McCoy et al., 1999). Despite digitalization, data transfer still required operator presence. Information was stored in device memory, and operators had to visit wells to collect data and manually upload them. Advantages included automatic calculation of diagram area with high precision, eliminating human error (Takacs, 2015). Archiving in digital databases allowed comparison of current and historical diagrams. Limitations included reactive maintenance, since data represented only snapshots. High operational costs and traffic risks from frequent visits remained (Lea & Bowen, 1992).

Technological basis included digital sonologs and dynamographs integrated into portable units. Compressed gas provided cleaner acoustic impulses, while digital signal processing enabled automatic recognition of well elements and reduced depth calculation errors (Gibbs, 1987). Software solutions enabled integration of collected data into simulation models, optimizing pump strokes and improving energy efficiency (Al Mubarak, 2022).

Figure 3 shows the Echometer Well Analyzer, while Figure 4 presents the sonolog and dynamograph used during the digitization phase

Figure 3. - Echometer Well Analyzer (Echometer Resigned, n.d.)

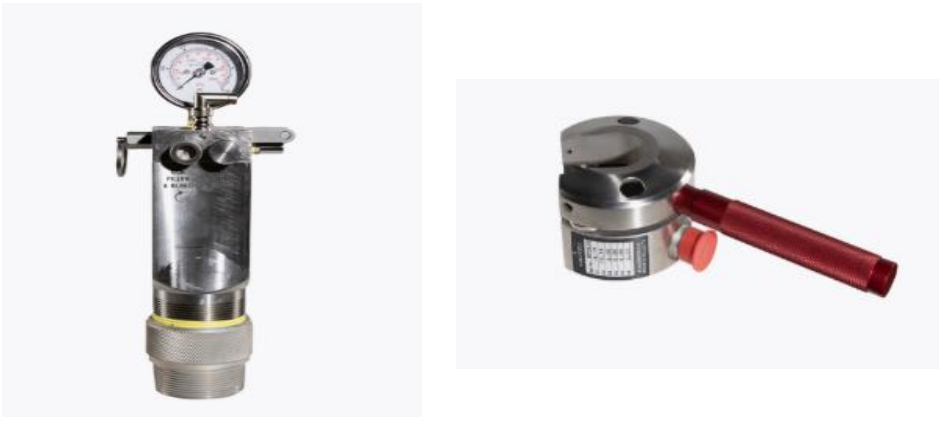

Figure 4 Digital sonolog and dynamograph (Echometer Resigned, n.d.)

Table 3 presents the technical characteristics of the digital sonolog, while Table 4 presents the technical characteristics of the digital dynamograph.

Table 3 Technical Characteristics of the Digital Sonolog

	Characteristic	Description
1	Working Pressure	Rated at 1500 psi
2	Microphone	Dual-disk, noise-canceling model
3	Pressure Gauge	1500 psi capacity
4	Dimensions	7.6 x 11.4 x 30.5 cm (3 x 4.5 x 12 in)
5	Weight	3.6 kg (8 lbs)

The device has a working pressure of 1500 psi and is equipped with a dual-disk noise-canceling microphone. The built-in pressure gauge also supports values up to 1500 psi.

Table 4 Technical Characteristics of the Digital Dynamograph

	Characteristic	Description
1	Installation	Between the pumping unit carrier bar and the polished rod clamp
2	Maintenance	No routine maintenance required
3	Data Processing	Uses Well Analyzer software
4	Calibration	Field recalibration possible
5	Sensors	Internal accelerometer
6	Throat / Opening	1.5 inc
7	Capacity	Rated up to 13600 lbs (30000 kg)

The device is installed between the pumping unit carrier bar and the polished rod clamp. The design requires no routine maintenance during operation. Data from the device is processed via the Well Analyzer, which analyzes collected information through integrated software. Measurement accuracy can be adjusted by field recalibration. The

dynamograph features an internal accelerometer and a 1,5 in throat. The maximum rated capacity is 13,600 kg (30,000 lbs)

6 REAL-TIME DATA TRANSMISSION PHASE

The phase of real-time data transmission in the Serbian oil industry appeared during the 2020s. In this development stage, sensors that were previously used as portable devices became fixed and permanently installed on each individual well. Collected data were no longer stored locally but transmitted through wireless networks such as GPRS, radio links, or satellite terminals directly to a central server. The process of transmitting information from the well to the user within the SCADA system took place through three hierarchical levels.

The first level included the field part and direct acquisition of data from the well. Key components consisted of pump unit controllers and intelligent control stations that collected signals from permanently installed load cells and position sensors based on the Hall effect (Liang et al., 2024); Yadav & Paul, 2021). At this level, primary signal processing was carried out and motor operation was optimized by applying frequency converters (Ogunmesa, 2021).

The second level represented the communication bridge between field units and the control center. Data from controllers were transmitted through routers and wireless technologies to programmable logic controllers and central servers (Liang et al., 2024; (Yadav & Paul, 2021). This segment ensured the integrity of information and its distribution in real time (Wali & Alshehry, 2024).

The third level included the management and analytical segment where visualization was performed within the SCADA system. At this level, automatic analysis of diagram overlaps, alarm management, and processing of large data sets were carried out, which enabled the transition to predictive maintenance (Danylenko & Sotnik, 2025). The architecture of the described intelligent management system (Figure 5) was presented in the corresponding illustration (Jankov et al., 2025).

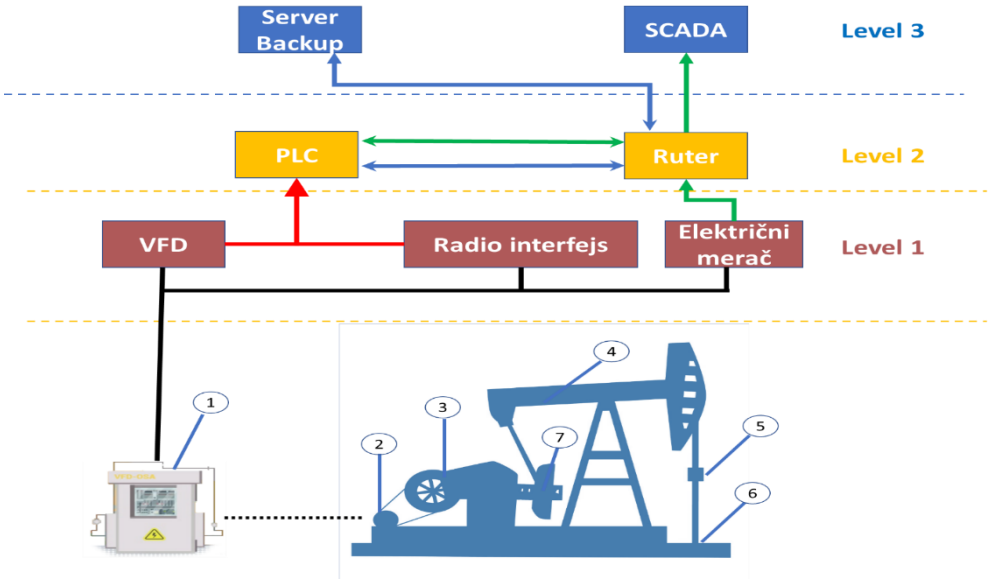

Figure 5 Data transfer from the well to the user (SCADA), (1-Intelligent Control Station (ISU), 2-electromotor, 3-gearbox, 4-balance beam, 5-dynamograph, 6-sonologist, 7-weights)

AVEVA[1] (https://www.aveva.com) develops software solutions that support and implement SCADA (Supervisory Control and Data Acquisition) systems through tools for process management, visualization, and data analysis. These solutions enable users to monitor and optimize industrial processes in real time, including direct integration with PLC and RTU devices. The AVEVA platform serves as a foundation for managing physical systems, providing the necessary infrastructure for operational oversight. The system is applied for process visualization, allowing specialists to respond to emergency situations.

Figure 6 shows the data collected from sensors which, following the described transmission, are used for analysis and decision-making. The interface displays well operating parameters in real time, allowing for the early detection of irregularities and providing the necessary time for their resolution

[1] A British multinational information technology consulting company headquartered in Cambridge. (AVEVA - Global Leader in Industrial Software).

Figure 6 Visualization of operating parameters in the AVEVA environment

The user could select the desired time interval for monitoring, with access to all historical data stored since the beginning of system use. Each parameter was analyzed individually, and due to the large amount of data, the system detected anomalies and predicted failure time. The intelligent management system automatically reported irregularities, after which specialists sent service requests before downtime occurred (Jankov et al., 2025).

In practice, sensor signals are acquired continuously, typically at intervals of 1 to 5 seconds depending on the parameter (load, stroke position, motor current). These raw data streams are locally processed and aggregated before transmission to the SCADA server. Due to memory and bandwidth limitations of the installed system, the SCADA platform does not store every single raw sample but instead updates the operator interface in a refresh cycle of approximately 30 seconds. This refresh interval therefore refers to the visualization layer, while the underlying acquisition occurs in much shorter intervals. At present, the 30 second cycle is a limitation of the installed system, and it represents a clear area for future improvement. Reducing the refresh interval in subsequent generations of SCADA platforms would provide additional benefits, including faster anomaly detection, more precise predictive maintenance, and improved operational efficiency.

There are many manufacturers of stationary sensors, which are mandatory in the third phase. One of them is Magmatek (https://www.mgtcontrol.ru), and their devices were used as an example for the description of the third phase.

For recording the dynamic level in this study, a stationary sonolog was used that records the level four times per day, with the option to adjust for a higher number of recordings. The sonolog also has the capability to measure and transmit data on pressure in the annular space. The manufacturer of the sonolog MGT APDU-1 is Magmatek, shown in Figure 7. The operation of the sonolog and the measurement of the level are presented in more detail in the referenced work (Jankov et al., 2025).

Figure 7 Sonolog MGT APDU-1 – stationary level meter in the annular space of the well (Приборы Контроля Параметров Скважин От Компании Магматэк, n.d.)

Table 5 presents the technical characteristics of the stationary sonolog, and Table 6 presents the technical characteristics of the stationary dynamograph.

Table 5 Technical characteristics of the stationary sonolog

	Characteristic	Description
1	Level measurement range	20 to 6,000 m
2	Level resolution	1 m or less
3	Pressure measurement range	0 to 100 kg/cm²
4	Pressure resolution	0.1 kg/cm²
5	Operating pressure	0.8 to 50 kg/cm²
6	Battery capacity	At least 4,000 measurements without charging
7	Charging time	Up to 3 hours
8	Communication	Bluetooth LE with NFC pairing
9	Communication range	30 m or more
10	Operating temperature	Between -40 and +50 °C
11	Service life	5 years or longer

In Figure 8, a dynamograph manufactured by Magmatek is shown, which is used as a stationary sensor.

Figure 8 Dynamograph MGT SDD-1 – stationary load meter of the sucker rod (Приборы Контроля Параметров Скважин От Компании Магматэк, n.d.)

Table 6 Technical characteristics of the stationary dynamograph

	Characteristic	Description
1	Measured load range	0 to 10,000 kgf
2	Measured stroke range	0 to 20 m (at 0.5 to 12 strokes/min)
3	Load measurement accuracy	≤1% full range
4	Load resolution	≤0.1% full range
5	Operation time (recording)	≥100 h
6	Power supply	Maintenance-free integrated battery
7	Communication channel	Bluetooth LE 4.x
8	Communication range	≥30 m
9	Setup method	NFC
10	Operating temperature	-40 to +50 °C
11	Calibration frequency	1 year
12	Service life	≥5 years
13	Weight	≤1.2 kg

7 RESULTS AND DISCUSSION

The results will be presented through analysis of each individual phase, as well as through comparative tables and diagrams. Data were collected from five measurements of each well per month, which is a total of 760 measurements for 152 wells.

The comparative results presented in Tables 7–10 confirm that the overall response time decreased from more than seven days in the paper phase to 30 seconds in the real time phase. It should be emphasized that the 30 second value refers to the refresh cycle of the SCADA visualization system, while the actual sensor acquisition occurs in much shorter intervals (1–5 seconds). This distinction highlights both the current limitation of the installed system and the potential for further improvement. Future upgrades aimed at reducing the refresh cycle would provide additional benefits in terms of faster anomaly detection and enhanced predictive maintenance.

7.1 Parameters of the first phase

In the first development phase, operational processes required significant time engagement due to the specifics of the mechanical instruments used. Work at the well site included installation of a massive mechanical dynamograph, preparation of the drum with a paper card, activation of the explosive charge, and manual reading of the record on the paper strip, which on average lasted 60 minutes. Transport and logistics required an additional 60 minutes due to the condition of road infrastructure and the need for regular maintenance of measuring devices, including cleaning of combustion residues from the explosive charge.

The key difference compared to later phases was in the process of data processing in the office, which required 30 minutes per well. Measurement results were not immediately available, and technical staff had to use a planimeter for manual calculation of the surface area of each individual chart. The total time required to process one recording was 150 minutes.

When calculating daily capacity within a 12-hour shift, taking into account effective working time of 10.5 hours after preparation of materials and servicing of instruments, a defined formula was applied for calculating operational output.

$$\frac{10{,}5\ hours}{2{,}5\ hours\ per\ well} = 4{,}2\ measurements\ per\ day\ per\ operator \tag{2}$$

The capacity of an operator (15 working days) was calculated using Formula 3.

Monthly

$$15\ days\ x\ 4{,}2\ \frac{measurements}{day} = 63\ measurements\ per\ month\ per\ operator \tag{3}$$

The required number of operators for 760 measurements is given by Formula 4.

$$\frac{760\ total\ measurements}{63\ measurements\ per\ operator} = 12{,}06\ operators \tag{4}$$

7.2 Parameters of the second phase

In the digitalization phase, operational processes required less time engagement compared to the previous period, but physical presence at the site still remained a key factor. Work at the well included installation of the digital dynamograph and sonolog, their connection to the computer unit via cables, as well as data reading, which on average lasted 30 minutes. Transport and logistics required an additional 45 minutes due to the specifics of road infrastructure and the spatial distance between individual wells.

Data processing in the office lasted 15 minutes per recording. Although the data were collected in digital format, it was still necessary to allocate time for synchronization with the central database and for final validation of the results. The total time required for complete processing of one recording amounted to 90 minutes. When calculating daily capacity within a 12-hour shift, taking into account effective working time of 10.5 hours after equipment preparation and instrument maintenance, a defined formula was applied to quantify operational output.

$$\frac{10{,}5\ hours}{1{,}5\ hours\ per\ operator} = 7\ measurements\ per\ day\ per\ operator \quad (5)$$

The capacity of an operator (15 working days) was calculated using Formula 36

Monthly

$$15\ days\ x\ 7\frac{measurements}{day} = 105 measurements\ per\ month\ per\ operator \quad (6)$$

The required number of operators for 760 measurements is given by Formula 7.

$$\frac{760\ total\ measurements}{105\ emasurements\ per\ operator} = 7{,}23 operators \quad (7)$$

For stable functioning of the system in the second phase (digital portable equipment), it is necessary to employ 8 operators (in order to cover deviations, equipment failures, and shift overlaps).

7.3 Parameters of the third phase

In this phase, the human factor in the measurement process was reduced to zero for routine checks. Sensors are fixed, and measurement is performed continuously (24/7) without human presence. The software (AVEVA/SCADA) automatically analyzes the chart. The engineer usually reacts only to an alarm (Jankov et al., 2025). One operator (dispatcher) can monitor all 152 wells in real time. The required number of operators in the field is drastically reduced, and they become exclusively an intervention team rather than a measurement team.

7.4 Comparative analysis of results

Comparative analysis of the number of operators

In Table 7, comparative data by phases are presented for the number of operators, time to information, measurement hours, and operator cost index.

Table 7 Comparative overview of exploitation efficiency for 152 wells

Parameter	Phase 1 (Paper)	Phase 2 (Digital)	Phase 3 (Online)
Required number of operators	12	8	1–2 (supervision)
Time to information	2–3 days	12–24 hours	30 seconds
Annual working hours (measurement)	22,800 h	13,680 h	~0 h
Labor cost (index)	100%	66%	<15%

The transition from the first to the third phase brings not only precision, but also frees up more than 80% of human resources that can be redirected to more complex engineering tasks. While in the first phase the focus was on data collection, in the third phase the focus is on optimization. The drastic reduction in response time (from several days to several minutes) directly prevents fluid losses caused by unnoticed failures, making the investment in the SCADA system pay off in record time.

Figure 9 presents graphical representation of the reduction in the number of required operators across the three phases, together with the reduction in response time for obtaining field information

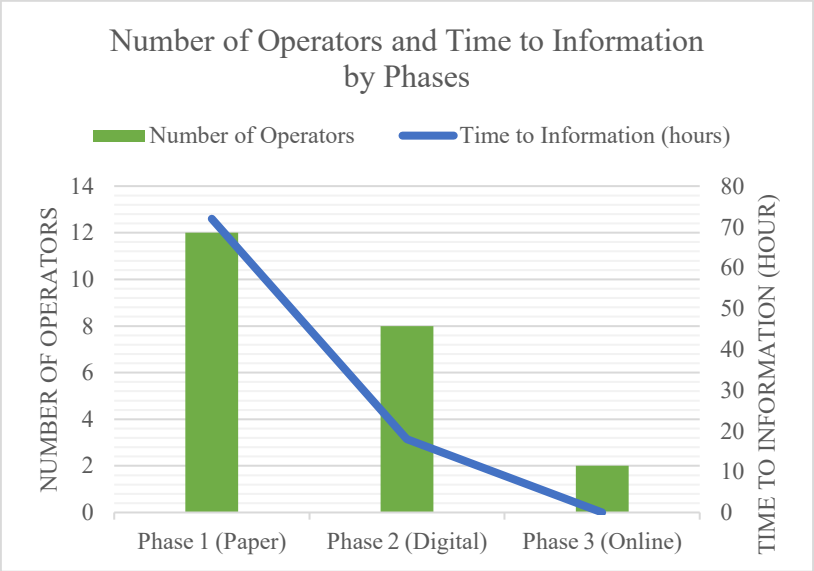

Figure 9 Graphical representation of the reduction in the number of required operators across the three phases, together with the reduction in response time for obtaining field information.

Comparative Overview of Response Time

Table 8 Comparative Overview of Response Time in Relation to Data Transmission Across Phases.

Table 8 Comparative Overview of Response Time from Failure to Information

Parameter	Phase 1 (Paper)	Phase 2 (Digital)	Phase 3 (Online)
Frequency of control	5 times per month	5 times per month	Continuous (24/7)
Failure detection time	5–7 days	2–3 days	30 seconds (Alarm)
Data processing time	30 min (Manual)	10 min (Software)	Instant (Automatic)
Total response time	7+ days	2–3 days	30 seconds

Economic Analysis

The economic feasibility analysis for the model of 152 wells is based on an average distance of 10 km between the locations and the base, with a unit transportation cost of 0.50 EUR per kilometer. In the first two development phases, which include manual and portable digital systems, each individual measurement requires a physical vehicle trip to the field. The calculation shows that with an annual intensity of 9,120 measurements, the total mileage reaches 91,200 km. This operational model generates annual transportation expenses of 45,600 EUR.

The transition to the third development phase, based on online data transmission systems, allows automation of the information collection process. Field activities in this model are carried out only upon detection of irregularities, applying the principle of management by exception. Statistical data show that, on average, 30% of wells per month require intervention, resulting in approximately 547 annual field trips. The annual mileage in this scenario amounts to 5,472 km, while the associated transportation costs are reduced to 2,736 EUR. The difference in costs indicates a high level of financial savings achieved through automated monitoring.

In this study, the analysis focused on transportation parameters and the reduction in the number of operators. The introduction of monitoring and remote-control systems, however, involves many additional aspects that need to be evaluated in order to provide a complete investment assessment and an approximate calculation of implementation profitability. The presented transportation savings represent only a part of the overall economic justification. A complete evaluation should also include capital expenditures (CAPEX), such as system investment cost, sensor installation, and software/communication infrastructure, as well as operational expenditures (OPEX) related to maintenance and data services. Preliminary estimates indicate that the reduction in manpower and logistics costs significantly offsets the initial investment, resulting in a positive return on investment (ROI) within the first years of system operation. A broader economic assessment, including CAPEX, OPEX, and ROI, will be addressed in future scientific works.

Reduction of CO_2 Emissions

The transition from manual monitoring (Phase 1/2) to online SCADA monitoring (Phase 3) across 152 wells reduces annual CO_2 emissions from 14,592 kg to 875 kg, representing a reduction of nearly 14 t (94%). This technological evolution directly contributes to ESG goals by lowering annual mileage from 91,200 km to 5,472 km, as shown in Table 10.

Table 10 Reduction of CO_2 Emissions in Phase 3 Compared to Phase 1

Parameter	Phase 1	Phase 3	Difference
Number of operators	12	2	−83%
Response time	7+ days	30 seconds	Reduced by >99%
Vehicle mileage	230 km/day	14 km/day	−94%
CO_2 emissions	High (baseline)	Reduced by 94%	−94%

Figure 10 shows a significant reduction of carbon dioxide emissions in the third phase compared to the first two. By eliminating routine manual inspections of 152 wells and applying the principle of management by exception, annual emissions are reduced from 14,592 kg to 875 kg. This reduction of 94%, amounting to approximately 14 tons annually, positions digital transformation as the primary tool for achieving environmental sustainability within the oil sector.

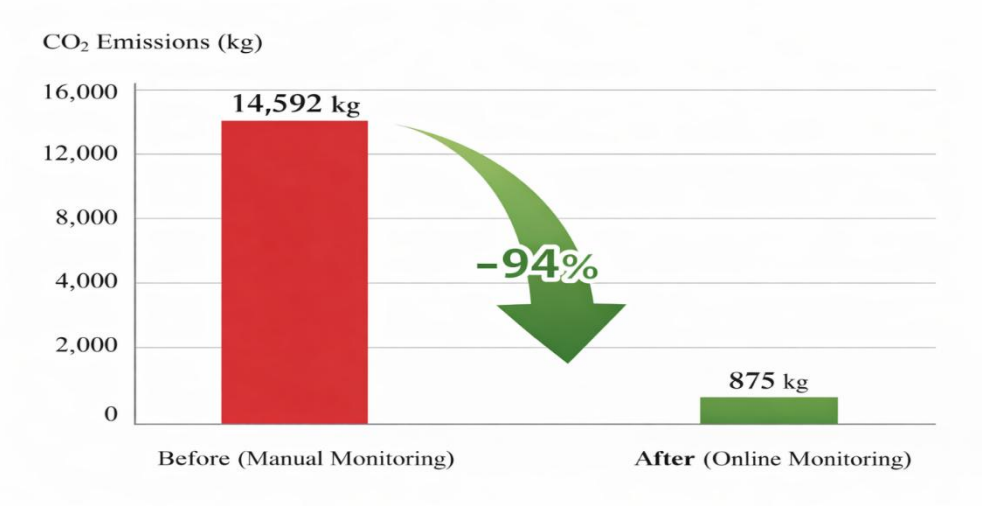

Figure 10 Comparative Display of Annual Emissions (kg) in the Field with 152 Wells Before and After Implementation of Online Monitoring

8 DISCUSSION

The comparative results presented in Tables 7 to 10 are based on directly measured field data from 152 wells, aggregated into averages for each phase. This approach ensures that the reported values reflect actual operational practice rather than estimates. The criteria for phase definition were consistent across all wells, and the same parameters (number of operators, response time, vehicle mileage, and measurement frequency) were applied uniformly. By presenting averaged values, the analysis highlights general trends while minimizing the influence of extreme individual cases.

The discussion of results connects the measured values with theoretical assumptions and previous research in the oil industry. The comparison of the three technological phases across 152 wells confirms that automation changes the structure of operational costs. The obtained data on the reduction of the number of operators by 83% correlate with the findings of the author (Gibbs, 1987) regarding the impact of electronic measuring cells on labor productivity.

The overall response time decreased from more than seven days in the paper phase, through two to three days in the digitalization phase, to 30 seconds in the real time phase represents a key change in production management. While traditional paper-based methods required manual processing and physical transfer of diagrams, the third phase enables immediate detection of irregularities in the operation of pumping units. Such results are consistent with research (Takacs & Kis, 2021) which emphasize the importance of real-time transmission for reducing fluid losses due to unplanned downtime.

Logistical parameters, such as the reduction of daily mileage from 230 km to 14 km, indicate a change in the maintenance model. The transition from reactive to predictive maintenance reduces the need for routine site visits. The results showing a 94% decrease in CO_2 emissions complement the techno-economic analysis with ecological indicators, which is consistent with modern requirements for sustainable oil exploitation. (Danylenko & Sotnik, 2025).

The observed limitations in data resolution of 30 seconds indicate the need for further refinement of compression algorithms. Although cloud analytics enables large-scale data processing, local recording still retains an advantage in diagnosing specific high-frequency dynamic processes. The discussion of these limitations opens space for the introduction of a fourth phase, which would employ deep learning methods for automatic interpretation of signals directly at the wellhead. (Ucar et al., 2024).

The identified intermediate phases and workforce resistance to new technologies confirm that technical solutions depend on the organization’s readiness for change. Operators’ fear of losing their role in the management process influences the speed of adoption of digital tools. This phenomenon requires further analysis from the perspective of

engineering management in order to ensure full integration of modern systems into everyday field operations.

9 CONCLUSION

The research conducted on a sample of 152 wells confirms that technological development is fundamentally transforming operational processes within the oil industry. The transition from manual data recording to automated real-time systems has resulted in a significant reduction in the workforce, decreasing the number of operators from 12 to 2. This 83% reduction in human resource engagement is a direct consequence of implementing modern measuring instruments and cloud analytics, which minimize the need for a physical presence on-site for routine measurements.

An analysis of logistical parameters indicates a drastic drop in daily vehicle mileage from 230 to 14 kilometers. This reduction in transport activities has cut annual fuel and maintenance costs by over 90%. Simultaneously, a 94% decrease in CO2 emissions was recorded, highlighting the environmental benefits of technological modernization. Furthermore, the results confirm that switching to wireless data transmission shortens the response time to operational changes from 48 hours to just 30 seconds.

However, certain research limitations remain, primarily regarding data transmission and resolution. The current 30-second refresh interval and cloud-based signal compression prevent the detection of specific high-frequency dynamic changes that are otherwise visible during local recording. Additionally, since the study was conducted on a specific oil field, variations in terrain and equipment age at other locations may affect the implementation speed of the third phase. Human resistance to new technologies also remains a limiting factor for total system automation.

Future work will focus on the fourth phase of development, involving the application of Artificial Intelligence (AI) and predictive maintenance. The primary focus will be the integration of deep learning algorithms to enable automated diagnostics without production downtime. Plans are also in place to examine increasing data resolution without straining network infrastructure. Further research will encompass a comprehensive analysis of the economic effects of full automation on the long-term stability of oil exploitation systems

Acknowledgment: The authors thank the Serbian Ministry of Education, Science, and Technological Development for their support and the funds provided under contract no. 451-03-136/2025-03/200126.

REFERENCES

ADERAMO, A. T., OLISAKWE, H. C., ADEBAYO, Y. A., & ESIRI, A. E. (2024). AI-driven HSE management systems for risk mitigation in the oil and gas industry. Comprehensive Research and Reviews in Engineering and Technology, 2(1), 1–22.

AL MUBARAK, O. M. M. (2022). Design and implementation of an industrial internet of things based Scada system: Case study the petroleum pipeline systems.

ÇINAR, Z. M., ABDUSSALAM NUHU, A., ZEESHAN, Q., KORHAN, O., ASMAEL, M., & SAFAEI, B. (2020). Machine learning in predictive maintenance towards sustainable smart manufacturing in industry 4.0. Sustainability, 12(19), 8211.

CLEGG, J., BUCARAM, S., & HEIN JR, N. (1993). Recommendations and Comparisons for Selecting Artificial-Lift Methods (includes associated papers 28645 and 29092). Journal of Petroleum Technology, 45(12), 1128–1167.

DANYLENKO, M., & SOTNIK, S. (2025). Comparative analysis of modern SCADA packages for production automation.

DYNAMOGRAPH DYN 77 | sonoechoTM. (n.d.). Retrieved March 19, 2026, from https://www.sonoecho.com/en/products/Dynamograph -dyn77.php

ECHOMETER MODEL M STRIP CHART RECORDER—Upc Global. (N.D.). Retrieved March 19, 2026, from https://www.upcoglobal.com/oil-well-products/echometer/model-m

ECHOMETER RESIGNED. (n.d.). Retrieved March 6, 2026, from https://www.echometer.com/products/model-m

GARRETT, M., ROWLAN, L., PODIO, A., EGNOTO, F., & MCCOY, J. (1996). Improved field measurements aid in sucker rod lift analysis. 109–113.

GIBBS, S. (1963). Predicting the behavior of sucker-rod pumping systems. Journal of Petroleum Technology, 15(07), 769–778.

GIBBS, S. (1982). A review of methods for design and analysis of rod pumping installations. Journal of Petroleum Technology, 34(12), 2931–2940.

GIBBS, S. (1987). Utility of motor-speed measurements in pumping-well analysis and control. SPE Production Engineering, 2(03), 199–208.

GIBBS, S. (1992). Design and diagnosis of deviated rod-pumped wells. Journal of Petroleum Technology, 44(07), 774–781.

GODASE, V. (2025). Smart energy management in manufacturing plants using PLC and SCADA. Advance Research in Power Electronics and Devices, 2(2), 14–24.

JANKOV, S. M., STANISAVLJEV, S. M., NOVAKOVIĆ, B. Z., & ĐORĐEVIĆ, L. R. (2025). Visualization of operation parameters and remote management of oil production through the implementation of SCADA system. Tehnika, 80(5), 501–506.

JANKOV, S., NOVAKOVIĆ, B., & DJORDJEVIĆ, L. (2025). Optimization of oil production by using sucker rod pumps by maintaining optimal system balance. Podzemni Radovi, 1(47), 45–73.

JANKOV, S., NOVAKOVIĆ, B., IVANOV, G., & ĐORĐEVIĆ, L. (2025). Optimization of oil production using reciprocating pumps through corrective adjustment of operating parameters. Mining and Metallurgy Engineering Bor, (2), 21–34.

JANKOV, S., NOVAKOVIĆ, B., MARKOVIĆ, M., ŠARENAC, U., LANDUP, D., PREMČEVSKI, V., & ĐORĐEVIĆ, L. (2026). Optimization of Oil Production Using Sucker Rod Pumps via Predictive Elimination of Paraffin Issues. Applied Sciences.

LEA, J. F., & BOWEN, J. (1992). Dynamic Measurements Of Beam-Pump Parameters. SPE Production Engineering, 7(01), 113–120.

LIANG, X., XING, Z., YUE, Z., MA, H., SHU, J., & HAN, G. (2024). Optimization of energy consumption in oil fields using data analysis. Processes, 12(6), 1090.

MARKOVIĆ, M., NOVAKOVIĆ, B., ĐURĐEV, M., JOVANOVIĆ, S., DESNICA, E., BLAŽIĆ, M., & TOLMAČ, J. (2025). Energy-Efficient Optimization Of Jaw-Type Blowout Preventer Activation Using Combined Experimental Design and Metaheuristic Algorithms. Energies, 18(18), 4852.

MCCOY, J., BECKER, D., PODIO, A., & DRAKE, B. (1997). Improved Analysis of Acoustic Liquid Level Depth Measurements Using Dual Channel Analog/Digital Strip Chart Recorder. Southwestern Petroleum Short Course, Lubbock, Texas.

MCCOY, J., DRAKE, W., COLLIER, F., OTT, R., & PODIO, A. (1999). Beam pump balancing based on motor power utilization. Journal of Canadian Petroleum Technology, 38(13).

MCCOY, J. N., PODIO, A. L., & HUDDLESTON, K. L. (1988). Acoustic determination of producing bottomhole pressure. SPE Formation Evaluation, 3(03), 617–621.

MCCOY, J., & PODIO, A. (1990). Well Performance Visualization and Analysis. SPE-20126.

MEDDAOUI, A., HAIN, M., & HACHMOUD, A. (2023). The benefits of predictive maintenance in manufacturing excellence: A case study to establish reliable methods for predicting failures. The International Journal of Advanced Manufacturing Technology, 128(7), 3685–3690.

NICOL, T. H., & PURCUPILE, J. (1984). Dynamic analysis of sucker rod pumping. In Energy Developments: New Forms, Renewables, Conservation (pp. 55–58). Elsevier.

NOVAKOVIĆ, B., DJURDJEV, M., DJORDJEVIĆ, L., DRAKULOVIĆ, V., RADOVANOVIĆ, L., & PREMČEVSKI, V. (2025). Predicting Operational Reliability of the Directional Control Valves of the Hydraulic Press System Using Taguchi Method and Regression Analysis. Machines, 13(12), 1124.

NOVAKOVIĆ, B., JANKOV, S., NIKOLIĆ, M., & ĐORĐEVIĆ, L. (2025). Multi-criteria optimization of sucker rod pump operation using AHP–TOPSIS based decision analysis for predictive paraffin control. Engineering Today.

OGUNMESA, O. (2021). Strategies Security Managers Used to Prevent Security Breaches in SCADA Systems' Networks.

OSARETIN, C. A. (2025). Feasibility study, design, dynamic modelling, simulation, and control of a solar-powered sucker rod oil pump.

RICCIO, C., MENANNO, M., ZENNARO, I., & SAVINO, M. M. (2024). A new methodological framework for optimizing predictive maintenance using machine learning combined with product quality parameters. Machines, 12(7), 443.

SNYTKO, A., JIMÉNEZ-CASTILLO, G., MUÑOZ-RODRÍGUEZ, F. J., & RUS-CASAS, C. (2025). Fault Diagnosis for Photovoltaic Systems: A Validated Industrial SCADA Framework. Applied Sciences, 15(23), 12656.

TAKACS, G. (2015). Sucker-rod pumping handbook: Production engineering fundamentals and long-stroke rod pumping. Gulf Professional Publishing.

TAKACS, G., & KIS, L. (2021). A new model to find optimum counterbalancing of sucker-rod pumping units including a rigorous procedure for gearbox torque calculations. Journal of Petroleum Science and Engineering, 205, 108792.

TIAN, H., DENG, S., WANG, C., NI, X., WANG, H., LIU, Y., MA, M., WEI, Y., & LI, X. (2021). A novel method for prediction of paraffin deposit in sucker rod pumping system based on CNN indicator diagram feature deep learning. Journal of Petroleum Science and Engineering, 206, 108986.

UCAR, A., KARAKOSE, M., & KIRIMÇA, N. (2024). Artificial intelligence for predictive maintenance applications: Key components, trustworthiness, and future trends. Applied Sciences, 14(2), 898.

VANI, G., NAVEENKUMAR, R., SINGHA, R., SHARKAR, R., & KUMAR, N. (2024). Advancing Predictive Data Analytics in IoT and AI Leveraging Real time Data for Proactive Operations and System Resilience.

WALI, A., & ALSHEHRY, F. (2024). A survey of security challenges in cloud-based SCADA systems. Computers, 13(4), 97.

WANG, X., HE, Y., LI, F., WANG, Z., DOU, X., XU, H., & FU, L. (2021). A working condition diagnosis model of sucker rod pumping wells based on deep learning. SPE Production & Operations, 36(02), 317–326.

YADAV, G., & PAUL, K. (2021). Architecture and security of SCADA systems: A review. International Journal of Critical Infrastructure Protection, 34, 100433.

Приборы контроля параметров скважин от компании Магматэк. (n.d.). Retrieved March 19, 2026, from https://www.mgtcontrol.ru/catalog/pribory-kontrolia-parametrov-skvazin

UNDERGROUND MINING ENGINEERING 48(2026) 83-90 UDK 62
UNIVERSITY OF BELGRADE - FACULTY OF MINING AND GEOLOGY ISSN 03542904

Original Scientific paper

DEVELOPMENT OF $LiGe_2(PO_4)_3$ CRYSTALLINE PHASE IN GLASS SUBJECTED TO NON ISOTHERMAL TREATMENT

Nataša Đorđević[1], Srđan Matijašević[2], Aleksandra Radulović[1], Slavica Mihajlović[2], Vladan Kašić[2], Milica Vlahović[3]

Received: April 13, 2026 **Accepted:** May 25, 2026

Abstract: The nucleation behavior of germanium phosphate glass under non isothermal conditions was examined using differential thermal analysis (DTA). The study focused on how both the duration and temperature of pre DTA heat treatment affect the characteristic DTA peak temperature (Tp). A complex relationship between these parameters was observed. At constant temperatures, extending the annealing time during the pre DTA treatment led to a reduction in the Tp value. Furthermore, the effect of pre DTA treatment temperature on DTA parameters revealed that, for annealing times longer than tind, the inverse dependence of Tp on T mirrored nfluence of temperature on nucleation rate (I), particularly in cases where the nucleation and crystallization regions partially overlapped. Differential thermal analysis (DTA), which we used in the manuscript, is one of the most reliable methods for monitoring phase transformations in glass systems. This method enables accurate detection of energy changes during heating. The application of this technique in non-isothermal conditions provides key data on the thermal stability of the samples and the kinetic parameters governing the crystallization process. Special importance is attached to the study of nucleation, which, as the initial phase of crystal growth, directly determines the final morphology and properties of the resulting glass-ceramic

Keywords: germanium phosphate glass, nucleation, non-isothermal conditions

[1] Institute of General and Physical Chemistry, 12 Studentski Trg, 11000 Belgrade, Serbia

[2] Institute for Technology of Nuclear and Other Mineral Raw Materials (ITNMS), 86 Franshet d' Esperey St., 11000 Belgrade, Serbia

[3] University of Belgrade, Institute of Chemistry, Technology and Metallurgy, National Institute of the Republic of Serbia, Njegoševa 12, 11000 Belgrade, Serbia

E-mails: natasa.djordjevic@iofh.bg.ac.rs, ORCID: https://orcid.org/0000-0002-2353-6751; s.matijasevic@itnms.ac.rs, ORCID: https://orcid.org/0000-0002-3897-8085; aradulovic@iofh.bg.ac.rs ORCID: https://orcid.org/0000-0001-8591-2946; s.mihajlovic@itnms.ac.rs, ORCID: https://orcid.org/0000-0003-0904-3878; v.kasic@itnms.ac.rs, ORCID: https://orcid.org/0000-0002-4430-567X; mvlahovic@tmf.bg.ac.rs ORCID: https://orcid.org/0000-0002-7893-9101

1 INTRODUCTION

NASICON (Na Super Ionic Conductor) type materials have been widely investigated due to their high ionic conductivity. In their crystalline form, these compounds follow the general formula $AB_2(PO_4)_3$, where A represents an alkali ion. The B site is typically occupied by a metal with a valency of four or higher, though trivalent elements can also substitute. Crystalline NASICON materials exhibit a rhombohedral $R\bar{3}c$ structure, characterized by (BO_6) octahedra connected through corner-sharing with (PO_4) tetrahedra. Their framework is notably "open," allowing alkali ions to migrate with reduced activation barriers, which makes them promising candidates for fast ion conductors (Rao, Sobha and Kumar, 2001; Anantharamulu et al., 2011).

Most syntheses of these materials rely on the traditional powder sintering technique, and many different compositions have been described. Alternatively, NASICON ceramics can be successfully prepared through glass ceramic processing (Cruz, Ferreira, and Rodrigues, 2009; Fu, 1998). Compared to sintered samples, glass ceramics offer significant advantages, as they can be easily shaped into desired dimensions and exhibit dense microstructures. Successful execution of this process depends on detailed knowledge of the crystallization characteristics of the glass precursor. Precisely defining the temperature ranges where phase transformations occur allows for the avoidance of undesirable secondary phases that could impair the electrical properties of the final product. Furthermore, controlling nucleation within the glass matrix directly influences microstructural homogeneity, which is vital for achieving high mechanical strength and stability under real operating conditions. Therefore, a detailed kinetic analysis of the process represents not only a theoretical challenge but also a practical necessity for the technological development of these materials.

NASICON materials have gained significant interest in the past few years as solid electrolytes for future lithium battery technologies, where ensuring safety and stability is essential. Because they unite excellent ionic conductivity with chemical stability, they are considered potential replacements for liquid electrolytes. Beyond ionic conductivity alone, it is essential to understand how the sample's thermal history influences grain-boundary formation, as these can act as significant barriers to ion transport. Optimizing these parameters through controlled glass crystallization offers a pathway toward developing materials that are not only high-performing but also economically viable for large-scale industrial production. Previous studies have shown that doping with elements such as Al, Ti, or Zr can further enhance conductivity and improve structural stability, but challenges remain in controlling nucleation and crystallization processes (Fokin et al., 2006; Wakasugi, Kadoguchi and Ota, 2001). Moreover, the compatibility of NASICON phases with metallic lithium is a crucial factor for their practical application in solid state batteries.

Germanophosphate glasses represent an attractive starting point for NASICON type glass ceramics because they combine high ionic conductivity with the ability to be

processed into various shapes. However, the parent glass is unstable in contact with molten lithium, which limits its direct application. Crystallization into $LiGe_2(PO_4)_3$ phases significantly improves chemical stability and compatibility with lithium anodes, while maintaining high lithium ion conductivity, often reaching values around 4×10^{-4} S/cm at room temperature (Matijašević et al., 2022). Furthermore, the incorporation of Al_2O_3 into the glass composition can lead to partial substitution of Ge^{4+} by Al^{3+}, compensated by Li^+ ions, resulting in the modified structure $Li_{1+x}Al_xGe_{2-x}(PO_4)_3$ and enhanced thermal stability (Đorđević et al., 2025).

In this study, emphasis is placed on the nucleation of the $LiGe_2(PO_4)_3$ phase in germanophosphate glass under non isothermal conditions. By investigating the influence of annealing time and temperature on nucleation behavior, the work aims to clarify the crystallization mechanism and its impact on ionic transport. The results are expected to contribute to a deeper understanding of NASICON type glass ceramics and their potential role as reliable solid electrolytes in advanced energy storage systems.

Reagent-grade Li_2CO_3, Al_2O_3, GeO_2, and $(NH_4)_2HPO_4$ were used as the initial raw materials. Following careful homogenization, the mixture was slowly heated to 300 °C to remove volatile species and subsequently melted at 1400 °C for half an hour in a platinum crucible. The resulting melt was poured onto a steel plate and allowed to cool in air. The obtained glass samples were transparent and free from visible gas inclusions. Chemical composition analysis was carried out using a spectrophotometer, specifically the AAS PERKIN ELMER Analyst 300.

2 EXPERIMENTAL

Non isothermal differential thermal analysis was conducted on a Netzsch STA 409 EP instrument, employing Al_2O_3 powder as the reference material. Each run used 100 mg of sample, heated at 10 °C per minute, and nucleation was examined in glass powders with particle sizes ranging from 0.50 to 0.65 mm. Heating was performed in alumina crucibles at 10 °C/min, starting from room temperature (T = 20 °C) up to selected temperatures in the range of 500–620 °C. These target temperatures were then maintained for varying durations of 15, 30, 60, 120, 180, and 300 minutes.

For the thermal treatment, a Carbolite CWF 13/13 furnace was used, offering automatic regulation and precise temperature control within ±1 °C. After annealing, the samples were cooled to room temperature and subsequently reheated in the DTA system at a constant heating rate of 10 °C/min, starting at 20 °C and reaching 800 °C.

To determine phase composition, XRD analysis was performed using a Philips PW 1710 diffractometer. The instrument employed a copper tube running at 40 kV and 32 mA. Patterns were recorded across the 2θ interval of 4–70°, with 0.25 s per step and increments of 0.02°. Divergence and receiving slits were maintained at 1 and 0.1 units,

respectively. Measurements were taken at room temperature with the sample mounted in a stationary holder.

3 RESULTS AND DISCUSSION

Chemical analysis confirmed that the obtained glass composition was $22Li_2O \cdot 10Al_2O_3 \cdot 30GeO_2 \cdot 38P_2O_5$ (mol%). This formulation is close to the stoichiometric NASICON type solid electrolyte $Li_{1.5}Al_{0.5}Ge_{1.5}(PO_4)_3$. Powder X ray diffraction (XRD) verified that the quenched melt was vitreous. The XRD pattern of samples subjected to thermal treatment at 800 °C for 100 h (Fig. 1) revealed the formation of $LiGe_2(PO_4)_3$ (JCPDS 80 1922) and GeO_2 (JCPDS 83 0543) phases during crystallization. Rietveld profile fitting indicated that the glass transformed into a two phase glass ceramic, consisting predominantly of $LiGe_2(PO_4)_3$ (97.5%) with GeO_2 as a minor secondary phase (2.5%).

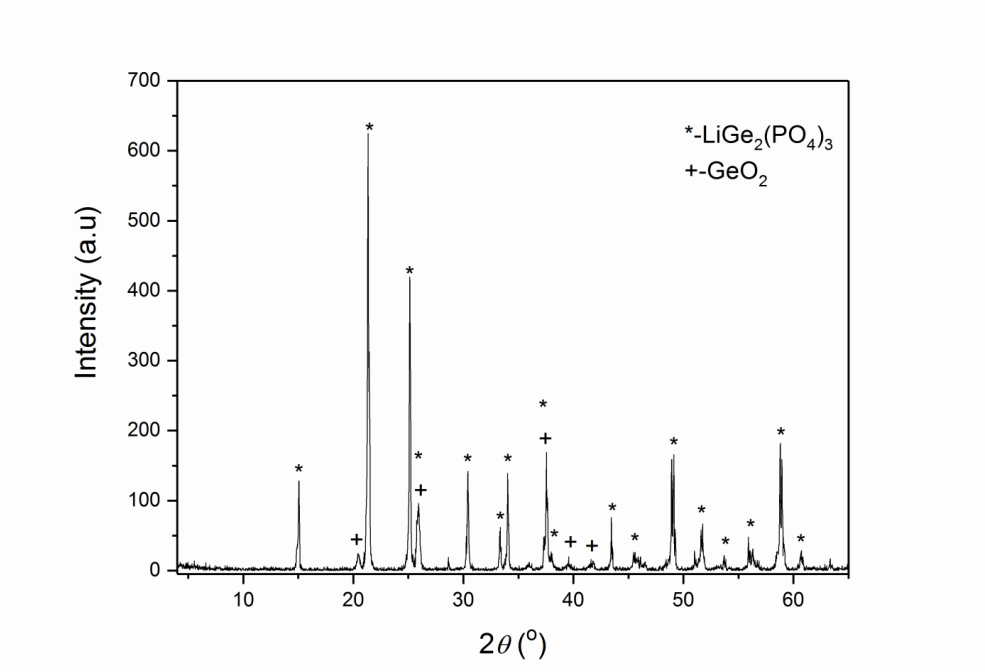

Figure 1 Diffraction pattern obtained from the glass sample after annealing at 800 °C for 100 h.

The results indicate that the trace presence of GeO_2 originates from slight deviations in the glass composition compared to the nominal formulation, caused by batch evaporation during melting. Consequently, only the crystallization of the $LiGe_2(PO_4)_3$ phase was taken into account. According to the JCPDS card, aluminium is not part of the $LiGe_2(PO_4)_3$ structure, although it is generally assumed that Al can enter the lattice as a

solid solution. When Al_2O_3 is introduced, Ge^{4+} cations are partially substituted by Al^{3+}, creating a charge imbalance that is compensated by Li^+ ions. This leads to the modified structure $Li_{1+x}Al_xGe_{2-x}(PO_4)_3$ and simultaneously enhances the thermal stability of the glass network. For the investigated composition, aluminium was present below the detection limit of XRD analysis (Đorđević et al., 2025).

A straightforward method for evaluating nucleation parameters in glasses was introduced through DTA analysis (Ray and Day, 1990; Kelton, 1992). The technique involves subjecting a small portion of the glass to isothermal treatment at a chosen temperature (T) for a specified duration (t), after which the sample is reheated in a DTA device at a constant rate until crystallization is completed. This procedure was carried out for several values of T, while parameters such as annealing time, heating rate (β), sample mass, and particle size remained unchanged. By plotting the reciprocal of the peak temperature (Tp^{-1}) against the nucleation temperature, a curve resembling the nucleation rate was obtained, enabling determination of the effective nucleation interval and the temperature at which nucleation reaches its maximumThe DTA curves showing the variation of Tp with annealing time at 550 °C are presented in Figure 2.

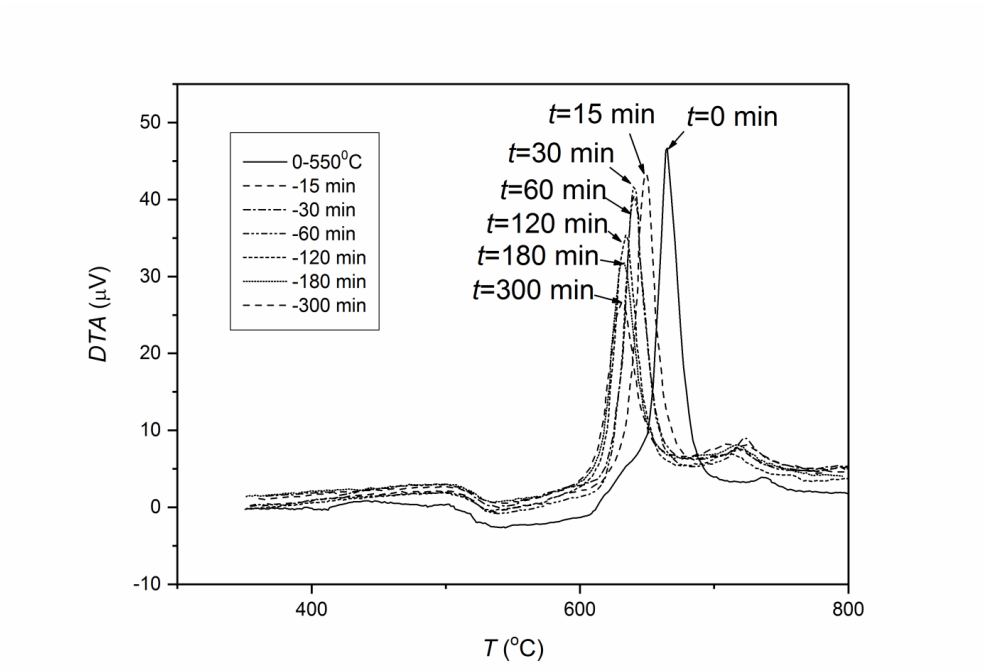

Figure 2 Differential thermal analysis curves of glass powders with particle sizes between 0.5 and 0.65 mm, subjected to annealing at 550 °C for different times.

It can be observed that the peak temperature (Tp) decreases with longer annealing times, and the intensity of the peak also diminishes over time. Such behavior corresponds to

polymorphic crystallization, in which prolonged heat treatment raises the number of nuclei and consequently shifts the exothermal peak to lower temperatures (Wakasugi, Kadoguchi, and Ota, 2001). A comparable trend was noted for the parameter ΔTp, defined as the difference between the crystallization peak temperatures of untreated and heat treated samples, although the change occurred in the opposite direction. In contrast, variations in the exothermal peak height (δTp) as a function of annealing time at selected temperatures differ from those observed for Tp^{-1} and ΔTp.

Figure 3 presents the curves showing the dependence of Tp^{-1} on temperature.

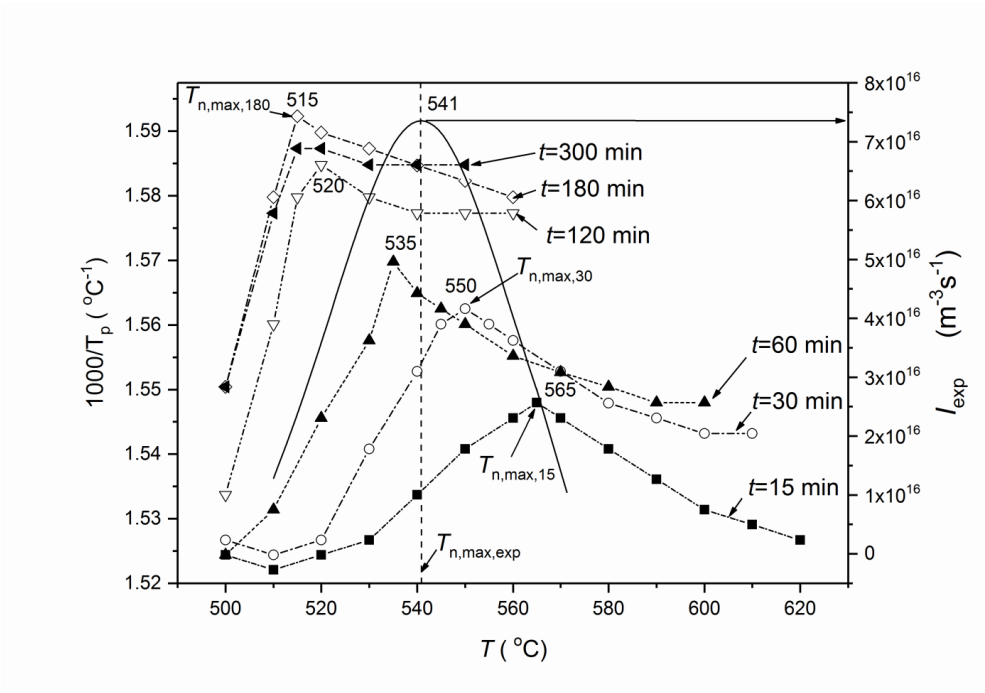

Figure 3 "Variation of parameters with temperature: a) Tp^{-1} plotted on the left ordinate (curves generated by fitting experimental observations).

"b) Right axis. The nucleation curve was measured under isothermal conditions. As depicted in Figure 3, Tp^{-1} shows a complex temperature dependence: it rises, reaches a maximum, and then declines, producing the well known bell shaped profile typical of glasses (Matijašević et al., 2022). For short treatment times below 30 minutes, the maxima were displaced to higher temperatures, while longer annealing progressively aligned them with the temperature of maximum nucleation.

"For annealing durations between 30 and 60 minutes, the curve maxima were located near the temperature corresponding to the highest nucleation rate (Tn,max). This trend reflects transient nucleation. At shorter treatment times, fewer nuclei developed, which caused the crystallization peaks to appear at elevated temperatures. In these cases, a

significant portion of the glass phase remained untransformed, producing curves shifted toward higher temperatures. With longer annealing, the crystalline fraction expanded, and the right side of the curves progressively moved to lower temperatures. When t exceeded 120 minutes, a pronounced narrowing of the right-hand side of the curves was evident. Because the nucleation and growth temperature ranges in this glass partly overlap, the crystalline fraction increased quickly with rising temperature, ultimately resulting in complete crystallization of the sample.

The maximum nucleation rate (Iexp = 7.34×10^{16} $m^{-3}s^{-1}$), determined from isothermal experiments, was found at Tn,max = (541 ± 5) °C (Figure 3, solid curve). The obtained glass composition exhibits a remarkably high nucleation rate compared to previously reported inorganic glass systems (Fokin et al., 2006)

4 CONCLUSION

"The nucleation characteristics of $22Li_2O{\cdot}10Al_2O_3{\cdot}30GeO_2{\cdot}38P_2O_5$ (mol%) glass under non isothermal conditions were examined. Results confirmed that the glass undergoes polymorphic crystallization, producing $LiGe_2(PO_4)_3$ phases. Analysis of pre DTA heat treatment effects on the peak temperature (Tp) revealed that, at constant temperatures between 500 and 620 °C, longer annealing times led to a reduction in Tp, approaching values typical of the quenched glass. When annealing times were varied between 15 and 300 minutes, the DTA parameters showed complex behavior. For short treatments ($t <$ 30 min), the maxima in Tp^{-1} vs. T plots were shifted above the temperature of maximum nucleation. At intermediate durations (30–60 min), the maxima aligned with the peak nucleation rate, while extended annealing shifted the maxima toward lower temperatures

Acknowledgment

The authors would like to thank the Ministry of Science, Technological Development and Innovations of the Republic of Serbia for support (Grant No: 451-03-33/2026-03/200023, and 451-03-66/2024-03/200026).

REFERENCES

RAO, K.J., SOBHA, K.C. and KUMAR, S. (2001) Infrared and Raman spectroscopic studies of glasses with Nasicon type chemistry. Chemical Science, 113, pp. 497-514. https://doi.org/10.1007/BF02708786

ANANTHARAMULU, N., et al. (2011) A wide-ranging review on Nasicon type materials. Journal of Materials Science, 46, pp.2821-2837. https://doi.org/10.1007/s10853-011-5302-5

CRUZ, A. M., FERREIRA, E.B. and RODRIGUES, A.C.M. (2009) Controlled crystallization and ionic conductivity of nanostructured LiAlGePO4 glass-ceramic. Journal of Non-Crystalline Solids, 355, pp. 2295-2301. https://doi.org/10.1016/j.jnoncrysol.2009.07.012

FU. J. (1998) Fast Li+ ion conduction in Li2O-(Al2O3, Ga2O3)-TiO2-P2O5 glass-ceramics. Journal of Materials Science, 33, pp. 1549-1553. https://doi.org/10.1023/A:1017559619391

Đorđević, N., et al. (2025) The Effect of Particle Size on the Crystallization LiGe2(PO4)3 Phase from Glass. Science of Sintering, 57, pp. 43-52. https://doi.org/10.2298/SOS231111064D

RAY, C.S. and DAY, D.E. (1990) Determining the Nucleation Rate Curve for Lithium Disilicate Glass by Differential Thermal Analysis. Journal of the American Ceramic Society, 73, pp. 439-442. https://doi.org/10.1111/j.1151-2916.1990.tb06532.x

KELTON, K.F. (1992) Estimation of the Nucleation Rate by Differential Scanning Calorimetry. Journal of the American Ceramic Society, 75, pp. 2449-2452. https://doi.org/10.1111/j.1151-2916.1992.tb05597.x

WAKASUGI, T., KADOGUCHI, T. and OTA, R. (2001), Evalution of the number density of nuclei in Li2O·SiO2 glass by DTA method. Journal of Non-Crystalline Solids, 290, pp. 64-72. https://doi.org/10.1016/S0022-3093(01)00718-9

MATIJAŠEVIĆ, S., et al. (2022) The Analysis of the Nucleation Process of the Lithium Germanium Phosphate Glass. Science of Sintering, 54, pp. 321-324. https://doi.org/10.2298/SOS2203321M

FOKIN, V.M., et al. (2006) Homogeneous crystal nucleation in silicate glasses: A 40 years perspective. Journal of Non-Crystalline Solids, 352, pp. 2681-2714. https://doi.org/10.1016/j.jnoncrysol.2006.02.074

UNDERGROUND MINING ENGINEERING 48(2026) 91-108 UDK 62
UNIVERSITY OF BELGRADE - FACULTY OF MINING AND GEOLOGY ISSN 03542904

Original scientific paper

CORRELATION BETWEEN UNIAXIAL COMPRESSIVE STRENGTH AND WATER CONTENT OF BEOČIN MARLS

Vladimir Čebašek[1], Veljko Rupar[1], Dragutin Jovković[1], Nikola Živanović[2]

Received: May 22, 2026 **Accepted:** June 24, 2026

Abstract: The uniaxial compressive strength (UCS) is one of the most important strength parameters for evaluating the mechanical behavior of rocks and is widely used as a fundamental input in rock mass characterization systems, empirical classifications, strength criteria, and various engineering design and calculation methods. Weak rocks, such as marls, exhibit a pronounced sensitivity to water content, which can significantly influence their strength and deformation characteristics. This paper investigates the correlation between water content and the reduction in UCS of marl samples. A series of laboratory tests were conducted on specimens with varying water contents. The results show a clear inverse relationship between water content and UCS, with strength decreasing progressively as water content increases. This reduction is attributed to the weakening of interparticle bonds, softening of the clay matrix, and increased pore water effects within the rock structure. The experimental data were analyzed to establish empirical relationships between water content and UCS reduction, providing a basis for predicting strength degradation under different environmental conditions. The findings highlight the critical role of water content in controlling the mechanical behavior of marls and emphasize the need to account for water content in geotechnical design and stability assessments in marl formations.

Keywords: uniaxial compressive strength (UCS), water content, marls

1 INTRODUCTION

The uniaxial compressive strength (UCS) is one of the most fundamental mechanical parameters used to characterize intact rock and plays a central role in rock mass classification systems, empirical strength criteria, and engineering design methods. Reliable estimation of UCS is essential for evaluating the stability of slopes, foundations, and underground excavations. However, in weak rocks such as marls, UCS is highly

[1] Faculty of Mining and Geology, University of Belgrade, Djusina 7, 11000 Belgrade, Serbia

[2] Faculty of Forestry, University of Belgrade, Knez Viseslava 1, 11030 Belgrade Serbia

E-mails: vladimir.cebasek@rgf.bg.ac.rs ORCID: https://orcid.org/0000-0002-8667-2339;
veljko.rupar@rgf.bg.ac.rs ORCID: https://orcid.org/0000-0002-0296-8467;
dragutin.jovkovic@rgf.bg.ac.rs ORCID: https://orcid.org/0000-0001-7324-6034;
nikola.zivanovic@sfb.bg.ac.rs ORCID: https://orcid.org/0000-0003-0340-5516

sensitive to environmental factors, particularly water content, which can significantly alter strength and deformability and introduce uncertainty into engineering design.

Marls are transitional sedimentary rocks composed of varying proportions of clay minerals and calcium carbonate. Figure 1 represents the conventional mineralogical composition of the marls. The yellow shadow is to highlight the three sections where the marls are located. Clay mineral range between 25–75% and calcium carbonate range 75 – 25%. The rest up to 10% is mostly in the form of quartz and feldspar (Bahhou et al., 2021).

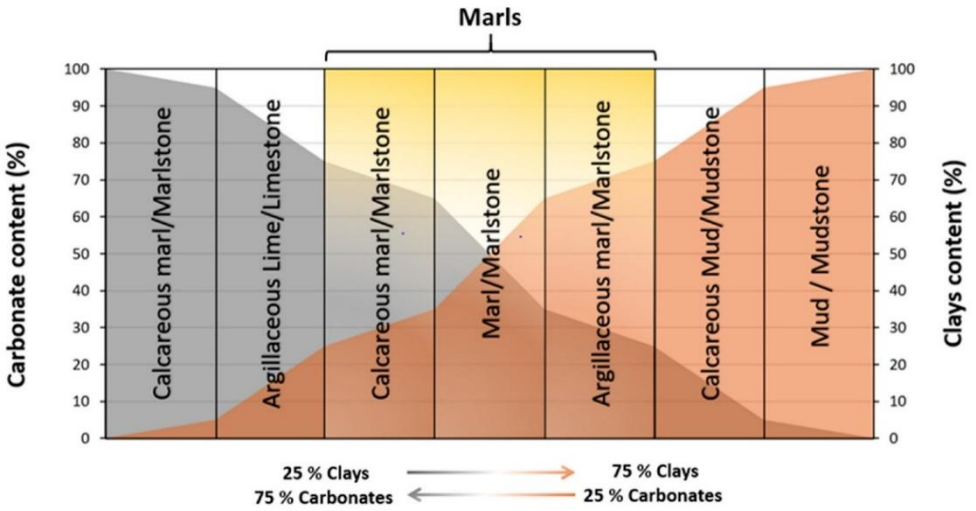

Figure 1 Conventional marls classification (Bahhou et al., 2021)

Due to this heterogeneous composition, marls exhibit complex mechanical behavior that can range from soil-like to rock-like depending on mineralogy, structure, and degree of cementation (Jaeger, 2007; Hoek & Brown, 1997). Their engineering properties are strongly controlled by factors such as clay content, porosity, and bonding, resulting in high variability in strength and stiffness (Bell, 2007). Recent studies further confirm that marl properties span a wide spectrum, from low-strength friable materials to well-cemented rocks with relatively high UCS values (Görög & Török, 2026).

A defining characteristic of marls is their strong sensitivity to water. Numerous experimental studies have demonstrated that increasing water content leads to a significant reduction in UCS (Vásárhelyi & Ván, 2006; Hawkins & McConnell, 1992). This behavior is primarily attributed to the softening of the clay matrix, degradation of interparticle bonding, and the influence of pore water pressure. Recent research confirms that the UCS of marls decreases noticeably under saturated conditions, even when initial dry strength is relatively high (Görög & Török, 2026). In addition, water affects the internal microstructure, leading to increased deformability and reduced stiffness.

The influence of water content on strength is not limited to marls but is a well-established phenomenon in other weak and clay-bearing rocks. Recent experimental and numerical studies show that water-rock interaction induces softening, crack propagation, and mechanical degradation under coupled hydro-mechanical conditions (Vásárhelyi & Ván, 2006; Cheng et al., 2024). Similarly, investigations on mudstones and other clay-rich geomaterials demonstrate that water absorption leads to swelling, microstructural changes, and significant reductions in strength due to physicochemical interactions (Wang & Yan, 2023; Comakli & Bayramov, 2024). These findings reinforce the understanding that water plays a critical role in weakening geomaterials, especially those containing clay minerals.

Recent literature has also focused on quantifying the relationship between water content and strength reduction. For example, studies on building stones indicate that UCS can decrease by up to 20–45% between dry and saturated states, with a large portion of strength loss occurring at relatively low water content levels (Tomor et al., 2024). This nonlinear behavior has also been observed in marls and similar materials, where rapid initial strength loss is followed by a more gradual decline with increasing saturation (Tomor et al., 2024; Bensaada et al., 2023). Such findings highlight the importance of considering partial saturation conditions in addition to fully dry and fully saturated states.

In parallel, recent research has explored stabilization and improvement techniques for marl materials to mitigate water content-induced weakening. For instance, the use of nanosilica additives has been shown to enhance the stability and durability of marl soils by modifying their microstructure and reducing deleterious reactions (Amiri et al., 2024). Other studies have investigated lime and thermal treatments, showing that controlled stabilization can significantly increase UCS and alter the material's microstructural behavior (Bensaada et al., 2023).

Despite these advances, predicting the strength behavior of marls remains challenging due to their inherent heterogeneity and sensitivity to environmental conditions. Existing empirical models often require calibration for specific materials and geological settings. Therefore, site-specific investigations are essential for accurately assessing the relationship between water content and UCS.

This paper focuses on marl formations located in Beočin, where such weak rocks are widely encountered in engineering practice. The geological conditions of this area provide a suitable framework for investigating the effects of water content on rock strength. The primary objective of this research is to examine the correlation between water content and UCS reduction through laboratory testing. By establishing empirical relationships tailored to the studied material, this work aims to improve the understanding of water content-dependent behavior and contribute to safer and more reliable geotechnical design in marl-dominated environments.

1.1 Cement Marl Mining at the "Filijala" Open Pit

The early exploitation of Beočin marlstone, locally referred to as “Beočin Kaja,” dates back to the 19th century. According to historical records from 1839, the British engineer Adam Clark used Beočin marlstone for the construction of the piers of the Széchenyi Chain Bridge between Buda and Pest. However, due to the lack of reliable documentation, it remains unclear whether Adam Clark can be credited with the “discovery” of this material, or whether it had already been exploited and used earlier, as suggested in some historical accounts (Vlajić et al., 2019).

In 1855, Josif Čik acquired the Beočin quarry from the company Weiner Wasser Bauamt and initiated the production of Roman cement at the present-day Filijala mining field, thereby establishing the first cement plant within the Habsburg Monarchy (Vlajić et al., 2019). The modernization of the production process was completed in 1869, when Portland cement manufacturing commenced. This period corresponds to the broader historical transition from natural (Roman) cement to Portland cement, which became the dominant construction material in the late 19th century (Varas et al., 2005).

The “Filijala” cement marl deposit, where the open-pit mine of the same name is located, represents the principal source of raw material for cement production today. The deposit consists of three mining sectors of unequal size and degree of exploitation: “Severno polje” (Northern Field), “Srednje polje” or “Međupolje” (Central Field), and “Južno polje” (Southern Field) (Ganić et al., 2012). The marl belongs to Upper Miocene (Pannonian) deposits and has been extensively studied in terms of its lithological and engineering-geological properties, Figure 2 and 3 (Ganic et al., 2010).

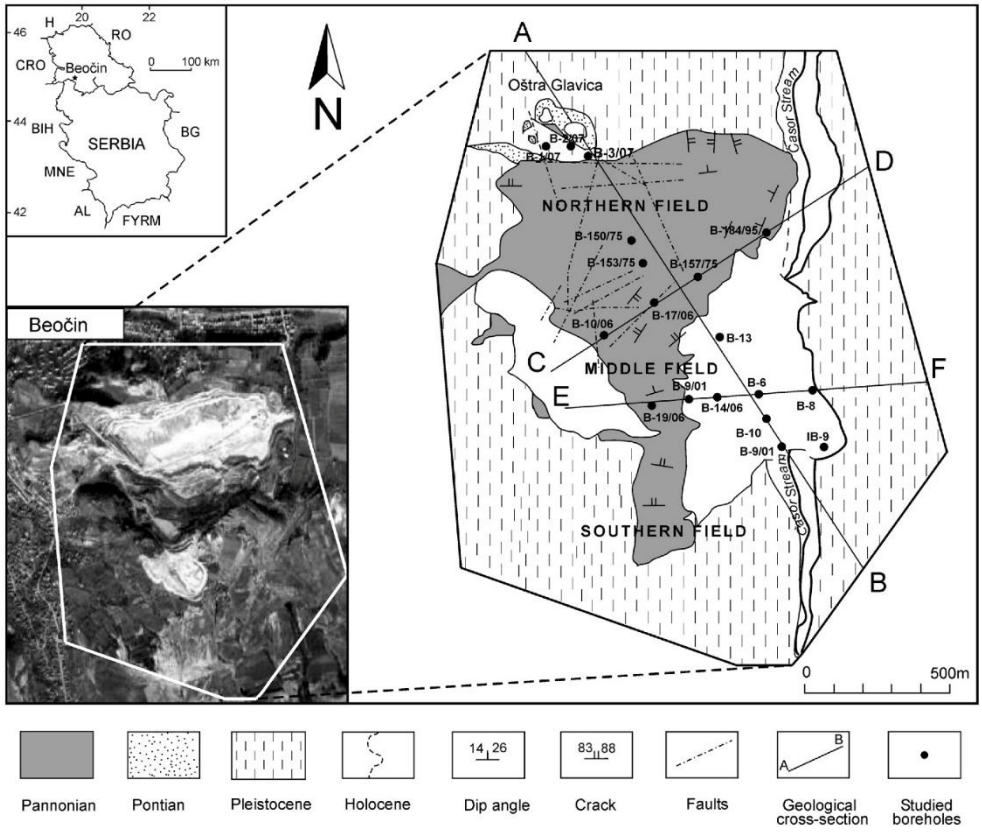

Figure 2 The geological sketch map of the "Filijala" Open Pit near Beočin. (Ganic et al., 2010)

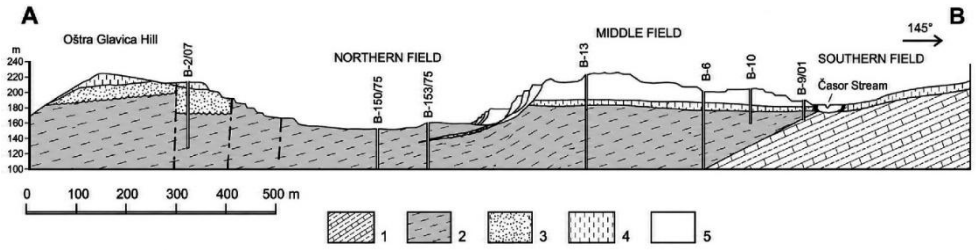

Figure 3 Geological cross-section A–B through the Miocene sediments on the "Filijala" Open Pit near Beočin. Legend: 1, Sarmatian (only in cross section) laminated marl, sandy marl, banded silty marl and siltstone, marly sandstone, stratified sandy limestone, lenses of conglomeratic marl, coaly clay, etc.; 2, Pannonian marl; 3, Pontian sand; 4, Pleistocene loess; 5, Holocene alluvial–prolluvial deposits, recent delluvial deposits and artificial deposits. (Ganic et al., 2010)

The “Filijala” Open Pit was initially developed within the “Severno polje” mining area. With the advancement and expansion of mining operations, the open-pit mine progressively evolved in accordance with production requirements and geological conditions (Vu et al., 2021).

The primary exploitation method is continuous mining technology, employing a bucket wheel excavator system, which remains widely used in large-scale surface mining due to its high production capacity and efficiency in homogeneous soft rock formations (Čelebić et al., 2024). However, due to variable geological and geotechnical conditions in cement marl deposits—such as heterogeneity, changes in water content, and variable strength—exclusive application of continuous mining is not feasible across the entire deposit (Vu et al., 2021).

Consequently, discontinuous mining technology is also applied. This method is used in zones where bucket wheel excavators cannot operate effectively due to high digging resistance, lithological variability, or selective extraction requirements (Čelebić et al., 2024). In addition, coordinated use of continuous and discontinuous systems is applied to ensure blending, quality control, and homogenisation of cement marl prior to processing in cement production plants (Vu et al., 2021).

Modern optimisation approaches in open-pit mining also highlight the importance of integrated production scheduling, equipment allocation, and haulage system design to improve efficiency and reduce operational costs, particularly in systems combining truck–shovel and continuous conveyor-based mining technologies (Čelebić et al., 2024).

1.2 Mineralogical–Petrographic and Chemical Composition of Marl

Mineralogical–petrographic investigations determined that the analyzed rock material can be classified as marl. The microcrystalline groundmass of the marl from the Filijala Deposit consists of approximately 75% finely dispersed carbonate material and about 23% clay fraction, dominated by montmorillonite with the presence of hydromica–illite. The coarser (sand-sized) fraction is represented by up to 2% of the rock mass and consists of rare angular grains of quartz, feldspar, fossil fragments, and occasional flakes of hydromica (Mihajlović et al., 2007).

Based on the statistical analysis of the chemical composition test results, the variability of the qualitative properties of the marl was determined. The statistical parameters describing the variability of the chemical properties of marl from the Filijala Deposit are presented in Table 1 (Mihajlović et al., 2007).

Table 1 Parameters of variability of chemical properties of marl

Component	Minimum value (%)	Maximum value (%)	Mean value (%)	Standard deviation (%)	Coefficient of variation (%)
SiO_2	7.420	31.841	18.362	2.838	15.454
Al_2O_3	2.71	7.957	6.061	0.994	16.401
Fe_2O_3	2.100	4.552	3.256	0.464	14.252
CaO	4.780	41.210	35.015	3.730	10.652
MgO	0.650	3.040	2.126	0.435	20.441
SO_3	0.526	3.934	1.738	0.415	23.857
$CaCO_3$	46.457	73.606	63.787	4.008	6.284
Loss on ignition (LOI)	23.216	37.760	31.520	1.640	5.204

With the modernization of the technological process and the application of the “dry process” for cement production, it is necessary to ensure that the technological requirement of a minimum $CaCO_3$ content of 60% is satisfied in the marl transported from the open-pit mine. The average $CaCO_3$ content in the “Severno polje” (Northern Field) mining sector is 64.42%, while in the “Južno polje” (Southern Field) it is 62.55%.

2 FIELD INVESTIGATIONS

At the test location within the "Filijala" Open-pit Mine, a detailed investigation program was conducted, comprising both field investigations and geomechanical laboratory testing. The field investigations included exploratory borehole drilling with continuous core recovery, followed by detailed core logging and mapping. A total of sixteen exploratory boreholes were drilled within the test zone of the open-pit mine, Figure 4

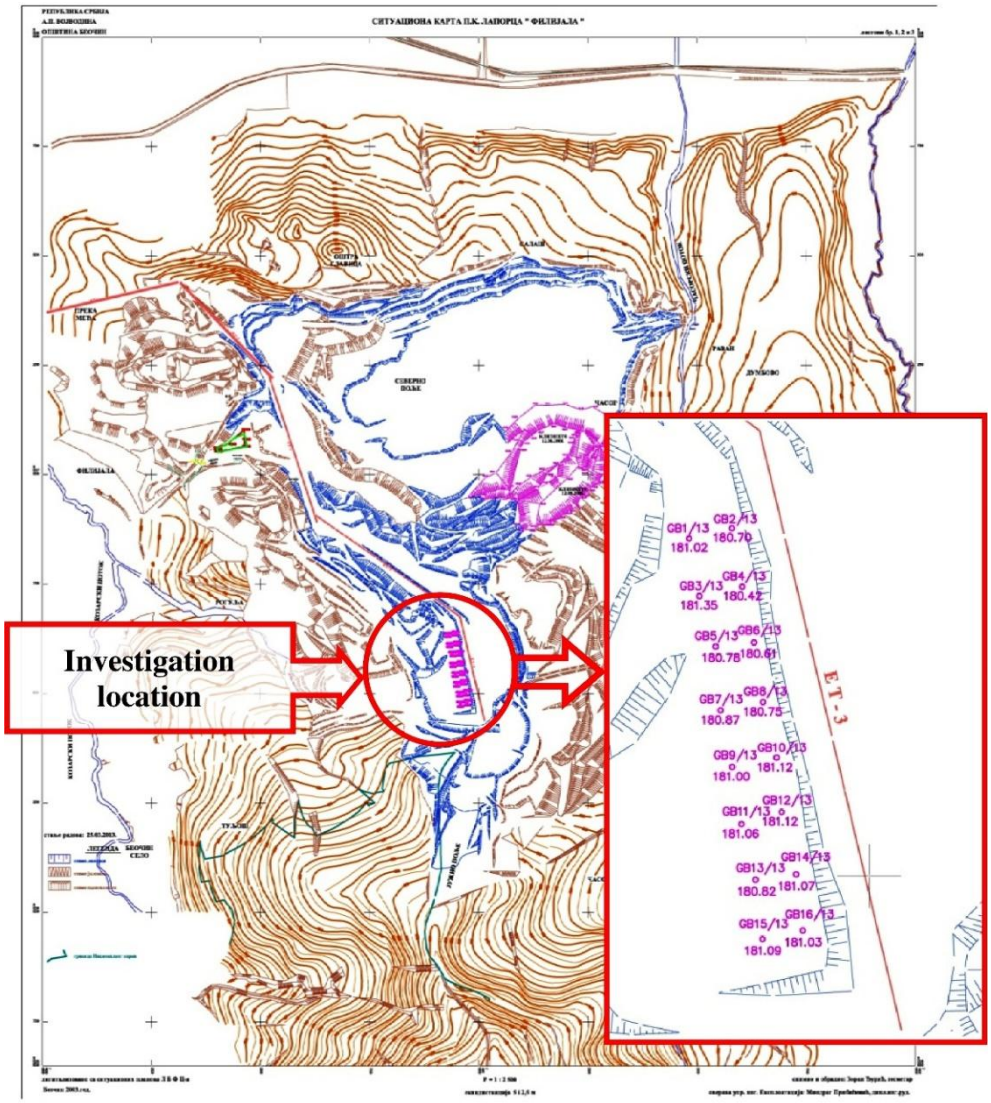

Figure 4 Disposition of investigation works at the test location within the "Filijala" Open Pit

Exploratory drilling was performed using a rotary drilling system with continuous coring. For this purpose, a GAK-300 drilling rig, together with the associated drilling equipment, was utilized. The primary objective of the field investigations was to determine the geological structure of the investigated micro-location. Based on the core logging results, representative intact rock material samples were selected, labeled, and prepared for subsequent geomechanical laboratory testing.

2.1 Methodology of Laboratory Testing

Cylindrical specimens were prepared in accordance with the recommendations of International Society for Rock Mechanics and ASTM International. The specimens were ground to obtain smooth, flat, and parallel end surfaces. The average specimen diameter was 85 mm, while the length-to-diameter ratio was 2.0.

Prior to testing, the dimensions and mass of each specimen were measured using a digital caliper and laboratory balance with precision of 0.01g. The water content condition of the samples was preserved during storage and preparation to ensure that the specimens used in the first testing group accurately reflected the in-situ conditions of the marl material.

Uniaxial compressive strength testing

Uniaxial compressive strength testing was conducted according to ISRM Suggested Methods (Ulusay & Hudson, 2007) and ASTM D7012 standards (ASTM D7012-07, 2007). Cylindrical specimens with a length-to-diameter ratio of approximately 2 were prepared from intact marl samples collected from the open-pit deposit. The specimen ends were ground flat and parallel prior to testing. Axial compression tests were performed using a servo-controlled hydraulic testing machine under displacement-controlled loading conditions at a constant stress rate of 0.5 MPa/s until failure, Figure 5. The UCS values were calculated as the ratio between the peak axial load and the original cross-sectional area of the specimen:

$$UCS = \frac{P}{A} \tag{1}$$

where:

- UCS is the uniaxial compressive strength (MPa),
- P is the maximum (peak) axial load (N),
- A is the initial cross-sectional area of the specimen (m^2).

a) Before testing *b) After testing*

Figure 5 Appearance of marl testing specimens before (a) and after (b) uniaxial compressive strength (UCS) testing

Water content testing

The water content was determined by oven drying representative samples at 105 °C until constant mass was achieved. The water content was calculated as:

$$w = \frac{m_w - m_d}{m_d} \cdot 100 \quad (2)$$

where:

w is the water content (%),

m_w is the wet mass,

m_d is the dry mass.

2.2 Test Results

Uniaxial compressive strength (UCS) tests were conducted in five groups, each consisting of six test specimens. After the first testing series, the remaining specimens were placed in a drying oven and dried at a temperature of 105 °C. Considering the relatively large volume of the specimens, the subsequent series of specimens were tested after 48 hours of drying. The results of the uniaxial compressive strength (UCS) tests and water content of the test specimens, obtained according to the previously described procedure, are presented in Table 2.

Table 2 Uniaxial compressive strength (UCS) and water content test results

Specimen group	Property	Specimen No.					
		1	**2**	**3**	**4**	**5**	**6**
1	UCS (MPa)	5.25	5.63	5.71	4.99	5.63	5.50
	w (%)	24.51	24.68	25.24	25.26	25.61	26.08
2	UCS (MPa)	6.17	6.50	6.41	5.86	6.48	6.28
	w (%)	12.07	13.36	13.77	14.03	14.19	14.28
3	UCS (MPa)	6.99	6.67	6.52	7.52	7.05	7.04
	w (%)	6.04	6.32	6.46	6.49	6.84	7.81
4	UCS (MPa)	7.26	7.39	6.94	7.71	6.91	7.06
	w (%)	2.9	3.3	3.55	3.88	4.31	4.57
5	UCS (MPa)	7.08	7.60	7.41	7.35	7.47	7.79
	w (%)	1.63	1.94	2.14	2.16	2.37	2.69

2.3 UCS–Water Content Correlation Analysis

The relationship between uniaxial compressive strength (UCS) and water content was analyzed in order to evaluate the influence of water content on the mechanical behavior of marl samples from the “Filijala” open-pit deposit. Variations in water content significantly affect the strength and deformation properties of weak sedimentary rocks due to softening of the clay fraction, degradation of carbonate cementation, and reduction of interparticle bonding (Hawkins & McConnell, 1992) (Vasarhelyi, 2005).

The laboratory-determined UCS values were correlated with the corresponding natural water content values obtained for each specimen. Correlation analysis was performed

using both linear and nonlinear regression models to identify the most representative relationship between the investigated parameters.

The general linear regression model can be expressed as:

$$UCS = a - b \cdot w \tag{3}$$

where:

- *UCS* is the uniaxial compressive strength (MPa),
- *w* is the water content (%),
- *a* and *b* are empirical regression coefficients.

In addition to the linear relationship, exponential regression analysis was evaluated because weak rocks commonly exhibit nonlinear strength degradation with increasing water content (Erguler & Ulusay, 2009).

The exponential model is defined as:

$$UCS = a \cdot e^{-b \cdot w} \tag{4}$$

where:

a and *b* are experimentally determined constants,

e is the base of the natural logarithm.

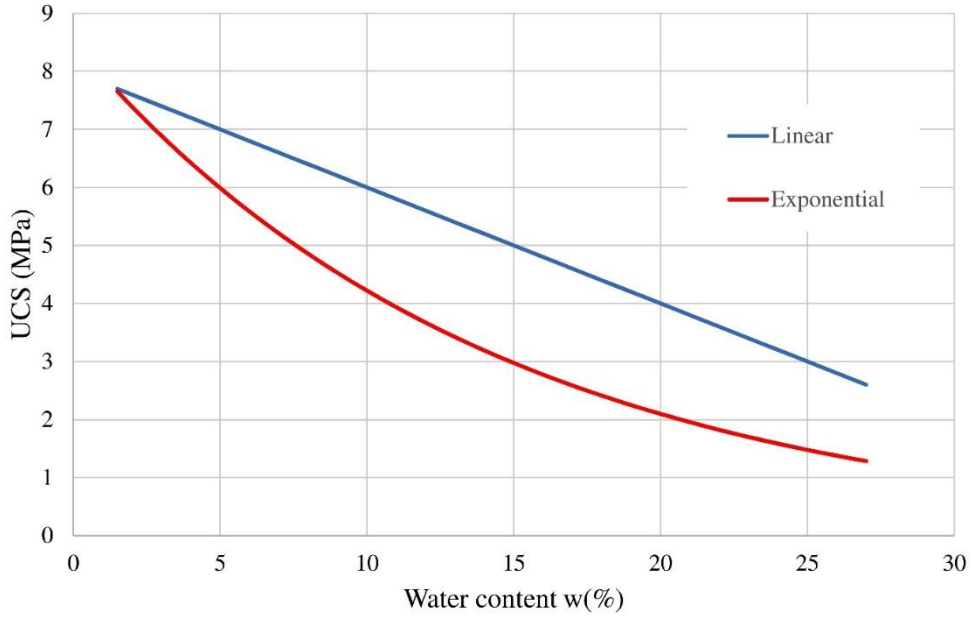

Figure 6 UCS–water content linear and nonlinear (exponential) correlation analysis

The goodness of fit of the regression models was evaluated using the coefficient of determination.

$$R^2 = 1 - \frac{\sum(y_i - \hat{y}_i)^2}{\sum(y_i - \bar{y})^2} \tag{5}$$

where:

- y_i represents measured UCS values,
- $\hat{y}_i$ represents predicted UCS values,
- $\bar{y}$ is the mean UCS value

A higher R^2 value indicates a stronger correlation between UCS and water content.

Based on the results presented in Table 2, the correlation analysis between UCS and water content (w) was performed for a linear correlation (Figure 7) and an exponential correlation (Figure 8).

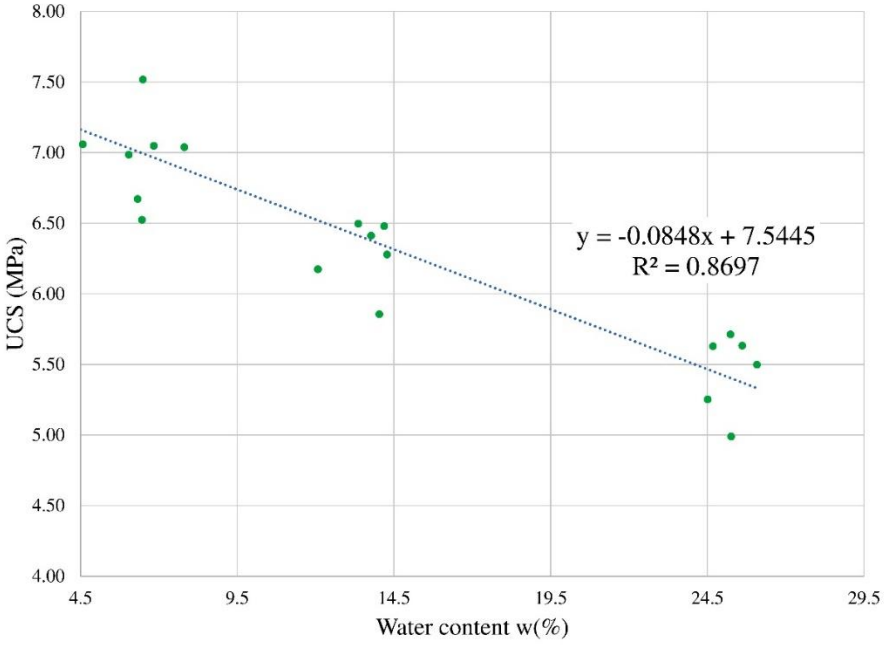

Figure 7 UCS–water content linear correlation analysis

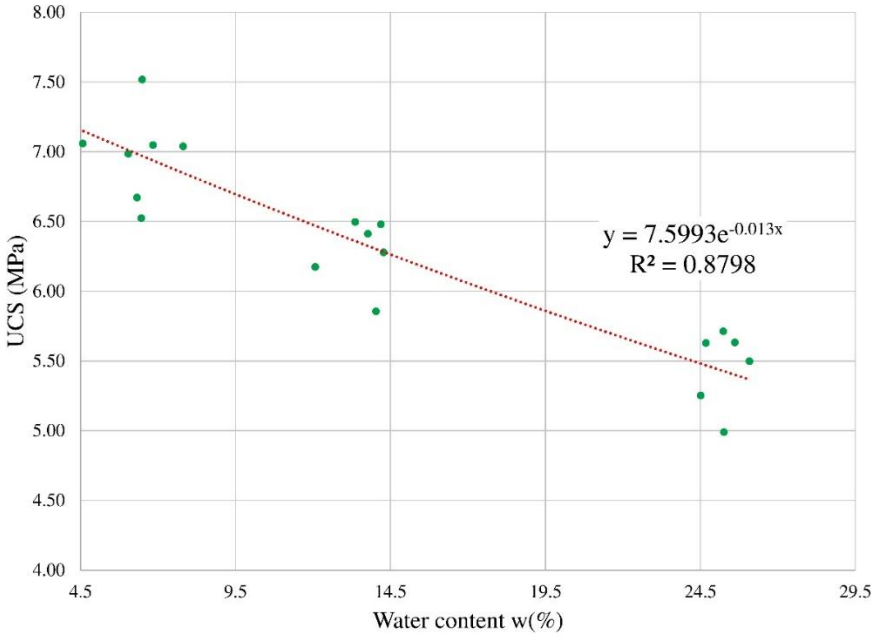

Figure 8 UCS–water content exponential (nonlinear) correlation analysis

Based on the analyses presented in Figures 7 and 8, the following correlation relationships between UCS and water content were established:

Linear correlation: $UCS = -0.0848 \cdot w + 7.5445$, $R^2 = 0.8697$

Exponential (nonlinear) correlation: $UCS = 7.5993 \cdot e^{-0.013 \cdot w}$, $R^2 = 0.8798$

Analysis of the coefficient of determination (R^2) values indicates that the exponential correlation has slightly greater potential for predicting UCS values for different water content (w) levels.

3 CONCLUSION

The investigated marls, known as "Pannonian marl" are composed of approximately 75% microcrystalline carbonate and 23% clay fraction (primarily montmorillonite and hydromica-illite). Chemical analysis confirms a mean $CaCO_3$ content of approximately 63.79%, meeting the industrial requirement of 60% for "dry process" cement production.

Previous investigations have demonstrated that increasing water content generally causes a substantial reduction in UCS due to:

- weakening of clay mineral bonds,
- dissolution and softening of carbonate cement,
- propagation of microcracks,
- reduction in matric suction,
- increase in pore-water pressure effects (Vasarhelyi, 2003).

These weakening mechanisms are especially pronounced in marls and other weak sedimentary rocks characterized by alternating carbonate and clay-rich components. water content-sensitive behavior significantly influences the stability of slopes, excavation faces, and foundation materials in open-pit mining and geotechnical engineering applications (Sabatakakis et al., 2008).

The paper confirms a significant inverse correlation between water content (w) and Uniaxial Compressive Strength (UCS). As water content increases, the UCS decreases due to the softening of the clay matrix and the degradation of interparticle bonding. Experimental data showed UCS values ranging from approximately 7.79 MPa at low water content ($w \approx 2.69\%$) to 4.99 MPa at high water content ($w \approx 25.26\%$).

Two regression models were developed to predict UCS based on water content:

- Linear Model: $UCS = -0.0848 \cdot w + 7.5445$, $R^2 = 0.8697$

- Exponential (Nonlinear) Model: $UCS = 7.5993 \cdot e^{-0.013 \cdot w}$, $R^2 = 0.8798$

The exponential model provides a slightly better fit (R^2 approx 0.88) for predicting the strength degradation of Beočin marl. This confirms that the mechanical weakening of these weak sedimentary rocks is nonlinear, with sensitivity to environmental water content being a critical factor for geotechnical stability and mining equipment selection (continuous vs. discontinuous mining) at the "Filijala" Open pit.

Acknowledgment: The authors thank the Serbian Ministry of Education, Science, and Technological Development for their support and the funds provided under Contract No. 451-03-34/2026-03/200126.

REFERENCES

AMIRI, M., ASAKEREH, A., FAROKHDEL, A., & ATASH POOSH, H. (2024). Enhancing marl soil stability: nanosilica's role in mitigating ettringite formation. International Journal of Geo-Engineering, 15(1), 19. https://doi.org/10.1186/s40703-024-00219-z

ASTM D7012-07. (2007). Test Methods for Compressive Strength and Elastic Moduli of Intact Rock Core Specimens under Varying States of Stress and Temperatures. ASTM International. https://doi.org/10.1520/D7012-07

BAHHOU, A., TAHA, Y., KHESSAIMI, Y. EL, HAKKOU, R., TAGNIT-HAMOU, A., & BENZAAZOUA, M. (2021). Using Calcined Marls as Non-Common Supplementary Cementitious Materials—A Critical Review. Minerals, 11(5), 517. https://doi.org/10.3390/min11050517

BELL, F. G. (2007). Engineering Geology (2nd ed.). Butterworth-Heinemann.

BENSAADA, A., CHOUNGACHE, B., & ZAITRI, R. (2023). Influence of the Incorporation of Alluvial Sand on the Mechanical Behavior of Marl Soil. Engineering, Technology & Applied Science Research, 13(2), 10363–10366. https://doi.org/10.48084/etasr.5712

ČELEBIĆ, M., BAJIĆ, D., BAJIĆ, S., BANKOVIĆ, M., TORBICA, D., MILOŠEVIĆ, A., & STEVANOVIĆ, D. (2024). Development of an Integrated Model for Open-Pit-Mine Discontinuous Haulage System Optimization. Sustainability, 16(8), 3156. https://doi.org/10.3390/su16083156

CHENG, X., SUN, H., PU, Y., GUO, J., & QIAO, W. (2024). Mechanical and energetic properties of rock-like specimens under water-stress coupling environment. Journal of

Petroleum Exploration and Production Technology, 14(5), 1113–1128. https://doi.org/10.1007/s13202-024-01766-y

COMAKLI, R., & BAYRAMOV, J. (2024). Effects of changing water content of clay-content rocks on field cutter consumption rate of roadheaders: a case study of porous ignimbrites. Bulletin of Engineering Geology and the Environment, 83(6), 210. https://doi.org/10.1007/s10064-024-03669-y

ERGULER, Z. A., & ULUSAY, R. (2009). Water-induced variations in mechanical properties of clay-bearing rocks. International Journal of Rock Mechanics and Mining Sciences, 46(2), 355–370. https://doi.org/10.1016/j.ijrmms.2008.07.002

GANIĆ, M., LAZIĆ, M., KNEŽEVIĆ, S., & RUNDIĆ, L. (2012). Geological And Engineering-Geological Conditions For Formation Of Landslide In Cement Marl At Open Pit "Filijala", Beočin. Undergound Mining Engineering, 20, 107–119.

GANIC, M., RUNDIC, L., KNEZEVIC, S., & CVETKOV, V. (2010). The Upper Miocene Lake Pannon marl from the Filijala Open Pit (Beocin, northern Serbia): New geological and paleomagnetic data. Geoloski Anali Balkanskoga Poluostrva, (71), 95–108. https://doi.org/10.2298/GABP1071095G

GÖRÖG, P., & TÖRÖK, Á. (2026). Influence of water on the physical properties of marl, calcareous marl, clayey marl, and limestone: a comparative study. Bulletin of Engineering Geology and the Environment, 85(2), 115/1-115/18. https://doi.org/10.1007/s10064-025-04772-4

HAWKINS, A. B., & MCCONNELL, B. J. (1992). Sensitivity of sandstone strength and deformability to changes in moisture content. Quarterly Journal of Engineering Geology, 25(2), 115–130. https://doi.org/10.1144/GSL.QJEG.1992.025.02.05

HOEK, E., & BROWN, E. T. (1997). Practical estimates of rock mass strength. International Journal of Rock Mechanics and Mining Sciences, 34(8), 1165–1186. https://doi.org/10.1016/S1365-1609(97)80069-X

JAEGER, J. C. , C. N. G. W. , & Z. R. W. (2007). Fundamentals of Rock Mechanics (4th ed.). Blackwell Publishing.

MIHAJLOVIĆ, B., SIMIĆ, D., ŽIVANOVIĆ, G., BELJIĆ, J., & MIHAJLOVIĆ, V. (2007). Report on Marl Reserves as a Cement Raw Material in the 'Filijala' Deposit near Beočin – Status as of June 30, 2007.

SABATAKAKIS, N., KOUKIS, G., TSIAMBAOS, G., & PAPANAKLI, S. (2008). Index properties and strength variation controlled by microstructure for sedimentary rocks. Engineering Geology, 97(1–2), 80–90. https://doi.org/10.1016/j.enggeo.2007.12.004

TOMOR, A. K., NICHOLS, J. M., & ORBÁN, Z. (2024). Evaluation of the Loss of Uniaxial Compressive Strength of Sandstones Due to Moisture. International Journal of Architectural Heritage, 18(5), 771–787. https://doi.org/10.1080/15583058.2023.2188313

ULUSAY, R., & HUDSON, J. A. (2007). The Complete ISRM Suggested Methods for Rock Characterization, Testing and Monitoring: 1974–2006. Commission on Testing Methods, International Society for Rock Mechanics.

VARAS, M. J., ALVAREZ DE BUERGO, M., & FORT, R. (2005). Natural cement as the precursor of Portland cement: Methodology for its identification. Cement and Concrete Research, 35(11), 2055–2065. https://doi.org/10.1016/j.cemconres.2004.10.045

VASARHELYI, B. (2003). Some observations regarding the strength and deformability of sandstones in dry and saturated conditions. Bulletin of Engineering Geology and the Environment, 62(3), 245–249. https://doi.org/10.1007/s10064-002-0186-x

VASARHELYI, B. (2005). Statistical Analysis of the Influence of Water Content on the Strength of the Miocene Limestone. Rock Mechanics and Rock Engineering, 38(1), 69–76. https://doi.org/10.1007/s00603-004-0034-3

VÁSÁRHELYI, B., & VÁN, P. (2006). Influence of water content on the strength of rock. Engineering Geology, 84(1–2), 70–74. https://doi.org/10.1016/j.enggeo.2005.11.011

VLAJIĆ, A., LIPCAJT, M., STIJEPOVIĆ, M., & PETROVIĆ, S. (2019). 180 Years Of Lafarge Beočin Cement Plant (pp. 1–52). Lafarge BFC doo Beočin.

VU, T., BAO, T., DREBENSTEDT, C., PHAM, H., NGUYEN, H., & NGUYEN, D. (2021). Optimisation of long-term quarry production scheduling under geological uncertainty to supply raw materials to a cement plant. Mining Technology: Transactions of the Institutions of Mining and Metallurgy, 130(3), 146–158. https://doi.org/10.1080/25726668.2021.1894398

WANG, T., & YAN, C. (2023). Investigating the influence of water on swelling deformation and mechanical behavior of mudstone considering water softening effect. Engineering Geology, 318, 107102. https://doi.org/10.1016/j.enggeo.2023.107102

UNDERGROUND MINING ENGINEERING 48(2026) 109-121 UDK 62
UNIVERSITY OF BELGRADE - FACULTY OF MINING AND GEOLOGY ISSN 03542904

Review paper

OIL AND NATURAL GAS PRICE DYNAMICS IN THE 21ST CENTURY: A REVIEW OF KEY FACTORS AND EVENTS

Nikoleta Aleksić[1], Milica Janković[2]

Received: June 23, 2026 **Accepted:** June 29, 2026

Abstract: This paper analyzes key factors and events in the 21st century that have determined the dynamics of crude oil and natural gas prices on the global market. Particular emphasis is placed on geopolitical and macroeconomic factors that have influenced shifts in supply-demand balance, as well as the emergence of increased volatility in energy markets. The study examines the Iraq War and the U.S. military intervention, the Arab Spring, the COVID-19 pandemic, the Russia-Ukraine war, and contemporary tensions between the United States, Israel, and Iran. These events, through disruptions in production, transportation, and global energy flows, have significantly affected price formation and market structures in both oil and natural gas markets. The results indicate that geopolitical and structural factors play a dominant role in shaping both short-term volatility and long-term trends in energy markets, with their effects directly reflected in global economic stability and energy security.

Keywords: crude oil, natural gas, energy markets, price volatility, geopolitical risk, global economy

1 INTRODUCTION

Oil and natural gas are among the most important energy resources of modern society, and their market prices have a significant impact on the global economy, energy security, and industrial development. Throughout more than 160 years of commercial exploitation, the prices of these strategic mineral resources have been subject to numerous fluctuations, manifested through periods of sharp increases and significant declines.

Changes in oil and natural gas market prices result from the complex interaction of various economic and non-economic factors. Among the most important are supply and demand, geological and geographical conditions, geopolitical circumstances, and technological development. Although all these factors influence price formation, their impacts are not equally significant. Previous studies have shown that the most

[1] University of Belgrade - Faculty of Mining and Geology, Djusina 7, 11000 Belgrade, Serbia

[2] NTC NIS – Naftagas, Novi Sad, Serbia

E-mails: nikoleta.aleksic@rgf.bg.ac.rs ORCID: https://orcid.org/0000-0001-9617-108X; milica.jankovic@nis.rs

pronounced price fluctuations are often associated with geopolitical events, political instability, and international conflicts.

Due to the interdependence of these factors, a change in one of them can trigger chain reactions affecting the entire market. Leading oil and gas producers and exporters, as well as international organizations, play a particularly important role in price formation, as their decisions can significantly influence global supply and demand.

Throughout the history of the oil and gas industry, numerous events have caused substantial changes in market prices. These fluctuations have been particularly pronounced in the oil market, whereas natural gas prices, although often linked to oil price movements, have generally exhibited a lower degree of variability. This paper analyzes the most significant changes in oil and natural gas prices during the 21st century, with particular emphasis on the factors and events that have shaped their development.

2 KEY FACTORS INFLUENCING OIL AND GAS PRICES

Oil continues to play an important role in the global economy, despite ongoing efforts to reduce its use and to find alternative energy sources. There are several factors that influence crude oil prices. They can be divided into external factors (general economic, political, geological, and market-related) and technological factors.

The most important factors include the current state of supply and demand, the condition and growth rate of the global economy, technological and technical progress (new technologies, materials, communication systems, alternative energy sources, etc.), the state and discovery of proven and potential oil reserves, as well as production costs (Miao et al., 2017).

The most significant non-economic factors include global military and political relations, strikes at production facilities and primary processing plants for mineral resources, port workers' strikes, and various forms of social unrest. Additional factors include upcoming labor contract negotiations in major producing countries, the imposition of embargoes on mineral resource imports from certain countries, the impact of natural conditions, local conflicts and open wars, partial or complete nationalizations, as well as policies related to the creation, replenishment, and sale of strategic reserves (stocks). Restrictive and protectionist policies, along with environmental protection and conservation measures related to human living and working conditions, also play an important role (Janković and Milovanović, 1985).

2.1 Supply and demand factor

Oil and natural gas prices are influenced by a wide range of factors, with the fundamental economic principles of supply and demand being particularly important. According to this relationship, an increase in supply leads to lower prices, while an increase in demand

leads to higher prices. Demand for oil depends on industrial production, economic growth, transportation, seasonal changes, and population growth, while on the supply side OPEC has traditionally played a key role through production control, and the United States increasingly contributes to global supply due to shale oil production (Pirog, 2005). In the case of natural gas, storage levels significantly affect supply stability by smoothing seasonal demand fluctuations, with inventories typically increasing from April to October (EIA, 2021). In addition, extreme weather conditions such as hurricanes and cold waves can disrupt production and supply chains, which under high demand conditions may lead to sharp price increases (Pirog, 2005; EIA, 2021).

2.2 Geological and geographical factors

Geological factors play an important role as they determine the presence of oil- and gas-bearing basins in different regions of the world. In addition, geographic location and reservoir accessibility influence transportation costs, which account for approximately one-fifth of the total oil price; therefore, location represents a key factor in price formation. The largest oil and gas reserves are found in countries such as Venezuela, Saudi Arabia, Canada, Iran, Iraq, Kuwait, the United Arab Emirates, Russia, Libya, and the United States (Fig. 1), with a significant share of these reserves concentrated in the Middle East and North Africa region, and more than half of the leading countries being OPEC members (Killian, 2009).

In addition to geological and geographical conditions, oil prices also depend on the quality of crude oil, which varies according to density and sulfur content, affecting its suitability for refining. Consequently, different benchmark crude oils are used as global price standards, such as Brent, West Texas Intermediate (WTI), and Dubai crude, as well as regional benchmarks including Urals, Bonny Light, Tapis, Duri, Isthmus, and Western Canadian Select (Gomez and Moya, 2020; Kostić, 2020).

Transport also plays a significant role in price formation, as the global pricing structure is partly based on the distance between producers and consumers, but also includes additional costs such as passage through maritime routes and transit channels, as well as risks associated with weather conditions, delays, and political instability (Melamid, 1962).

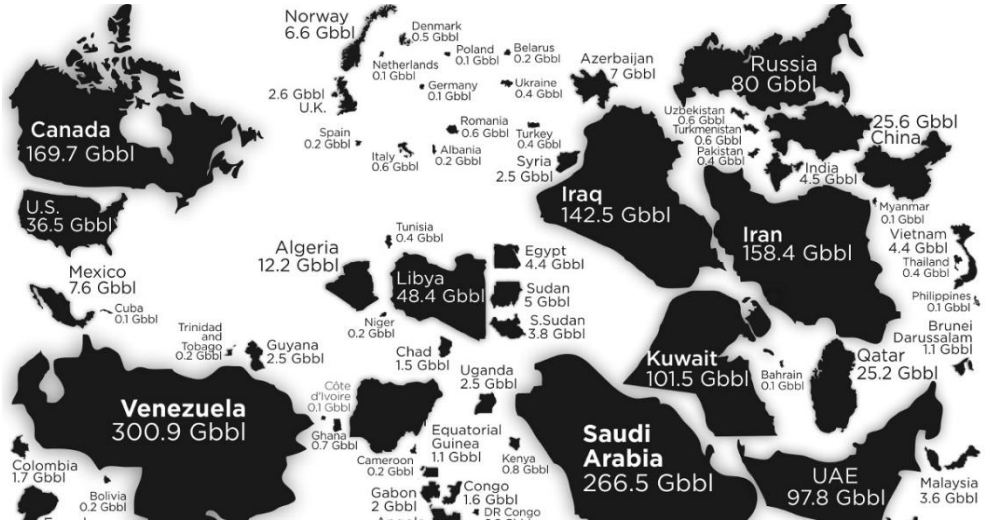

Figure 1 Geographical location of countries with the largest oil reserves (Desjardins, 2019).

2.3 Geopolitical factors

Countries with large oil production, such as the United States, Venezuela, Canada, Saudi Arabia, Iran, and Iraq, significantly determine market supply, and tensions involving any of these nations can lead to major disruptions. A similar situation applies to natural gas, where countries with the largest reserves include Russia, Iran, and Qatar. As a result, if war or conflict occurs in oil- and gas-producing regions, or if such events are anticipated, supply may be threatened, ultimately leading to price changes. Therefore, geopolitics has traditionally been an important factor influencing oil and gas prices (Hughes & Long, 2015; Zhao et al., 2023)

2.4 Technological and technical factors

Technological and technical progress reduces the costs of oil exploration, production, transportation, and storage, which leads to a decrease in crude oil prices. Innovations in geological exploration (remote sensing, geophysics, mathematical simulation, geothermal modeling), as well as in oil production (horizontal and directional drilling, new offshore platform designs, and faster production rates), have contributed to lower costs and, consequently, reduced oil prices (Deku and Lim, 2024).

3 KEY EVENTS AFFECTING OIL AND GAS PRICES IN THE 21ST CENTURY

Throughout the 21st century, a number of key geopolitical and economic events have significantly influenced the price dynamics of oil and natural gas. Among the most important are the military intervention of the United States and the United Kingdom in Iraq, the Arab Spring, the COVID-19 pandemic, the armed conflict between Russia and Ukraine, as well as the escalation of tensions and armed conflicts between the United States, Israel, and Iran. All of these events have led to disruptions in global supply and energy security, which has directly affected the volatility of energy prices on the world market.

3.1 Military intervention of the United States and the United Kingdom in Iraq

The Iraq War, also known as the Second Gulf War, was a conflict conducted in two phases. The first phase was a short, conventional war in March-April 2003, during which combined forces from the United States and the United Kingdom (with smaller contingents from several other countries) invaded Iraq and rapidly defeated Iraqi military and paramilitary forces. This was followed by a longer second phase in which U.S. forces occupied Iraq. Following the stabilization of the situation in the country in 2007, the United States gradually reduced its military presence in Iraq and formally completed its withdrawal in December 2011.

The military intervention in Iraq led to a significant disruption in Iraqi oil production, with a maximum lost production capacity of approximately 2.4×10^6 bbl/day, while the average production loss in 2003 amounted to about 1.4×10^6 bbl/day. Three wars and decades of instability severely damaged the country's oil industry, and production did not fully recover until the beginning of 2008 (McNally, 2017).

Iraq has approximately 3.7×10^9 m³ of proven natural gas reserves, accounting for about 2% of global reserves and ranking 12th in the world. Its proven reserves are around 1,194 times higher than annual consumption. Although Iraq's gas basins are significant, due to underdeveloped infrastructure, about one-third of the produced gas (associated gas from oil production) is flared, limiting both exports and domestic supply. During periods of war and sanctions, exports of oil and gas were disrupted, which led to an increase in prices from approximately 0.90 USD/m³ in 2000 to 1.26 USD/m³ in 2003, reaching a peak of 2.60 USD/m³ in 2008, followed by a decline to about 1.10 USD/m³ in 2009 (McNally, 2017).

3.2 „The Arab Spring“

“The Arab Spring” refers to a series of pro-democracy protests that, since 2011, spread across several predominantly Muslim countries, including Tunisia, Egypt, Libya, Syria, and Bahrain, with long-term political and social consequences. Although in some cases they led to regime changes (Tunisia, Egypt), in many countries they resulted in increased instability. In Libya, a disruption of approximately 1.5×10^6 bbl/day in oil supply to the market occurred, contributing to oil prices rising above 100 USD/bbl, while during the period 2011–2014 prices ranged between 100 and 125 USD/bbl (McNally, 2017). In parallel, the civil war in Syria that followed the protests led to a prolonged political and humanitarian crisis and significant population migration flows. Prior to 2011, Syria produced around 400,000 bbl/day of oil (of which approximately 140,000 bbl/day were exported), while proven natural gas reserves were estimated at 8.5–9 trillion m³. Following the outbreak of the crisis, oil production fell to about 25,000 bbl/day, turning the country from a net exporter into a state dependent on imports and alternative supply routes, whereas natural gas production was less affected due to the need to maintain electricity supply under conflict conditions (Al-Ghazi, 2021).

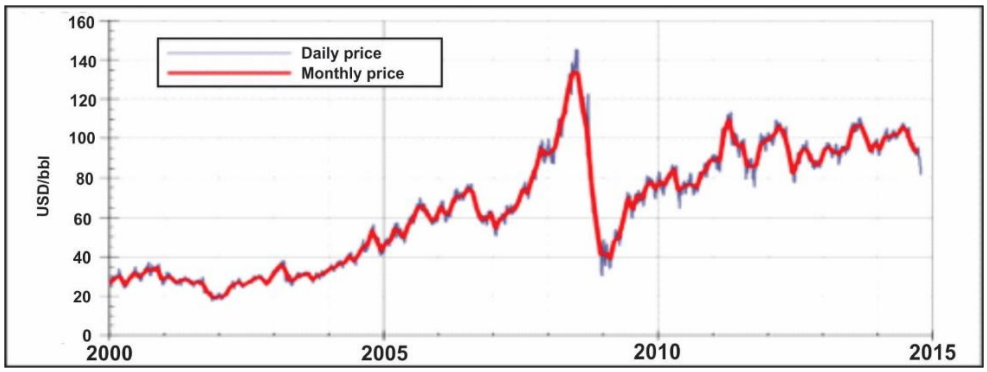

Figure 2 Price trend chart 2000-2015 (Theanphibian, 2012)
Note. Data adapted from Theanphibian, 2012.

3.3 COVID-19 Pandemic

The COVID-19 pandemic led to one of the most pronounced disruptions in the modern oil market. After a period of relatively stable prices during 2018-early 2020, the decline in oil prices began due to disagreements between major OPEC producers and was subsequently intensified by the global COVID-19 pandemic and a collapse in demand. Due to mobility restrictions across many countries, oil consumption nearly came to a halt, while storage capacities reached maximum levels for the first time, resulting in

extreme market disruptions, including negative storage pricing conditions. During this period, production was temporarily reduced to approximately 12 × 10^6 bbl/day, while demand in April 2020 was about 29 × 10^6 bbl/day lower compared to the same month of the previous year, representing the lowest level since 1995 (Lahn & Bradley, 2020). Oil prices experienced a sharp decline in March 2020, with Brent crude reaching around 51 USD/bbl (Fig. 3), while Urals crude fell to 11–20 USD/bbl, reflecting a severe imbalance between global supply and demand in the oil market.

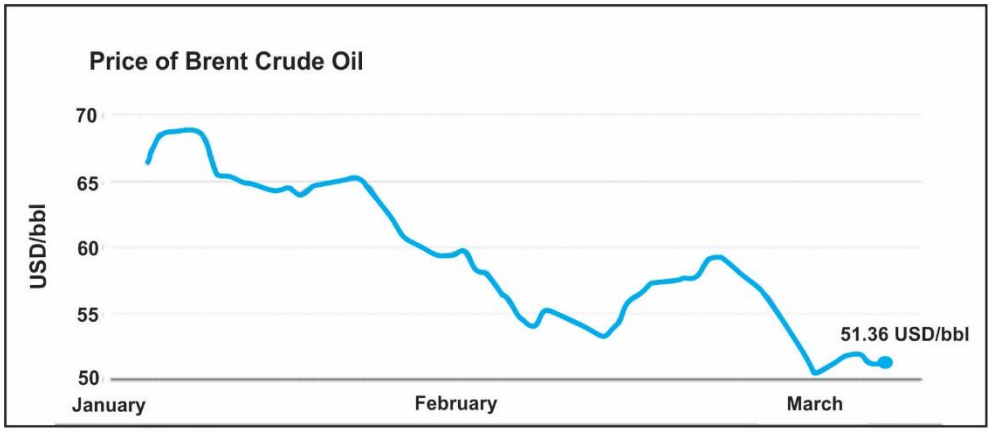

Figure 3 Chart of Brent crude oil price movements during January, February, and March 2020 (BBC, 2020).

Note. Adapted from BBC News (2020).

3.4 Russia-Ukraine conflict

The Russian military intervention in Ukraine in 2022 caused significant disruptions to the global oil and natural gas markets, leading to a major restructuring of trade flows and supply routes. As a result of Western sanctions and reduced exports to Europe, Russia increasingly redirected its oil exports toward Asian markets, particularly China and India, often at substantial discounts and using high-risk logistical solutions such as ship-to-ship transfers. At the same time, European refineries compensated for the loss of Russian crude oil by increasing imports from West Africa and the United States, with U.S. crude exports to Europe rising by more than 15% compared to March levels and reaching approximately 1.45 million bbl/day (Fattouh, 2022). These developments represent one of the most significant restructurings of global oil trade flows since the expansion of unconventional oil production in the United States. Despite the initial market disruptions and the surge in oil prices to over 139 USD/bbl in March 2022, prices gradually stabilized at around 110 USD/bbl in the following months, while the price of Urals crude averaged approximately 76 USD/bbl (Cahill, 2022). Russian exports

partially recovered to pre-conflict levels as early as April, despite the substantial changes in market structure.

From 2023 to 2026, the global oil and natural gas market continued to adjust to the consequences of the Russia-Ukraine conflict and the sanctions imposed on Russia. Although Russian oil export volumes remained relatively stable due to the redirection of flows toward China and India, export revenues declined because of lower selling prices and the implementation of price-cap mechanisms by Western countries (Babina et al., 2025; Johnson et al., 2023). During this period, Brent crude oil prices gradually stabilized, averaging approximately 82.5 USD/bbl in 2023, 80.5 USD/bbl in 2024, and around 69 USD/bbl in 2025, reflecting a combination of weaker global demand and relatively stable supply conditions (Fig. 4).

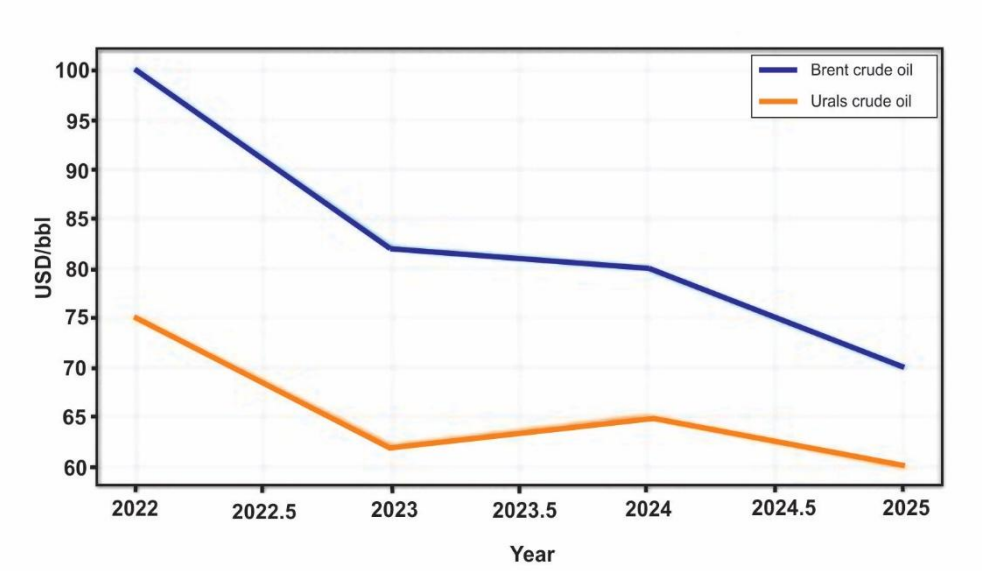

Figure 4 Brent vs Urals crude oil prices 2022-2025 (European Commission, 2025).

Note. Data adapted from European Commission (2025).

The natural gas market showed a higher degree of stabilization compared to the 2022 energy crisis, although it remained sensitive to geopolitical developments. The European TTF benchmark averaged about 37 EUR/MWh in 2024, increasing to approximately 42 EUR/MWh in 2025 (Fig. 5), corresponding to roughly 0.40–0.50 USD/m³ in energy-equivalent terms. At the same time, the European Union continued to diversify its energy supply through increased liquefied natural gas (LNG) imports, referring to natural gas that is cooled to approximately -162°C and transported in liquid form via specialized tankers before regasification and integration into the European gas network, as well as through alternative pipeline sources. This significantly reduced dependence on Russian natural gas and contributed to the gradual stabilization of the market. Nevertheless,

global energy markets remained influenced by geopolitical tensions and ongoing structural changes in trade flows (European Commission, 2025).

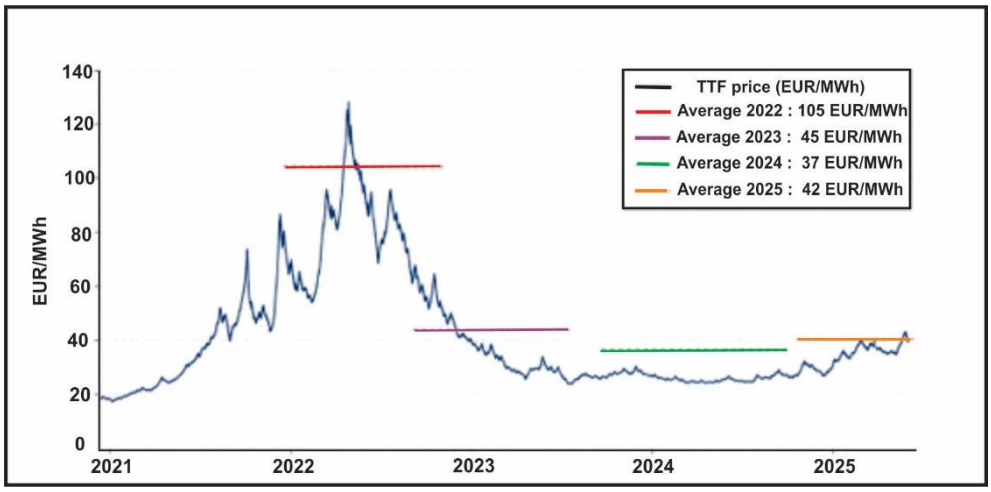

Figure 5 Evolution of European natural gas prices (TTF) during the Russia-Ukraine conflict 2022-2025 (European Commission, 2025).

Note. Data adapted from European Commission (2025).

3.5 US-Israel-Iran conflict

The escalation of the conflict between Iran, the United States, and Israel during 2026 led to a significant increase in geopolitical risk in global energy markets and pronounced volatility in oil prices. A particularly important factor is the potential disruption of transportation through the Strait of Hormuz, through which approximately 20% of global seaborne oil trade passes, making it a critical determinant of global supply conditions (Reuters, 2026a).

During periods of intensified conflict and restrictions on maritime traffic, Brent crude oil prices recorded a sharp increase from approximately 95-100 USD/bbl to levels above 110–120 USD/bbl while in phases of de-escalation and diplomatic progress prices declined below 90 USD/bbl, and in some instances toward 80 USD/bbl (Reuters, 2026b; Reuters, 2026c). These movements indicate a pronounced geopolitical risk premium embedded in oil prices (Fig. 6).

In periods of partial or perceived closure of the Strait of Hormuz, markets reacted with immediate price spikes due to expectations of reduced global supply and disruptions in supply chains. Conversely, announcements of de-escalation and progress in negotiations between the United States and Iran led to rapid downward corrections, confirming the high sensitivity of energy markets to geopolitical information (Reuters, 2026d).

Overall, the 2026 developments demonstrate that geopolitical factors, particularly the Iran-related conflict and the status of the Strait of Hormuz, were the dominant drivers of short-term movements in global oil prices.

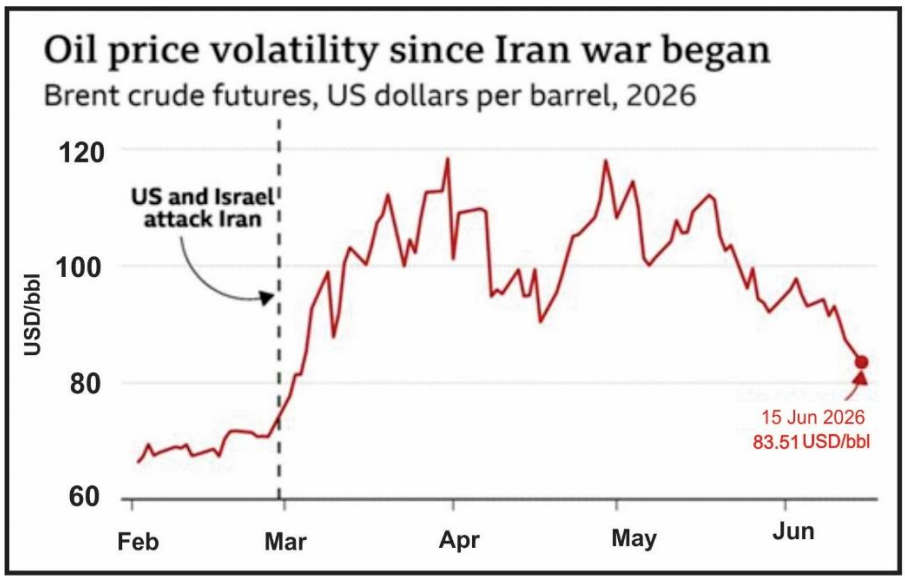

Figure 6 Brent crude oil price fluctuations during the US-Israel-Iran conflict (February-June 2026).
Note. Adapted from BBC News (2026).

4 CONCLUSION

In the 21st century, the dynamics of crude oil and natural gas prices have been driven by a complex interaction of fundamental market forces and recurrent geopolitical and macroeconomic disruptions. Conflicts in key producing regions, sanctions regimes, OPEC and OPEC+ production decisions, global financial crises, as well as disruptions in supply chains and strategic transport routes, have repeatedly resulted in pronounced volatility across global energy markets.

These developments have had significant implications for the global economy, given that oil and natural gas remain essential inputs for transportation, industrial production, electricity generation, and heating. Periods of sharp energy price increases have contributed to higher inflation, reduced real purchasing power, and slower economic growth, particularly in net energy-importing economies. Conversely, periods of declining prices have temporarily alleviated cost pressures but have also negatively affected fiscal stability and investment capacity in major exporting countries.

Overall, oil and natural gas price movements in the 21st century highlight the persistent vulnerability of the global economic system to energy supply disruptions and geopolitical risks. The increasing interconnectedness of global energy markets, combined with the continued structural dependence of modern economies on fossil fuels, confirms that energy commodities remain key determinants of industrial development, macroeconomic stability, and international economic relations.

Acknowledgment: The authors thank the Serbian Ministry of Education, Science, Technological Development and Innovation for their support and the funds provided under Contract No. 451-03-34/2026-03/200126.

REFERENCES

AL-GHAZI, S. (2021). *The Syrian regime's oil and gas crisis* (Policy brief). ORSAM. https://orsam.org.tr/en/yayinlar/the-syrian-regimes-oil-and-gas-crisis/

BABINA, T., HILGENSTOCK, B., ITSKHOKI, O., MIRONOV, M., RIBAKOVA, E., & SHAPOVAL, N. (2026). *Russian oil exports under international sanctions*. *Energy Economics, 153*, 109006. https://doi.org/10.1016/j.eneco.2025.109006

BBC News. (2020, March 9). *What on earth is going on with the oil price?* https://www.bbc.com/news/business-51753142

BBC News. (2026). *Oil price rises amid geopolitical tensions involving US, Israel and Iran*. Retrieved from https://www.bbc.com/news/articles/c6217106px6o

CAHILL, D. (2022). *I only pay attention to interesting things…and that's a problem: Investor attention in financial markets*. University of Western Australia. https://doi.org/10.26182/k41b-vq19

DESJARDINS, J. (2019, March 25) *Map: The countries with the most oil reserves*. Visual Capitalist. https://www.visualcapitalist.com/map-countries-most-oil-reserves/

DEKU, S., & LIM, K. Y. (2024). *Oil Price Effects On Optimal Extraction–Exploration*. Energy Economics, 129, 107263.

EUROPEAN COMMISSION. (2025). *Commission notice on crude oil price cap and market prices*. https://finance.ec.europa.eu/

EUROPEAN COMMISSION. (2025). *Quarterly report on European gas markets*. Publications Office of the European Union. https://energy.ec.europa.eu/data-and-analysis/market-analysis_en

FATTOUH, B. (2022). *Russia-Ukraine crisis and its impact on oil markets*. Oxford Institute for Energy Studies. https://www.oxfordenergy.org/

GÓMEZ, R., & MOYA, J. (2020). *Oil and its geography*. Atalayar Report.

HUGHES, L., & LONG, A. (2015). Is there an oil weapon? Security implications of changes in the structure of the international oil market. *International Security, 39*(3), 155–170.

JANKOVIĆ, S., & MILOVANOVIĆ, D. (1985). *Ekonomska geologija i osnovi ekonomike mineralnih sirovina*. Rudarsko-geološki fakultet, 315–322.

JOHNSON, S., RACHEL, L., & WOLFRAM, C. (2023). Design and implementation of the price cap on Russian oil exports. *Journal of Comparative Economics, 51*(4), 1244–1252.

KILLIAN, L. (2016). *The impact of the fracking boom on Arab oil producers*. CESifo Working Paper Series, 5751.

KOSTIĆ, A. (2020). *Ležišta istraživanja nafte i gasa*. Univerzitet u Beogradu, Rudarsko-geološki fakultet, p.137–146.

LAHN, G., & BRADLEY, S. (2020). *How COVID-19 is changing the opportunities for oil and gas-led growth*. OECD Development Matters. https://oecd-development-matters.org/2020/07/10/how-covid-19-is-changing-the-opportunities-for-oil-and-gas-led-growth/

MCNALLY, R. (2017). *Crude volatility: The history and the future of boom-bust oil prices*. Columbia University Press. https://doi.org/10.7312/mcna17814

MELAMID, A. (1962). Geography of the world petroleum price structure. *Economic Geography, 38*, 283–290.

MIAO, H., RAMCHANDER, S., WANG, T., & YANG, D. (2017). Influential factors in crude oil price forecasting. *Energy Economics*, 1–5.

PIROG, R. (2005). *World oil demand and its effect on oil prices*. CRS Report for Congress, 6–7.

REUTERS. (2026a, June 21). *Oil falls after US–Iran talks ease supply risks; Brent drops below $80*. https://www.reuters.com/business/energy/brent-oil-rises-more-than-1bbl-after-bumpy-start-us-iran-peace-talks-2026-06-21/

REUTERS. (2026b, June 22). *European shares subdued as investors weigh US–Iran talks and Strait of Hormuz developments*. https://www.reuters.com/markets/europe/european-shares-muted-investors-weigh-us-iran-talks-2026-06-22/

REUTERS. (2026c, March 23). *Factbox: Analysts hike oil price outlooks as Iran conflict persists*. https://www.investing.com/news/commodities-news/factboxanalysts-hike-oil-price-outlooks-as-iran-conflict-persists-4574186

REUTERS. (2026d, March 31). *Iran war shock drives steepest hike yet in oil price forecasts*. https://www.kitco.com/news/off-the-wire/2026-03-31/iran-war-shock-drives-steepest-hike-yet-in-oil-price-forecasts

THEANPHIBIAN. (2012). *Crude oil price WTI EIA since 2000*. Wikimedia Commons. https://commons.wikimedia.org/wiki/File:Crude_oil_price_WTI_EIA_since_2000.svg

U.S. Energy Information Administration (2021) *Natural gas storage and seasonal demand*. https://www.eia.gov/naturalgas/

ZHAO, Y., CHEN, L., & ZHANG, Y. (2024). *Spillover effects of geopolitical risks on global energy markets: Evidence from CoVaR and CAViaR-EGARCH model*. Energy Exploration & Exploitation, 42(2), 772–788.

UNDERGROUND MINING ENGINEERING 48(2026) 123-131 UDK 62
UNIVERSITY OF BELGRADE - FACULTY OF MINING AND GEOLOGY ISSN 03542904

Professional paper

1D ADJUSTMENT OF THE GEODETIC NETWORK AT THE SCHOOL MINE "CRVENI BREG" ON AVALA

Nevena Đurđev[1], Aleksandar Ganić[1], Zoran Gojković[1], Aleksandar Milutinović[1]

Received: April 27, 2026 **Accepted:** June 03, 2026

Abstract: The objective of this paper is to present the procedure for obtaining the most probable values of height differences through one-dimensional adjustment of the geodetic network of the school mine "Crveni Breg" on Avala. Since the terrain is not connected to the national levelling network, the first step involves determining adjusted height differences. Once the initial point is linked to a national benchmark, accurate elevations of all points within the school polygon will be established. The survey was conducted using the geometric levelling method from the middle (''forward-backward''), and the results were processed by conditional adjustment. Accuracy assessment indicated that the obtained standard deviation corresponds to technical levelling of increased precision, confirming the quality of the fieldwork and measurements.

Keywords: conditional adjustment, geodetic network, accuracy assessment.

1 INTRODUCTION

In contemporary research practice, numerous scientific disciplines are based on measuring specific quantities, their analysis, and interpretation. Throughout the process of measuring, we obtain values/results with lower or higher accuracy compared to the true value, which cannot be directly reached by measurement. By repeatedly measuring the same value, different results are usually obtained, leading to the conclusion that all measurements are burdened with errors. Some errors can be eliminated through measurement procedures by subsequently introducing corrections, however, random errors remain and are an integral part of measurement results [Ganić, 2008; Džeparovski, 1995; Ghilani, 2010].

In order to minimize random errors in measurement results and to achieve their closer approximation to the true values, as well as to the computed parameters derived from these results, it is necessary to ensure measurement redundancy. This is accomplished

[1] University of Belgrade - Faculty of Mining and Geology, Đušina 7, Belgrade Serbia
Emails: nevena.djurdjev@dok.rgf.bg.ac.rs ORCID: https://orcid.org/0009-0005-1919-5025;
aleksandar.ganic@rgf.bg.ac.rs ORCID: https://orcid.org/0000-0002-3431-7909;
zoran.gojkovic@rgf.bg.ac.rs ORCID: https://orcid.org/0009-0000-2642-1493;
aleksandar@milutinovic.rgf.bg.ac.rs ORCID: https://orcid.org/0000-0002-9450-2903

not only by performing an adequate number of repeated observations of the same quantities, but also by observing a greater number of quantities than strictly required for the unique determination of the unknowns (in the case of mining surveys, these unknowns are the coordinates and/or elevations of points) [Ganić, 2008; Džeparovski, 1995; Ghilani, 2010].

The indeterminacy of such a mathematical system is resolved by applying rigorous adjustment methods, which are based on the condition that the sum of the squares of the corrections to the observed values (v_i) is minimized (equations 1a and 1b) [Ganić, 2008; Džeparovski, 1995; Ghilani, 2010].

$$\sum_{i=1}^{n}(i=1)^{n} v_i \, v_i = min \tag{1a}$$

respectively

$$\sum_{i=1}^{n} p_i v_i \, v_i = min \tag{1b}$$

depending on whether the measurements are of equal or varying precision

Given the stated minimum condition, the results of repeated measurements of the same values are subjected to direct adjustment, thereby yielding the most probable values of the observed quantities. Subsequently, since a redundant number of observations are available, all most probable values of the measured quantities are incorporated into the procedure of indirect or conditional adjustment, with the aim of obtaining the most probable values of the unknown parameters. Namely, the coordinates and/or elevations of points [Ganić, 2008; Džeparovski, 1995; Ghilani, 2010].

During mining surveying, we observe angles, distances, and height differences, and through their processing and further calculations, the coordinates and elevations of points are derived. These serve as the basis for solving a wide range of tasks encountered during the exploitation of mineral resources, as well as for the graphical representation of terrain or the staking out of designed structures.

The polygon of the school mine “Crveni Breg” on Avala, consisting of trigonometric points and benchmarks on the surface terrain, as well as all points of the underground traverse in the lower gallery, is not vertically connected to the national levelling network. Consequently, all these points possess only approximate local elevations. For this reason, measurements of height differences were carried out within the surface polygon, and their processing was performed using conditional adjustment to obtain the most probable values of the height differences, as a first step. This paper presents the procedure of one-

dimensional conditional adjustment of the polygon of the school mine “Crveni Breg” on Avala [Đurđev, 2023].

In the future, once a point of the polygon is connected to the national levelling network and its true elevation is determined, the true elevations of all other points in the polygon will subsequently be calculated based on the most probable values of height differences.

2 FIELD MEASUREMENTS OF HEIGHT DIFFERENCES AND MEASUREMENT RESULT

The school mine “Crveni Breg” on Avala dates to Roman times, and traces of their exploitation are still visible in certain parts of the mine. “Crveni Breg” is a lead and silver mine, officially opened in 1886/1887 and officially closed in 1953. Today, the “Crveni Breg” mine is used for educational purposes.

The geodetic basis of the polygon of the school mine on the surface terrain in front of the lower gallery consists of six points: four trigonometric points (101–104) and two benchmarks (Rp and Rz), as shown in Figure 2.1.

Figure 2.1 Research location: School Mine “Crveni Breg” on Avala and the Geodetic Basis of the School Mine (Source: Google maps)

The geodetic basis of the school mine on Avala is not strictly connected to the national levelling network, and therefore the elevations of its points are of approximate character. For this reason, conditional adjustment of the measured height differences within the network will be applied, yielding their most probable values. The elevations of the

network points will not be calculated at this stage, however, once the network is connected to the national benchmarks, the most probable values of the height differences obtained in this way will be used to calculate the most probable elevations of all points in the network [Đurđev, 2023].

Within the geodetic network, nine height differences were measured, thereby ensuring redundant observations. A sketch showing the mentioned control points and the measured height differences (Δh_i) of the levelling lines is presented in Figure 2.2. [Đurđev, 2023].

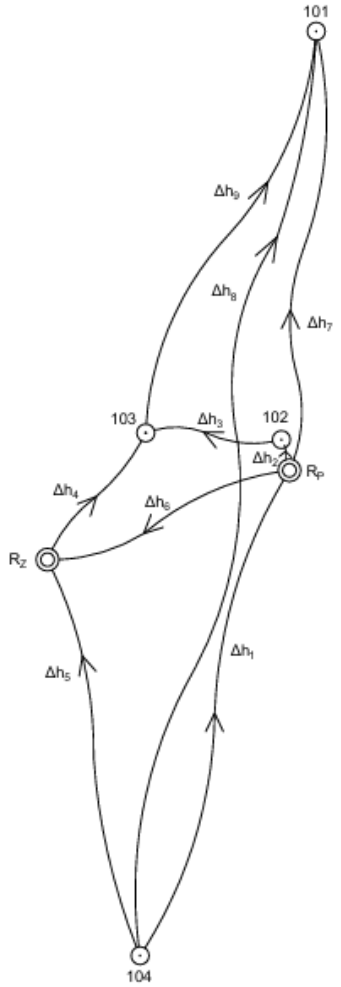

Figure 2.2 Sketch of the Levelling Network (Approximate scale) [Đurđev, 2023]

The measurements were carried out using a digital levelling instrument "Leica Sprinter 150M," whose standard deviation at a distance of 30 m amounts to ±0.6 mm [Leica

Geosystems]. Supporting equipment was used, including aluminum levelling bars and iron shoes for the stabilization of reference points.

The height differences were measured using the method of geometric levelling from the midpoint (backsight–foresight). The readings on the staffs were taken according to the BFFB principle (back–front–front–back) with a change in instrument height. In this way, four independent measurements were ensured for each levelling line in the network.

Table 2.1 presents the calculated average values of the measured height differences, as well as the achieved and permissible maximum deviations of the height differences.

The average achieved deviation of the measured height differences throughout the entire levelling network is 1.4 mm. The permissible deviations of the measured height differences were calculated according to the formula for technical levelling of higher accuracy on favorable terrain [Mihajlović, 1982], while the achieved deviations are significantly smaller than the permissible ones

Table 2.1 Calculated Average Values of the Measured Height Differences and Achieved Standard Deviations [Đurđev, 2023]

Traverse number	from	to	Discrepancy Forward (m)		Discrepancy Backward (m)		Average (m)		Deviations (mm)	
			Δh_p	S_p	$-\Delta h_z$	S_z	Δh	S	Ach[2].	Perm. [3]
1	104	R_p	0.8800	113	0.8785	112	0.87925	112.25	1.5	6.7
2	R_p	102	0.5400	7	0.5405	7	0.54025	7	0.5	1.7
3	102	103	5.2380	30	5.2400	30	5.239	30	2	3.5
4	R_z	103	5.2715	35	5.2720	36	5.27175	35.5	0.5	3.8
5	R_z	104	-1.3830	88	-1.3850	88	-1.384	88	2	5.9
6	R_z	R_p	-0.5075	32	-0.5065	32	-0.507	32	1	3.6
7	R_p	101	14.6675	122	14.6665	121	14.667	121.5	1	7.0
8	104	101	15.5485	207	15.5465	209	15.5475	208	2	9.2
9	103	101	8.8900	112	8.8875	112	8.88875	112	2.5	6.7

3 DATA PROCESSING AND MOST PROBABLE VALUES OF HEIGHT DIFFERENCES

The levelling network of the school mine on Avala was adjusted by the method of conditional adjustment, treated as a free levelling network in the local system. Since the elevations of all six points are unknown, a local elevation was adopted for benchmark Rz, while the elevations of the remaining five points of the network remain as unknown. Given that nine height differences were measured, this implies the availability of four redundant observations, and for each redundant observation it is necessary to establish one independent conditional equation [Đurđev, 2023].

[2]Achieved deviation

[3]Permissible deviation

The final conditional equations are of the form

$$-\Delta h'_1 + \Delta h'_5 - \Delta h'_6 = 0 \quad (2)$$

$$-\Delta h'_2 - \Delta h'_3 + \Delta h'_4 + \Delta h'_6 = 0 \quad (3)$$

$$\Delta h'_4 + \Delta h'_5 - \Delta h'_8 + \Delta h'_9 = 0 \quad (4)$$

$$-\Delta h'_1 - \Delta h'_7 + \Delta h'_8 = 0 \quad (5)$$

The conditional adjustment of the levelling network was carried out by applying matrix solution techniques in the program "Microsoft Excel". For the purposes of adjustment using matrix calculations, based on the final conditional equations, the following were formed:

- Coefficient matrix of the conditional equations *A*:

$$A = \begin{bmatrix} -1 & 0 & 0 & -1 \\ 0 & -1 & 0 & 0 \\ 0 & 1 & 0 & 0 \\ 0 & -1 & 1 & 0 \\ 1 & 0 & 1 & 0 \\ -1 & 1 & 0 & 0 \\ 0 & 0 & 0 & -1 \\ 0 & 0 & -1 & 1 \\ 0 & 0 & -1 & 0 \end{bmatrix}$$

- Vector of independent terms ω:

$$\omega = \begin{bmatrix} -0.00225 \\ -0.0005 \\ -0.003 \\ 0.00125 \end{bmatrix}$$

- Weight matrix *P*:

$$P = \begin{bmatrix} 8.9087 & 0 & 0 & 0 & 0 & 0 & 0 & 0 & 0 \\ 0 & 142.85714 & 0 & 0 & 0 & 0 & 0 & 0 & 0 \\ 0 & 0 & 33.3333 & 0 & 0 & 0 & 0 & 0 & 0 \\ 0 & 0 & 0 & 28.1690 & 0 & 0 & 0 & 0 & 0 \\ 0 & 0 & 0 & 0 & 11.3636 & 0 & 0 & 0 & 0 \\ 0 & 0 & 0 & 0 & 0 & 31.2500 & 0 & 0 & 0 \\ 0 & 0 & 0 & 0 & 0 & 0 & 8.2304 & 0 & 0 \\ 0 & 0 & 0 & 0 & 0 & 0 & 0 & 4.8077 & 0 \\ 0 & 0 & 0 & 0 & 0 & 0 & 0 & 0 & 8.9286 \end{bmatrix}$$

Based on these, the following values are calculated according to the equations:

- Coefficient matrix of the normal equations *N:*

$$N = A^T \cdot P^{-1} \cdot A \tag{6}$$

Inverse matrix of the normal equation coefficients N^{-1}

- Vector of correlates *k*:

$$k = -N^{-1} \cdot \omega \tag{7}$$

- Correction vector *v:*

$$Nv = P^{-1} \cdot A \cdot k \tag{8}$$

By adding the calculated corrections to the measured height differences, their most probable values are obtained, which satisfy the imposed conditional equations:

$$\Delta h'_1 = \Delta h_1 + v_1 = +0.8784 \text{ m } (104 - \mathrm{R_p})$$
$$\Delta h'_2 = \Delta h_2 + v_2 = +0.5402 \text{ m } (\mathrm{R_p} - 102)$$
$$\Delta h'_3 = \Delta h_3 + v_3 = +5.2387 \text{ m } (102 - 103)$$
$$\Delta h'_4 = \Delta h_4 + v_4 = +5.2721 \text{ m } (\mathrm{R_z} - 103)$$
$$\Delta h'_5 = \Delta h_5 + v_5 = -1.3852 \text{ m } (\mathrm{R_z} - 104)$$
$$\Delta h'_6 = \Delta h_6 + v_6 = -0.5068 \text{ m } (R_z - R_p)$$
$$\Delta h'_7 = \Delta h_7 + v_7 = +14.6677 \text{ m } (R_p - 101)$$
$$\Delta h'_8 = \Delta h_8 + v_8 = +15.5461 \text{ m } (101 - 104)$$
$$\Delta h'_9 = \Delta h_9 + v_9 = +8.8887 \text{ m } (103 - 101)$$

The reference standard deviation of unit weight σ_o amounts to:

$$\sigma_o = \sqrt{\frac{v^T \cdot P \cdot v}{n - r}} = \pm 3.32 mm/km \tag{9}$$

where the difference *n* - *r* represents the number of redundant measurements in the network.

The standard deviations of the adjusted height differences are calculated according to the equation:

$$\sigma_{\Delta h_i'} = \sigma_o \cdot \sqrt{Q_{h_i} \cdot Q_{h_i}} \tag{10}$$

Where:

$$Q_{h_i} = P^{-1} \cdot P^{-1} \cdot A \cdot N^{-1} \cdot A^T \cdot P^{-1} \tag{11}$$

And they amount to:

$$\sigma_{\Delta h_1} = \pm 0.72 \text{ mm}$$
$$\sigma_{\Delta h_2} = \pm 0.27 \text{ mm}$$
$$\sigma_{\Delta h_3} = \pm 0.46 \text{ mm}$$
$$\sigma_{\Delta h_4} = \pm 0.49 \text{ mm}$$
$$\sigma_{\Delta h_5} = \pm 0.72 \text{ mm}$$
$$\sigma_{\Delta h_6} = \pm 0.46 \text{ mm}$$
$$\sigma_{\Delta h_7} = \pm 0.76 \text{ mm}$$
$$\sigma_{\Delta h_8} = \pm 0.90 \text{ mm}$$
$$\sigma_{\Delta h_9} = \pm 0.77 \text{ mm}$$

4 CONCLUSION

In this study, the procedure for calculating the most probable values of the measured height differences in the polygon of the school mine “Crveni Breg” on Avala, in front of the lower adit, is presented. The calculation of the most probable values of the measured height differences within the polygon was carried out using the method of conditional adjustment. The polygon was adjusted as a free local network, since in the future it will be connected to the national levelling network, at which time the points will obtain their official elevations.

The accuracy assessment after adjustment showed that the standard deviation of the measured height differences in the network is ±3.32 mm/km. This deviation is smaller than the permissible deviation in a levelling network of increased technical accuracy, which amounts to ±5 mm/km, thus indicating the high quality of the fieldwork and measurements performed. Finally, the most probable values of the height differences were computed, satisfying the imposed mathematical conditions, as well as their standard deviations, which range between ±0.27 mm and ±0.90 mm.

In future work, when the school polygon is connected to the national benchmarks, it will be possible to calculate the true elevations of all points forming the polygon. Moreover, the standard deviations of the elevations of the polygon points, given the small standard deviations of the adjusted height differences, will predominantly depend on the standard

deviation of the connected point from the national network, and within the entire network will approximately equal the standard deviation of that connected point.

REFERENCES

GANIĆ A. (2008) RAČUN IZRAVNANJA. Belgrade, Serbia: Faculty of Mining and Geology, University of Belgrade.

DŽEPAROVSKI, V. (1995) RAČUN IZRAVNANJA sa algoritmima za rešavanje zadataka. Belgrade, Serbia: Faculty of Mining and Geology, University of Belgrade.

GHILANI C. D. (2010) Adjustment Computations: Spatial Data Analysis, 5th Edition. Hoboken, New Jersey: John Wiley & Sons. ISBN: 978-0-470-46491-5.

ĐURĐEV N. (2023) 1D izravnanje geodetske mreže na školskom rudniku „Crveni Breg“ na Avali (Bachelor thesis), Faculty of Mining and Geology, University of Belgrade.

LEICA GEOSYSTEMS. (n.d.). Leica Sprinter 150M. Available from: https://bctechnologies.co.in/products/leica-sprinter-150m-digital-auto-level. Accessed on: 1.06.2026.

MIHAJLOVIĆ, K. (1982) Geodezija II (II deo), University of Belgrade, Naučna knjiga

UNDERGROUND MINING ENGINEERING 48(2026) 133-144 UDK 62
UNIVERSITY OF BELGRADE - FACULTY OF MINING AND GEOLOGY ISSN 03542904

Review paper

ENERGY EFFICIENCY OF MODERN UNDERGROUND MINE VENTILATION CONTROL STRATEGIES: A CRITICAL REVIEW OF RESEARCH FINDINGS

Sanja Bajić[1], Radmila Gaćina[1], Luka Crnogorac[1], Katarina Urošević[1]

Received: June 24, 2026 **Accepted:** June 29, 2026

Abstract: Underground mine ventilation serves both as a critical safety system and as one of the major consumers of electrical energy in underground mining operations. This paper presents a critical review of the energy performance of ventilation management strategies, focusing on ventilation network optimization, fan speed control, Ventilation-on-Demand (VoD), model-based control, computational fluid dynamics (CFD) applications, and sensor-based monitoring. The review is organized according to the level of intervention and validation, encompassing industrial measurements, pilot-scale and laboratory studies, as well as numerical simulations. The findings indicate that direct energy savings are most commonly achieved through the reduction of network resistance and pressure losses, fan speed adjustment, and the spatial and temporal alignment of airflow distribution with actual operational requirements. CFD analyses and monitoring systems do not constitute energy-saving measures by themselves; rather, they provide the basis for defining safe operating limits and enabling closed-loop control strategies. Reported energy savings are not directly comparable due to differences in baseline operating conditions, system boundaries, and validation methodologies. Reliable implementation requires the maintenance of minimum safety airflow rates, the provision of backup safety measures, and automatic transition to predefined safe operating modes in the event of sensor, communication, or actuator failures.

Keywords: mine ventilation; energy efficiency; Ventilation-on-Demand; variable frequency drive control; validation

1 INTRODUCTION

Ventilation in underground mines ensures the supply of fresh air, the dilution and removal of gases and airborne contaminants, the control of heat and humidity, and the maintenance of environmental conditions required for the safe operation of personnel

[1] University of Belgrade - Faculty of Mining and Geology, Djusina 7, 11000 Belgrade, Serbia
E-mails: sanja.bajic@rgf.bg.ac.rs ORCID: https://orcid.org/0000-0003-4387-9601;
radmila.gacina@rgf.bg.ac.rs ORCID: https://orcid.org/0000-0002-3856-4202;
luka.crnogorac@rgf.bg.ac.rs ORCID: https://orcid.org/0000-0002-9897-270X;
katarina.urosevic@rgf.bg.ac.rs ORCID: https://orcid.org/0000-0002-5529-2552

and equipment. At the same time, due to the continuous operation of main and auxiliary ventilation fans, it represents a significant component of the Mine's overall energy consumption (McPherson, 1993; Hartman et al., 1997).

Ventilation systems are commonly designed to satisfy worst-case or peak-demand operating conditions, whereas actual airflow requirements vary with the location of active workings, equipment utilization, contaminant emissions, and the ongoing development of the ventilation network. The mismatch between design conditions and real-time demand frequently results in excessive airflow, throttling losses at regulators, fan operation outside the optimum efficiency range, and unnecessary energy losses in inactive sections of the network. Although designing mine ventilation systems according to maximum anticipated demand is a rational engineering approach, the expansion of underground infrastructure, often driven by exploration and mine development activities, can make the delivery of adequate airflow to all working areas increasingly challenging, particularly when overall energy costs must be minimized.

The use of diesel-powered underground equipment, oxidation of sulphide ores, geological conditions involving carbonate formations, methane, hydrogen, radon, or sulphur-bearing strata, as well as the generation of nitrogen oxides following blasting operations, are only some of the factors contributing to the complexity of underground mine ventilation (Semin et al., 2020; Brake, 2006).

The objective of this paper is to compare contemporary ventilation management strategies with respect to three key questions:

- by which mechanisms they influence energy consumption,
- how their performance has been validated, and
- which safety and infrastructure constraints determine their applicability.

On this basis, the reviewed approaches are classified into direct energy-efficiency interventions targeting ventilation networks and fans, and enabling technologies such as CFD modelling, monitoring systems, and predictive control models.

2 METHODOLOGICAL FRAMEWORK

The analysis encompassed monographs, peer-reviewed journal articles, and conference papers published between 1989 and 2025. Relevant sources were identified using combinations of the following keywords: *mine ventilation, underground mine energy efficiency, ventilation on demand, variable frequency drive, mine ventilation optimization, CFD mine ventilation, and ventilation monitoring*.

The literature selection has been focused on studies addressing underground mine ventilation and presenting a technical intervention, mathematical model, or control strategy, together with either quantified energy performance indicators or a justified assessment of their influence on ventilation system safety.

For each selected source, the level and type of intervention, ventilation system characteristics, validation methodology, reported energy-related outcomes, and identified safety constraints were examined. The results were evaluated according to the method of validation, namely industrial measurements, pilot-scale and laboratory investigations, or numerical and optimization-based analyses. Due to differences in baseline operating conditions, system boundaries, and monitoring periods among the reviewed studies, reported energy-saving values were not aggregated into a single average indicator

3 ENERGY PERFORMANCE INDICATORS AND EVALUATION CRITERIA

The primary objective of mine ventilation is to ensure controlled airflow throughout the underground network. The analysis of mine ventilation systems is fundamentally based on the continuity equation, according to which the volumetric airflow rate through a given cross-section is expressed as (McPherson, 1993; Hartman et al., 1997):

$$Q = A \cdot v \tag{1}$$

Where:

Q - volumetric airflow rate (m^3/s),

A - cross-sectional area (m^2),

v - average air velocity (m/s).

As air flows through underground openings, pressure losses occur due to friction, local resistances, cross-sectional changes, network branching, air leakage, and the presence of equipment. In mine ventilation engineering, this relationship is commonly described using the Atkinson equation, or quadratic airflow law (McPherson, 1993; Acuña and Lowndes, 2014):

$$\Delta p = R \cdot Q^2 \tag{2}$$

Where:

Δp – pressure drop across the airway (Pa),

R – aerodynamic resistance of the airway,

Q – volumetric airflow rate (m³/s).

For the assessment of energy efficiency, fan power demand is of particular importance and may be expressed as (McPherson, 1993; Hartman et al., 1997):

$$P = \frac{Q \cdot \Delta p}{\eta} \tag{3}$$

Where:

P – required fan power (W),

Q – airflow rate (m³/s),

Δp – pressure rise generated or overcome by the fan (Pa),

η – overall efficiency of the fan and drive system.

Nowadays, an energy-performance outcome is considered directly validated when a study reports a measured change in power demand, electrical energy consumption, or operating cost relative to a clearly defined baseline operating condition. Results obtained solely through numerical simulations are classified as estimated values, whereas CFD analyses, monitoring systems, and network calibration procedures are treated as enabling tools unless they are integrated with active control measures and validated through field implementation.

4 BASELINE OPERATING CONDITIONS AND SOURCES OF ENERGY LOSSES

In many underground mines, the baseline ventilation configuration consists of fans operating at approximately constant speed, while airflow distribution is controlled through regulators and ventilation doors. Such systems are generally robust and straightforward to operate; however, they are often designed for peak-demand conditions and therefore do not adequately respond to short-term variations in production activity (Jovičić, 1989; Lilić et al., 2000).

Energy losses are not confined to the fan itself. The total power demand of a ventilation system is influenced by airway resistance, air leakage, abrupt changes in airflow direction, poorly designed intake and return airways, throttling losses, and fan operation away from the optimum efficiency point. Consequently, improving a single component does not necessarily lead to improved performance of the overall system.

Papar et al. (1999) describe this challenge as the need for a systems-based approach in which the power supply, motor, drive system, fan, control devices, and ventilation airways are considered as an integrated whole. In the mine investigated by these authors,

aerodynamic redesign of intake and discharge components enabled the required airflow to be achieved without installing higher-capacity fans.

This baseline framework is essential for interpreting reported energy savings. Reductions in energy consumption may result from lower airflow requirements, reduced network resistance, improved fan efficiency, or decreased operating time. Meaningful comparison between studies is therefore possible only when the underlying energy-saving mechanism is clearly identified.

5 ENERGY-EFFICIENT MINE VENTILATION MANAGEMENT

5.1 Ventilation Network Optimization

Ventilation network optimization encompasses the reduction of aerodynamic resistance, improvement of airflow distribution, selection of regulator settings, and coordination of multiple fan systems. Energy savings are achieved when the required airflow is delivered with a lower overall pressure drop or when airflow is redistributed from inactive to active sections of the mine without increasing total airflow demand (Acuña and Lowndes, 2014).

Network simulation models provide an efficient means of evaluating alternative operating scenarios; however, the resulting energy savings remain potential benefits until validated through measurements of airflow, pressure, and power consumption. A major limitation is the sensitivity of optimization results to uncertainties in airway resistance and leakage estimates. For this reason, network calibration should precede the implementation of any control strategy.

5.2 Fan and Drive Control

Variable Frequency Drive (VFD) technology enables fan speed to be adjusted according to actual airflow requirements, rather than dissipating excess pressure through throttling devices. Because fan power demand is approximately proportional to the cube of rotational speed, the greatest savings potential exists in systems operating for extended periods under partial-load conditions.

Using a model-based analysis of an auxiliary ventilation system, Gonen (2021) estimated annual energy savings of approximately 53%. However, such results are highly dependent on the operating profile, minimum permissible airflow rates, and assumptions regarding baseline energy consumption.

Field investigations reported by Papar et al. (1999) demonstrate that speed control is not the only available intervention. By modifying the aerodynamic configuration of the ventilation system, existing fans were able to deliver the required design airflow, thereby avoiding the installation of additional fan capacity exceeding 224 kW. This case

highlights that VFD implementation should follow a thorough assessment of system sizing, airway configuration, leakage conditions, and fan operating points.

5.3 Ventilation-on-Demand and Model-Based Control

Ventilation-on-Demand (VoD) systems adjust airflow according to the location and timing of actual ventilation requirements. Control signals may be derived from production schedules, operational events, personnel and equipment tracking systems, or measurements of mine atmospheric conditions. Energy benefits are achieved only when monitoring information is translated into adjustments of fan speed, regulator settings, or the operating status of individual ventilation branches. Based on industrial case studies from multiple mines, Costa and da Silva (2020) reported annual energy savings ranging from approximately 21% to 30% following the implementation of different combinations of VoD and VFD technologies. These values should not be interpreted as a universal efficiency indicator, since the mines differed substantially with respect to depth, reliance on auxiliary ventilation, degree of automation, and baseline operating conditions.

Model-based control extends the VoD concept by simultaneously determining optimal operating points for fans and regulators. Sjöström et al. (2020) implemented model-based control of main and booster fans at the Garpenberg Mine and reported an approximately 40% reduction in ventilation energy consumption over a ten-month monitoring period, while continuously tracking airflow and differential pressure throughout the network.

Chatterjee et al. (2015) further demonstrated that optimization strategies can incorporate time-varying electricity tariffs. In such cases, a distinction must be made between reductions in energy consumption and reductions in operating cost, as these objectives are not necessarily equivalent.

The reliability of VoD systems depends on measurement quality and network response characteristics. Ihsan et al. (2024) developed Adaptive Neuro-Fuzzy Inference System (ANFIS) models for predicting optimal fan power requirements and hazardous gas dilution times. Although the models demonstrated promising performance, validation was conducted under laboratory-scale conditions. Consequently, the results confirm methodological feasibility rather than proven energy savings in full-scale mining operations.

5.4 CFD Modelling as a Tool for Defining Safe Operating Limits

Computational Fluid Dynamics (CFD) comprises a set of numerical methods used to simulate velocity, pressure, temperature, and contaminant concentration fields within complex underground geometries. In the context of energy efficiency, its contribution is indirect: CFD can identify airflow recirculation, stagnant zones, inefficient mixing, and localized leakage pathways, but the simulation itself does not reduce energy consumption (Lilić et al., 2000; Yi et al., 2022).

Cheng et al. (2016) applied CFD modelling to optimize methane control while simultaneously preventing spontaneous combustion in a longwall mining environment. Their results demonstrated that increasing airflow rates could effectively reduce methane concentrations; however, higher airflow also increased oxygen ingress into the goaf area, thereby elevating the risk of spontaneous heating. Consequently, the recommended airflow range represented a safety compromise rather than an energy-optimization outcome in a strict sense.

The review research of Brodny and Tutak (2021) and Yi et al. (2022) indicate that CFD is particularly valuable for the design and assessment of auxiliary ventilation systems, smoke and gas dispersion analyses, dust transport studies, and thermal environment evaluations. Its contribution to energy efficiency becomes measurable only when CFD-derived solutions are incorporated into operational control strategies and subsequently validated against baseline operating conditions.

Because CFD results are highly sensitive to geometric representation, boundary conditions turbulence models, and numerical mesh quality, simulation outcomes should always be verified through field measurements before implementation.

5.5 Sensor-Based Monitoring, Network Calibration, and Control Reliability

Monitoring airflow rates, pressure, gas concentrations, temperature, and equipment location constitutes the foundation of a closed-loop ventilation control system. Sensor data enable verification that required airflow quantities are being delivered, facilitate early detection of abnormal operating conditions, and support continuous updating of ventilation network models (Shriwas and Pritchard, 2020).

Continuous airflow monitoring can significantly improve network-model calibration and reduce discrepancies between simulated and actual operating conditions (Zhou et al., 2022). Accurate calibration is particularly important in mines where network resistance changes continuously due to development activities, production advances, and modifications of ventilation infrastructure. Monitoring itself does not generate energy savings; rather, it serves as a prerequisite for reliable ventilation management. Robust systems should incorporate redundant measurement and control channels, signal validation procedures, clearly defined alarm thresholds, and provisions for manual operator intervention.

In the event of communication failure, sensor malfunction, or unreliable measurements, the control system should automatically revert to a predefined safe operating mode, even when such operation results in higher energy consumption Table 1 summarizes studies reporting quantified energy-performance outcomes, whereas Table 2 highlights methods whose primary contribution lies in modelling, validation, or safety enhancement. This distinction prevents simulation-based potential from being interpreted as industrially verified energy savings.

Table 1 Studies Reporting Quantified Energy Performance

Source	Intervention	Validation Method	Energy Outcome
Costa and da Silva (2020)	VoD/VFD implementation in multiple mines	Industrial case studies	21–30% reported annual energy savings
Gonen (2021)	VFD control of auxiliary fans	Model-based analysis	53% estimated annual energy savings
Papar et al. (1999)	Aerodynamic system redesign	Field measurements	Avoided installation of >224 kW additional fan capacity
Sjöström et al. (2020)	Model-based ventilation control	Ten-month industrial monitoring campaign	Approximately 40% reduction in energy consumption
Saleem (2025)	Mathematical and machine-learning model	Numerical analysis	31.24% modelled reduction in energy consumption

Table 2 Enabling Technologies without directly verified Mine-Scale energy savings

Source	Tool/Method	Validation Approach	Contribution to Energy Optimization
Cheng et al. (2016)	CFD modelling	Numerical simulation of a real mine geometry	Determination of safe airflow operating ranges
Ihsan et al. (2024)	ANFIS-based VoD model	Laboratory-scale validation	Prediction of fan power requirements and gas dilution times
Shriwas and Pritchard (2020)	Monitoring and control systems	Review of industrial practice	Foundation for closed-loop ventilation control
Zhou et al. (2022)	Continuous network calibration	Experimental study	Improved reliability and accuracy of network models

Note: Reported energy-saving percentages are not directly comparable because of differences in system boundaries, baseline operating conditions, and calculation methodologies.

The reviewed studies indicate that the largest reported energy savings are generally achieved through the adjustment of fan operation to actual ventilation requirements, primarily by means of VFD control and VoD strategies. In contrast, ventilation network optimization often yields less immediately measurable but potentially more sustainable long-term improvements.

6 DISCUSSION

The results of this review demonstrate that substantial energy savings are rarely achieved through a single intervention. Instead, the greatest benefits arise from the integration of multiple complementary measures. Ventilation network optimization reduces unnecessary pressure losses, VFD control enables fan operation to match airflow demand, and VoD systems direct airflow to locations where mining activities are taking place. Monitoring systems and predictive models provide the information required to determine when and to what extent airflow rates can be safely adjusted.

The applicability of these approaches depends strongly on site-specific mining conditions. Mines characterized by frequent changes in active workings, extensive diesel equipment fleets, and well-developed communication infrastructure are particularly suitable for the implementation of VFD and VoD technologies. Conversely, operations relying on aging infrastructure, unreliable communication systems, or facing significant gas-related hazards may require a gradual implementation strategy beginning with improved monitoring of airflow, gas concentrations, and fan performance.

Reported energy-saving values cannot be directly compared because they originate from different validation environments. Some results are based on measurements obtained in operating mines, whereas others are derived from laboratory experiments, numerical simulations, or optimization models. Consequently, studies supported by before-and-after field measurements provide the strongest evidence for practical implementation. Energy-efficiency objectives must never compromise ventilation safety. Minimum airflow quantities, acceptable air velocities, maximum permissible concentrations of hazardous gases, thermal comfort requirements, and emergency response procedures for fires or equipment failures must always take precedence over energy-saving targets. Therefore, modern ventilation systems should be capable of automatically reverting to a safe operating mode whenever sensors, communication systems, or automated control functions become unreliable.

7 CONCLUSION

The energy efficiency of underground mine ventilation systems can be improved through the reduction of network losses, the appropriate selection of fan operating modes, and the adjustment of airflow quantities to actual ventilation requirements. Variable Frequency Drive (VFD) control and Ventilation-on-Demand (VoD) systems offer the greatest practical potential, particularly when integrated with reliable monitoring systems and continuously updated ventilation network models.

CFD simulations, sensor-based monitoring systems, and predictive control models do not directly generate energy savings; however, they enable more reliable assessment of airflow distribution, gas dispersion, and the consequences of modifying ventilation

operating conditions. Their practical value depends on the quality of input data and the validation of results through field measurements.

In mines with limitation of infrastructure, advanced ventilation management technologies should be implemented progressively. Initial efforts should focus on improving measurement systems, reducing air leakage, and optimizing auxiliary ventilation networks, after which VFD control and more sophisticated VoD solutions may be introduced. Throughout this process, personnel safety and the maintenance of stable underground atmospheric conditions must remain the primary aim governing any energy-optimization strategy.

Acknowledgment: The authors thank the Serbian Ministry of Education, Science, and Technological Development for their support and the funds provided under Contract No. 451-03-34/2026-03/ 200126 and No. 451-03-33/2026-03/ 200126.

Editorial Disclaimer: Authors Luka Crnogorac and Katarina Urošević are Editors of this journal. They were not involved in the peer review, editorial evaluation, or decision-making process for this manuscript. Editorial responsibility was delegated to an independent editor.

REFERENCES

MCPHERSON, M.J. (1993) Subsurface Ventilation and Environmental Engineering. Dordrecht: Springer. Available from: https://doi.org/10.1007/978-94-011-1550-6.

HARTMAN, H.L., MUTMANSKY, J.M., RAMANI, R.V. and WANG, Y.J. (1997) Mine Ventilation and Air Conditioning. 3rd ed. New York: John Wiley & Sons.

СЕМИН, М. А., ГРИШИН, Е. Л., ЛЕВИН, Л. Ю., & ЗАЙЦЕВ, А. В. (2020). Автоматизированное управление вентиляцией шахт и рудников. Проблемы, современный опыт, направления совершенствования. *Записки Горного института*, *246*, 623-632. DOI: 10.31897/PMI.2020.6.4

BRAKE, R. (2006). The Importance of Underground Mine Ventilation.*AusIMM Bulletin*. Available from: https://www.researchgate.net/profile/Rick-Brake/publication/297810462_The_importance_of_underground_mine_ventilation/links/5a6883b8a6fdcc03e077817f/The-importance-of-underground-mine-ventilation.pdf

ACUÑA, E.I. and LOWNDES, I.S. (2014) A review of primary mine ventilation system optimization. Interfaces, 44 (2), pp. 163–175. Available from: https://doi.org/10.1287/inte.2014.0736.

DE SOUZA, E. (2017) Application of ventilation management programs for improved mine safety. International Journal of Mining Science and Technology, 27 (4), pp. 647–650. Available from: https://doi.org/10.1016/j.ijmst.2017.05.018.

KOUL, P. (2025) Design and optimization of ventilation systems for deep underground mines. Podzemni radovi / Underground Mining Engineering, 47, pp. 1–44. Available from: https://doi.org/10.5937/podrad2547001K.

JOVIČIĆ, V. (1989) Ventilacija rudnika. Beograd: Rudarsko-geološki fakultet, Univerzitet u Beogradu.

LILIĆ, N., STANKOVIĆ, R. and OBRADOVIĆ, I. (2000) Hibridni sistem za planiranje i analizu ventilacije rudnika. Beograd: Rudarsko-geološki fakultet, Univerzitet u Beogradu.

PAPAR, R., SZADY, A., HUFFER, W.D., MARTIN, V. and MCKANE, A. (1999) Increasing energy efficiency of mine ventilation systems. In: Proceedings of the 8th U.S. Mine Ventilation Symposium, pp. 611–617.

GONEN, A. (2021) Energy savings in auxiliary ventilation systems of underground mines. International Journal of Engineering Technologies and Management Research, 8 (10), pp. 72–82. Available from: https://doi.org/10.29121/ijetmr.v8.i10.2021.1055.

SALEEM, H.A. (2025) Energy consumption reduction in underground mine ventilation system: An integrated approach using mathematical and machine learning models toward sustainable mining. Sustainability, 17 (3), 1038. Available from: https://doi.org/10.3390/su17031038.

ACUÑA, E. and ALLEN, C. (2017) Ventilation control system implementation and energy consumption reduction at Totten Mine with Level 4 Tagging and future plans. In: Proceedings of the First International Conference on Underground Mining Technology. Perth: Australian Centre for Geomechanics. Available from: https://doi.org/10.36487/ACG_rep/1710_06_Acuna.

CHATTERJEE, A., ZHANG, L. and XIA, X. (2015) Optimization of mine ventilation fan speeds according to ventilation on demand and time of use tariff. Applied Energy, 146, pp. 65–73. Available from: https://doi.org/10.1016/j.apenergy.2015.01.134.

COSTA, L. DE V. and DA SILVA, J.M. (2020) Cost-saving electrical energy consumption in underground ventilation by the use of ventilation on demand. Mining Technology, 129 (1), pp. 1–8. Available from: https://doi.org/10.1080/25726668.2019.1651581.

IHSAN, A., WIDODO, N.P., CHENG, J. and WANG, E.-Y. (2024) Ventilation on demand in underground mines using neuro-fuzzy models: Modeling and laboratory-scale

experimental validation. Engineering Applications of Artificial Intelligence, 133, 108048. Available from: https://doi.org/10.1016/j.engappai.2024.108048.

CHENG, J., LI, S., ZHANG, F., ZHAO, C., YANG, S. and GHOSH, A. (2016) CFD modelling of ventilation optimization for improving mine safety in longwall working faces. Journal of Loss Prevention in the Process Industries, 40, pp. 285–297. Available from: https://doi.org/10.1016/j.jlp.2016.01.018.

BRODNY, J. and TUTAK, M. (2021) Applying computational fluid dynamics in research on ventilation safety during underground hard coal mining: A systematic literature review. Process Safety and Environmental Protection, 151, pp. 373–400. Available from: https://doi.org/10.1016/j.psep.2021.05.016.

YI, H., KIM, M., LEE, D. and PARK, J. (2022) Applications of computational fluid dynamics for mine ventilation in mineral development. Energies, 15 (22), 8405. Available from: https://doi.org/10.3390/en15228405.

SHRIWAS, M. and PRITCHARD, C. (2020) Ventilation monitoring and control in mines. Mining, Metallurgy & Exploration, 37, pp. 1015–1021. Available from: https://doi.org/10.1007/s42461-020-00231-8.

ZHOU, L., THOMAS, R.A., YUAN, L. and BAHRAMI, D. (2022) Experimental study of improving a mine ventilation network model using continuously monitored airflow. Mining, Metallurgy & Exploration, 39, pp. 887–895. Available from: https://doi.org/10.1007/s42461-022-00574-4.

SJÖSTRÖM, S., KLINTENÄS, E., JOHANSSON, P. and NYQVIST, J. (2020) Optimized model-based control of main mine ventilation air flows with minimized energy consumption. International Journal of Mining Science and Technology, 30 (4), pp. 533–539. Available from: https://doi.org/10.1016/j.ijmst.2020.05.016.

УНИВЕРЗИТЕТ У БЕОГРАДУ
РУДАРСКО-ГЕОЛОШКИ ФАКУЛТЕТ
11120 Београд 35, Ђушина 7, п.п. 35-62
Тел: (011) 3219-100, Факс: (011) 3235-539

UNIVERSITY OF BELGRADE,
FACULTY OF MINING AND GEOLOGY
Republic of Serbia, Belgrade, Djusina 7
Phone:(381 11) 3219-100, Fax:(381 11) 3235-539

РУДАРСКИ ОДСЕК

Студијски програм
РУДАРСКО ИНЖЕЊЕРСТВО

Модули:
Површинска експолатација лежишта минералних сировина
Подземна експолатација лежишта минералних сировина
Подземна градња
Рударска мерења
Механизација у рударству
Припрема минералних сировина

Студијски програм
ИНЖЕЊЕРСТВО НАФТЕ И ГАСА

Студијски програм
ИНЖЕЊЕРСТВО ЗАШТИТЕ ЖИВОТНЕ СРЕДИНЕ

Деканат

- Тел.: +381 11 3219 101
- Факс.: +381 11 3235 539
- E-mail: dekan@rgf.bg.ac.rs

Рударски одсек

- Секретар: Томашевић Александра
- Тел.: +381 11 3219 102
- E-mail: ro@rgf.bg.ac.rs

Секретар факултета

- Ђокановић Слађана
- Тел.: +381 11 3219 105
- E-mail: sladja@rgf.bg.ac.rs

Геолошки одсек

- Секретар: Јевтовић Бошко
- Тел.: +381 11 3219 103
- E-mail: gorgf@rgf.bg.ac.rs